AD NUMBER
ADB002165
LIMITATION CHANGES

TO:

Approved for public release; distribution is unlimited.

FROM:

Distribution authorized to U.S. Gov't. agencies only; Test and Evaluation; FEB 1975. Other requests shall be referred to Air Force Armament Lab., Eglin AFB, FL 32542.

AUTHORITY

AFATL ltr 26 May 1977

~~ .. ~ ~ 1975

INVESTIGATION OF FACTORS AFFECTING THE WIND TUNNEL MEASUREMENTS OF CARRIAGE-POSITION AIRLOADS ON EXTERNAL STORE MODELS AT TRANSONIC MACH NUMBERS

David W. Hill, Jr.
ARO, Inc.

PROPULSION WIND TUNNEL FACILITY
ARNOLD ENGINEERING DEVELOPMENT CENTER
AIR FORCE SYSTEMS COMMAND
ARNOLD AIR FORCE STATION, TENNESSEE 37389

February 1975

Final Report for Period March 23 — July 23, 1973

Prepared for

NOTICES

When U. S. Government drawings specifications, or other data are used for any purpose other than a definitely related Government procurement operation, the Government thereby incurs no responsibility nor any obligation whatsoever, and the fact that the Government may have formulated, furnished, or in any way supplied the said drawings, specifications, or other data, is not to be regarded by implication or otherwise, or in any manner licensing the holder or any other person or corporation, or conveying any rights or permission to manufacture, use, or sell any patented invention that may in any way be related thereto.

Qualified users may obtain copies of this report from the Defense Documentation Center.

References to named commercial products in this report are not to be considered in any sense as an endorsement of the product by the United States Air Force or the Government.

APPROVAL STATEMENT

This technical report has been reviewed and is approved for publication.

FOR THE COMMANDER
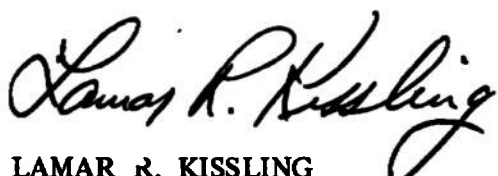
LAMAR R. KISSLING
Lt Colonel, USAF
Chief Air Force Test Director, PWT
Directorate of Test
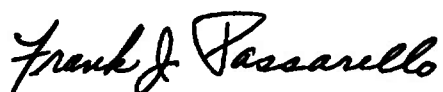
FRANK J. PASSARELLO
Colonel, USAF
Director of Test

REPORT DOCUMENTATION PAGE		READ INSTRUCTIONS BEFORE COMPLETING FORM
1. REPORT NUMBER AEDC-TR-75-12 AFATL-TR-75-22	2 GOVT ACCESSION NO.	3 RECIPIENT'S CATALOG NUMBER
4 TITLE (and Subtitle) INVESTIGATION OF FACTORS AFFECTING THE WIND-TUNNEL MEASUREMENTS OF CARRIAGE-POSITION AIRLOADS ON EXTERNAL STORE MODELS AT TRANSONIC MACH NUMBERS		5 TYPE OF REPORT & PERIOD COVERED Final Report—March 23– July 23, 1973
		6. PERFORMING ORG. REPORT NUMBER
7 AUTHOR(s) David W. Hill, Jr., ARO, Inc.		8 CONTRACT OR GRANT NUMBER(s)
9 PERFORMING ORGANIZATION NAME AND ADDRESS Arnold Engineering Development Center Arnold Air Force Station, Tennessee 37389		10. PROGRAM ELEMENT, PROJECT, TASK AREA & WORK UNIT NUMBERS Program Element 64602F Project 5613
11 CONTROLLING OFFICE NAME AND ADDRESS Air Force Armament Laboratory (DLJC) Eglin AFB, Florida 32542		12. REPORT DATE February 1975
		13. NUMBER OF PAGES 112
14. MONITORING AGENCY NAME & ADDRESS(if different from Controlling Office)		15. SECURITY CLASS. (of this report) UNCLASSIFIED
		15a. DECLASSIFICATION/DOWNGRADING SCHEDULE N/A

16 DISTRIBUTION STATEMENT (of this Report)

Distribution limited to U.S. Government agencies only; this report contains information on test and evaluation of military hardware; February 1975; other requests for this document must be referred to Air Force Armament Laboratory (DLJC), Eglin AFB, Florida 32542.

17 DISTRIBUTION STATEMENT (of the abstract entered in Block 20, if different from Report)

18 SUPPLEMENTARY NOTES

Available in DDC

19 KEY WORDS (Continue on reverse side if necessary and identify by block number)

wind tunnel	position	transonic flow
test methods	aerodynamic loading	Mach numbers
measurements	drag	
carriages	external stores	

20 ABSTRACT (Continue on reverse side if necessary and identify by block number)

A wind tunnel test was conducted to investigate the factors affecting the M-117 and BLU-1C/B (finned and unfinned) store carriage-position airloads beneath the wing of a 0.05-scale A-7D aircraft. The investigation included store afterbody modifications, the presence of stings of various diameters and shapes, misalignment of store relative to its carriage position, variations of aircraft yaw attitude, and various store carriage

DD FORM 1473 1 JAN 73   EDITION OF 1 NOV 65 IS OBSOLETE

20. ABSTRACT (Continued)

positions on the multiple ejector rack (MER). The rigid loads
technique which simulated the captive trajectory system (CTS)
technique was used to measure carriage-position airloads and
the results compared to the CTS results. The test was conducted
at Mach numbers 0.7, 0.9, and 1.05 with the aircraft angle of
attack ranging from -2 to 12 deg. The results indicated that
the M-117 carriage-position airloads were the most sensitive to
any of the factors and the unfinned BLU-1C/B the least sensitive
to all the factors investigated. The carriage-position airloads
were most sensitive to store afterbody modifications. Most of
the effects were greater at Mach number 1.05. The differences
between the carriage-position airloads data using the CTS and
rigid loads technique were no greater than the repeatability of
the data from the CTS technique.

AFSC
Arnold AFB Tenn

PREFACE

The work reported herein was conducted by the Arnold Engineering Development Center (AEDC), Air Force Systems Command (AFSC), at the request of the Air Force Armament Laboratory (AFATL), under Program Element 64602F, Project 5613. The project monitor was Capt. Steve Braud, AFATL (DLJC). The results of the test were obtained by ARO, Inc. (a subsidiary of Sverdrup & Parcel and Associates, Inc.), contract operator of AEDC, AFSC, Arnold Air Force Station, Tennessee, under ARO Project No. PA026. The testing was conducted during the period from March 23 to July 23, 1973, and the data analysis was completed on' October 31, 1973. The manuscript (ARO Control Number ARO-PWT-TR-74-116) was submitted for publication on November 26, 1974.

CONTENTS

ILLUSTRATIONS

TABLES

1.0 INTRODUCTION

To verify safe separation of external stores from aircraft, wind tunnel techniques were devised to investigate the store separation characteristics. One of the techniques is the captive trajectory system (CTS) which is used in the Aerodynamic Wind Tunnel (4T) of the Propulsion Wind Tunnel Facility. In the CTS technique, the store model is positioned in the aircraft flow field by a servo-controlled independent store sting. When using this technique, the afterbody generally has to be modified for access of the support sting. The alteration usually consists of increasing the base diameter which may result in a decrease in tail fin planform area or reduction in length of the body.

Disagreement between some flight tests and wind tunnel trajectory data of stores separated from multiple ejector racks (MER) led to concern that the store tail modifications and presence of sting might affect the measured aerodynamic force and moment data, thus altering the calculated trajectory motion. As a result of this disagreement, a wind tunnel study program was conducted in order to evaluate the effects on store force and moments of store afterbody modification, presence of stings of various diameters and shapes, misalignment of the store relative to its carriage position, and aircraft yaw attitude. The "rigid loads" technique was used to make these measurements and the results compared with the CTS technique.

In the rigid loads technique, the store model is supported by the aircraft model in its carriage position by an internal balance. Since the requirement for mounting the store model on a sting is eliminated, the store model may be constructed to duplicate the geometry of the full-scale store. Using this technique, effects of afterbody modifications may be ascertainted by measuring the difference between store carriage loads for simulated full-scale models and simulated captive trajectory models. Effects of store support sting interference may be ascertained in a similar manner by testing with and without the presence of dummy stings.

The tests were conducted using 0.05-scale models of the M-117 and BLU-1C/B (finned and unfinned) stores mounted from MER racks on the center wing pylon stations of the A-7D aircraft. Testing was conducted at Mach numbers 0.7, 0.9, and 1.05 over an angle-of-attack range from -2 to 12 deg.

2.0 APPARATUS

2.1 TEST FACILITY

The Aerodynamic Wind Tunnel (4T) is a closed-loop, continuous flow, variable density tunnel in which the Mach number can be varied from 0.2 to 1.3. At all Mach numbers,

the stagnation pressure can be varied from 300 to 3700 psfa. The test section is 4 ft square and 12.5 ft long with perforated, variable porosity (0.5- to 10-percent open) walls. It is completely enclosed in a plenum chamber from which the air can be evacuated, allowing part of the tunnel airflow to be removed through the perforated walls of the test section. A more complete description of the test facility can be found in the Test Facilities Handbook[1].

For carriage loads measurement tests, the parent-aircraft model is inverted in the test section and supported by an offset sting attached to the main pitch sector. The store model is either mounted to the aircraft or is supported by the CTS support which extends down from tunnel top wall and which provides store movement independent of the parent-aircraft model. Figures 1 and 2 show a sketch of an installation of a CTS and rigid loads test.

2.2 TEST ARTICLES

The test articles used were 0.05-scale models of stores and A-7D aircraft (including pylons, racks, and models used for configuration loading). The A-7D model was geometrically similar to the full-scale aircraft except for some modifications incident to the wind tunnel installation and CTS operation. A sketch of the A-7D model showing basic dimensions and location of the wing pylon stations is shown in Fig. 3. Dimensions of the wing pylons are presented in Fig. 4. When installed on the aircraft, all pylon surfaces for store and rack mounting are at a 3-deg nose down attitude with respect to the aircraft waterline. Multiple ejection rack details are shown in Fig. 5. These racks were mounted on the pylons to align the 30-in. lug attachments. Figures 6 through 8 present the basic and modified BLU-1C/B finned, BLU-1C/B unfinned, and M-117GP store models used in the CTS and rigid loads installation.

Figure 9 shows the details and dimensions of the 0.2- and 0.4-in.-diam straight dummy stings and 0.4-in.-diam bent dummy sting used in the rigid loads installation. The dummy stings were supported by the main sting. Figure 9 is a photograph showing the dummy sting installed.

In CTS testing, the store models were mounted on a six-component internal balance which was an intergal part of an offset sting.

A photograph showing the CTS installation is shown in Fig. 10. Photographs showing the rigid loads installation with and without the dummy sting installed are shown in Figs. 11 and 12.

---

[1] Test Facilities Handbook (Tenth Edition). "Propulsion Wind Tunnel Facility, Vol. 4." Arnold Engineering Development Center, May 1974.

2.3 INSTRUMENTATION

For CTS testing, a 0.40-in.-diam, six-component balance was used. The pylons and racks were instrumented with spring-loaded plungers (touch wires) which were electrically connected to give the data system an indication of when the store contacted the touch wire at the carriage position. The CTS system was electrically connected to automatically stop the CTS movement if the store model or CTS contacted the aircraft model, aircraft support sting, or the test walls.

For rigid loads testing, a 0.30-in.-diam, four-component balance (no axial and rolling-moment gages) was used. The balances were mounted to the MER racks as shown in Figs. 13 and 14.

The aircraft angle of attack was set using an absolute angle-of-attack sensor mounted in the fuselage of the A-7D model.

3.0 TEST DESCRIPTION

3.1 TEST CONDITIONS

Pitch polar data were taken at Mach numbers 0.7, 0.9, and 1.05. The tunnel stagnation pressure was varied to produce a constant free-stream dynamic pressure of 500 psf. The tunnel stagnation temperature varied between 90 and 100°F. The tunnel conditions were held constant while each configuration was tested through a -2- to 12-deg angle-of-attack range. The test section wall porosity was varied with free-stream Mach number in order to achieve minimum lift interference while alleviating blockage effects.

3.2 DATA ACQUISITION

To obtain carriage-position loads data using the CTS technique, the parent aircraft was positioned at the desired initial angle of attack. The store model was then automatically moved by the CTS to its carriage position at the touch point. Force and moment data were then recorded at this position and at various selected distances from the carriage position. The store model was then automatically moved clear of the parent model. The next data point was initiated by a manually controlled angle-of-attack movement of the parent model.

In the rigid loads technique, the aircraft model support is controlled by the automatic model attitude-positioning system (AMAPS). The AMAPS is a computer-controlled system which automatically stops the model through a pre-programmed sequence of aircraft angle of attack and takes data at each set position.

The model parameters used in the reduction of force and moment data to aerodynamic coefficients are presented in Table 1.

3.3 CORRECTIONS

In CTS testing, balance angular and translational deflections caused by aerodynamic loads on the store models were accounted for in the data reduction program to calculate store model attitude.

In both CTS and rigid loads testing, corrections were also made for model weight tares to calculate the net aerodynamic forces on the store model.

3.4 PRECISION OF DATA

Uncertainties in aerodynamic force and moment coefficient data on the store models were calculated taking into consideration probable inaccuracies in the balance measurements and tunnel conditions. The maximum uncertainties in the coefficients are presented below:

ΔC_N	ΔC_Y	ΔC_m	ΔC_n
±0.007	±0.011	±0.032	±0.040

The estimated uncertainties in model positioning resulting from the ability of the CTS to set a specific value are:

$\Delta X, \Delta Y, \Delta Z$	$\Delta\theta, \Delta\psi$
±0.050	±0.150

The estimated uncertainty in setting Mach number was no greater than ±0.003 and the uncertainty in parent-model angle of attack was estimated to be ±0.10 deg.

4.0 RESULTS AND DISCUSSION

The data presented herein consist of store-model aerodynamic coefficient variations with aircraft angle of attack for the M-117 and BLU-1C/B (unfinned and finned) at Mach numbers of 0.7, 0.9, and 1.05. For the same store model, comparisons of carriage-position aerodynamic coefficients are made with the basic and modified store base geometry, and for variations in the dummy sting geometries, store pitch and yaw attitudes relative to the carriage position, displacement of the store from its carriage position, and aircraft yaw attitude. Comparisons are also made between the CTS and rigid loads techniques.

Table 2 describes the wing-loading configurations used in the data presentation. Information pertaining to data obtained during the test is presented in Tables 3 and 4. The L or R notation for each configuration denotes left or right wing, respectively.

4.1 EFFECTS OF STORE BASE GEOMETRY MODIFICATIONS

Figures 16 through 21 present the carriage-position aerodynamic coefficient data for the basic and modified M-117 and BLU-1C/B (unfinned and finned) stores. In general, the effect of modifying the tail base geometry on the store aerodynamic coefficients is a function of Mach number, wing-loading configuration, and aircraft angle of attack. The data indicate the M-117 is the most sensitive and the unfinned BLU-1C/B the least sensitive to geometrical changes around the base of the store.

4.2 EFFECTS DUE TO PRESENCE OF STORE STINGS

The 0.4-in.-diam bent and straight dummy stings were used in combination with models simulating the geometry of stores used in captive trajectory testing. The 0.4-in.-diam bent sting was used to evaluate the aerodynamic interference effect due to sting geometry changes, and the 0.4-in.-diam straight sting simulated the actual sting arrangement normally used in captive trajectory testing.

Figures 22 through 33 present the carriage-position aerodynamic coefficients for the basic and modified M-117 and BLU-1C/B (unfinned and finned) stores with and without the presence of stings. The aerodynamic coefficient data of the M-117 with the basic tail geometry (Fig. 22) were significantly affected by the presence of the 0.2-in.-diam sting, whereas the unfinned BLU-1C/B (Figs. 24 and 25) and finned BLU-1C/B (Figs. 26 and 27) store aerodynamic data were relatively unaffected by the presence of the sting.

For the modified CTS store shape, the M-117 carriage-position aerodynamic coefficients (Figs. 28 and 29) were the most sensitive to the presence of 0.4-in.-diam stings. The 0.4-in.-diam straight sting had the greater effect of the two stings on measured aerodynamic coefficients of the M-117.

In general, the effect of the presence of the stings on any store was smaller than the effect of modifying the base geometry.

4.3 EFFECTS OF ANGULAR AND TRANSLATIONAL STORE POSITIONING

Effects of store positioning were investigated because minor alignment errors are known to occur during routine tests due to uncorrectable store support and parent sting deflections. Effects of store positioning on carriage-position airloads were evaluated using the CTS technique.

Figures 34 through 37 present the aerodynamic coefficient data for the BLU-1C/B store showing variations with distance from the carriage position (Fig. 34), pitch attitude relative to carriage position (Fig. 35), yaw attitude relative to carriage position (Fig. 36), and aircraft yaw angle (Fig. 37). The translational and angular store positioning and aircraft yaw angle may have significant effects on the store aerodynamic coefficient data, depending on the store location on the MER or wing configuration loading. Of the angular misalignments investigated, the store and aircraft yaw appear to produce the more significant gradients in carriage-position aerodynamic coefficients.

4.4 COMPARISON OF DATA OBTAINED BY THE CTS TECHNIQUE AND RIGID LOADS TECHNIQUE

Figures 38 through 43 show the comparison of CTS and rigid loads technique measurements of the carriage-position aerodynamic coefficients for the M-117 (Figs. 38 and 39, unfinned BLU-1C/B (Figs. 40 and 41), and finned BLU-1C/B (Figs. 42 and 43). The data indicate significant differences in aerodynamic coefficients for the M-117 and finned BLU-1C/B stores. It was anticipated that the data obtained from the two techniques would be in better agreement because the rigid loads technique used stores and stings which simulated the models used in the CTS technique. A possible explanation for the disagreement is store carriage-position misalignment produced by the CTS technique. Repeat test runs of aerodynamic coefficient data for the finned BLU-1C/B using the CTS technique and the modified finned BLU-1C/B store, and 0.2- and 0.4-in.-diam stings using the rigid loads technique are presented in Fig. 44. It can be seen that the aerodynamic coefficient data bands are very significant for the CTS technique repeatability when compared to the rigid loads data bands. Therefore, it is very difficult to evaluate the CTS technique because the difference between the two techniques is no greater than the repeatability of the CTS technique.

5.0 CONCLUSIONS

As a result of this wind tunnel investigation, the following conclusions have been reached:

1. In general, the M-117 carriage-position aerodynamic coefficients are the most sensitive to changes in afterbody geometry, sting interference, store positioning, and MER position. The unfinned BLU-1C/B is the least sensitive.

2. The magnitudes of all effects for any store studied depend on MER station location and are greater at the higher Mach numbers.

3. The store afterbody modification is the most significant with respect to changes in carriage-position aerodynamic coefficients.

4. Measured aerodynamic data for the store in its carriage position are very sensitive to store positioning.

5. The difference between the carriage-position aerodynamic coefficients of the CTS and rigid loads techniques is no greater than the repeatability of the CTS technique.
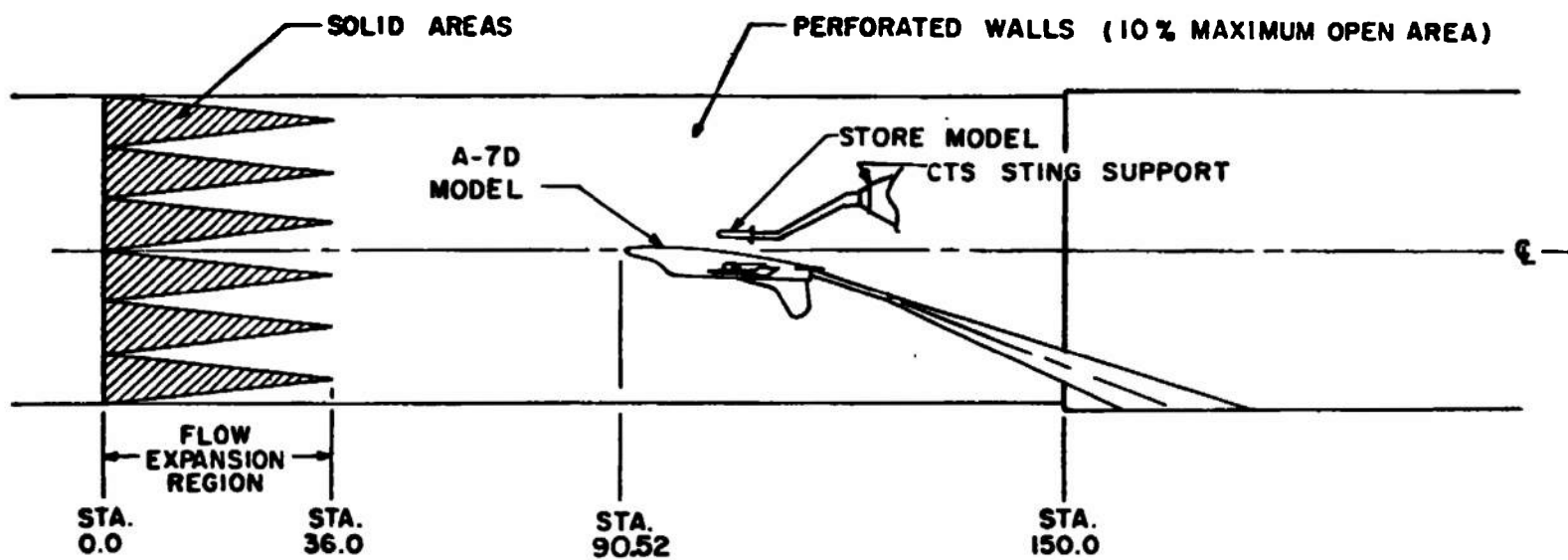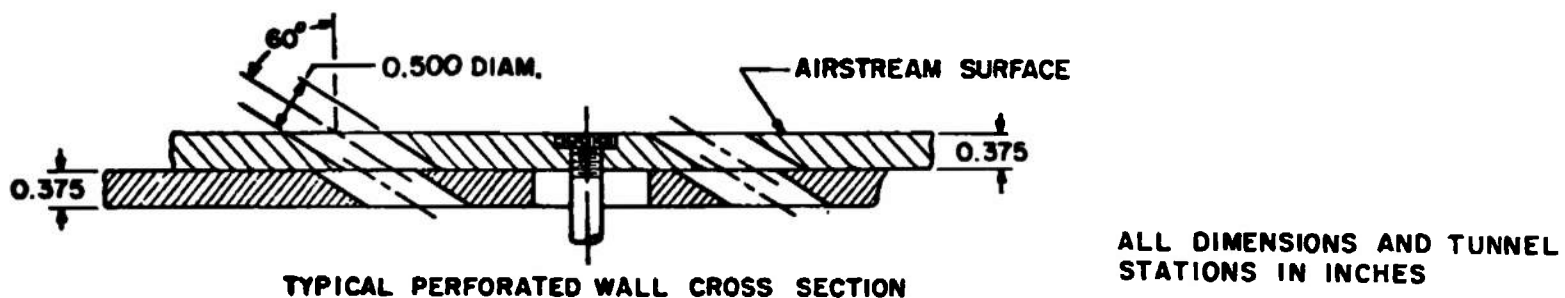
Figure 1. Schematic of the tunnel test section showing model location and CTS model support.

TUNNEL ℄

BLU-I C/B UNFINNED
MER/CENTER PYLON

A-7D
WITH HORIZONTAL TAIL REMOVED

TUNNEL FLOOR
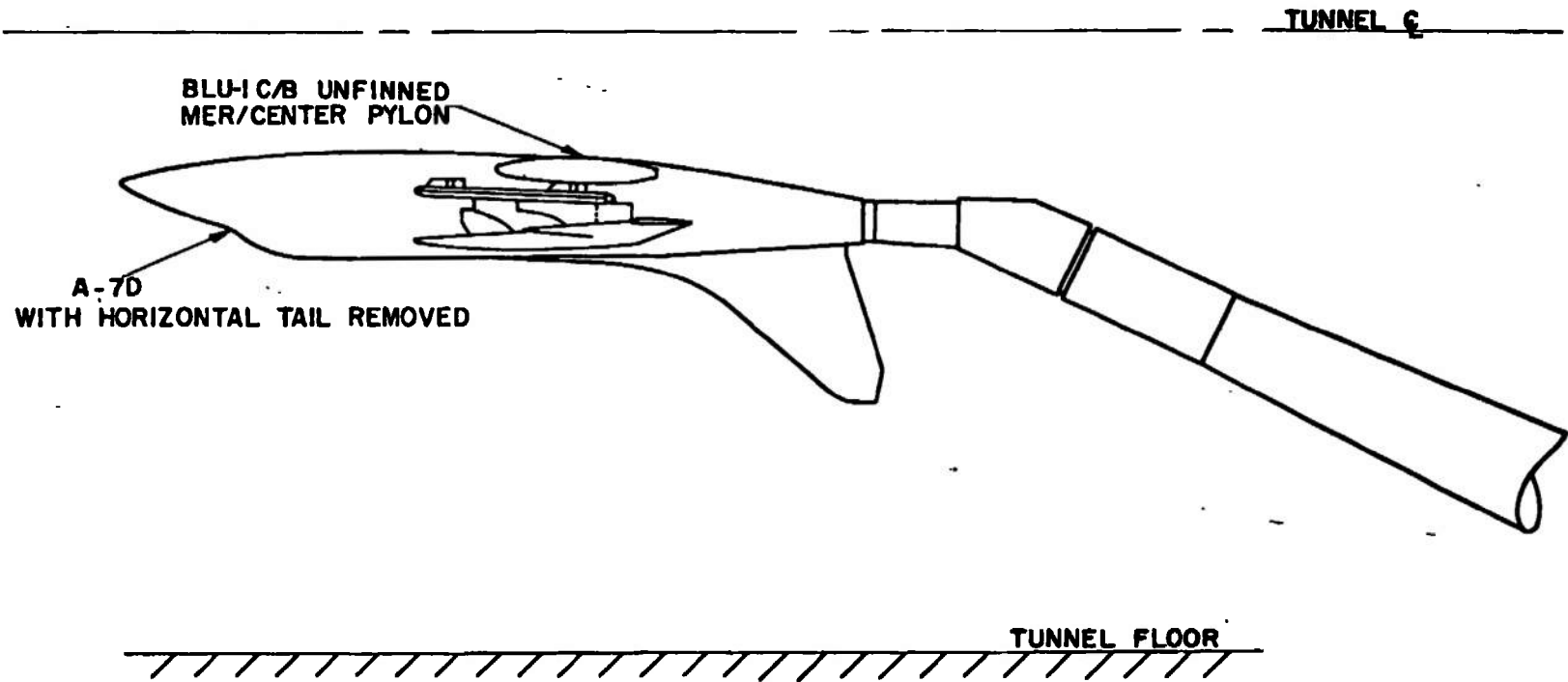
Figure 2. Schematic of the A-7D showing the BLU-1C/B supported by the aircraft.

BL 0.000

BL-3.060

BL-4.860

BL-6.831

BL-11.619

ALL DIMENSIONS IN INCHES

MS 0.000

13.304 13.758 15.468

28.805
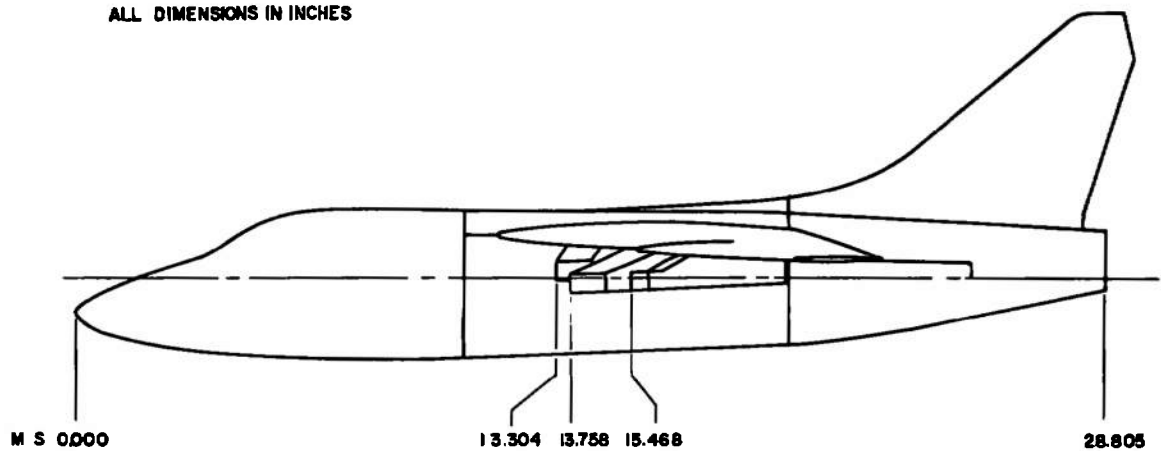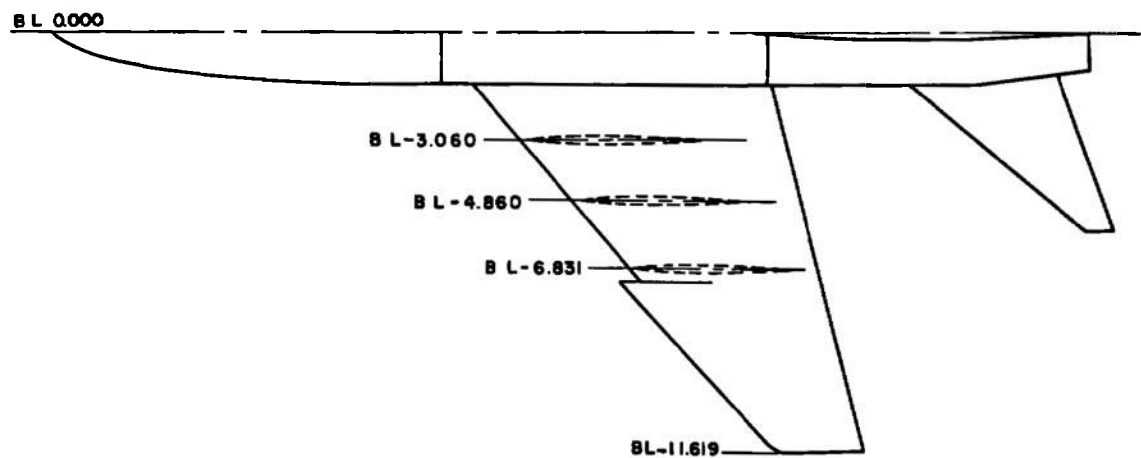
Figure 3. Sketch of the A-7D aircraft model.

17

FWD 30-IN. SUSPENSION POINT
FWD 14-IN. SUSPENSION POINT

W L 0.0 (Ref.)

3°

ALL DIMENSIONS IN INCHES
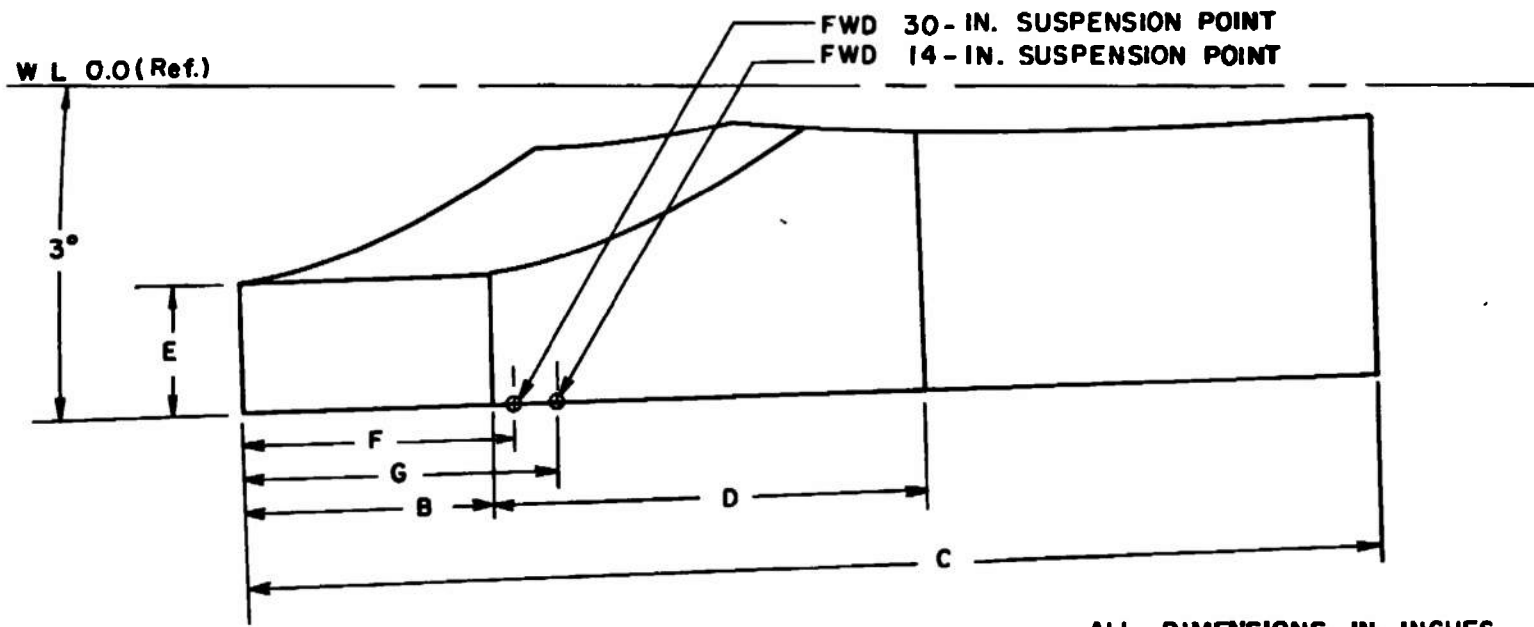
	INBOARD	CENTER	OUTBOARD
B	1.030	1.030	0.515
C	4.580	4.850	4.437
D	1.630	1.905	2.008
E	0.575	0.575	0.513
F	0.950	0.950	0.750
G	1.350	1.350	1.150

Figure 4. Details and dimensions of the A-7D wing pylon models.

ALL DIMENSIONS IN INCHES
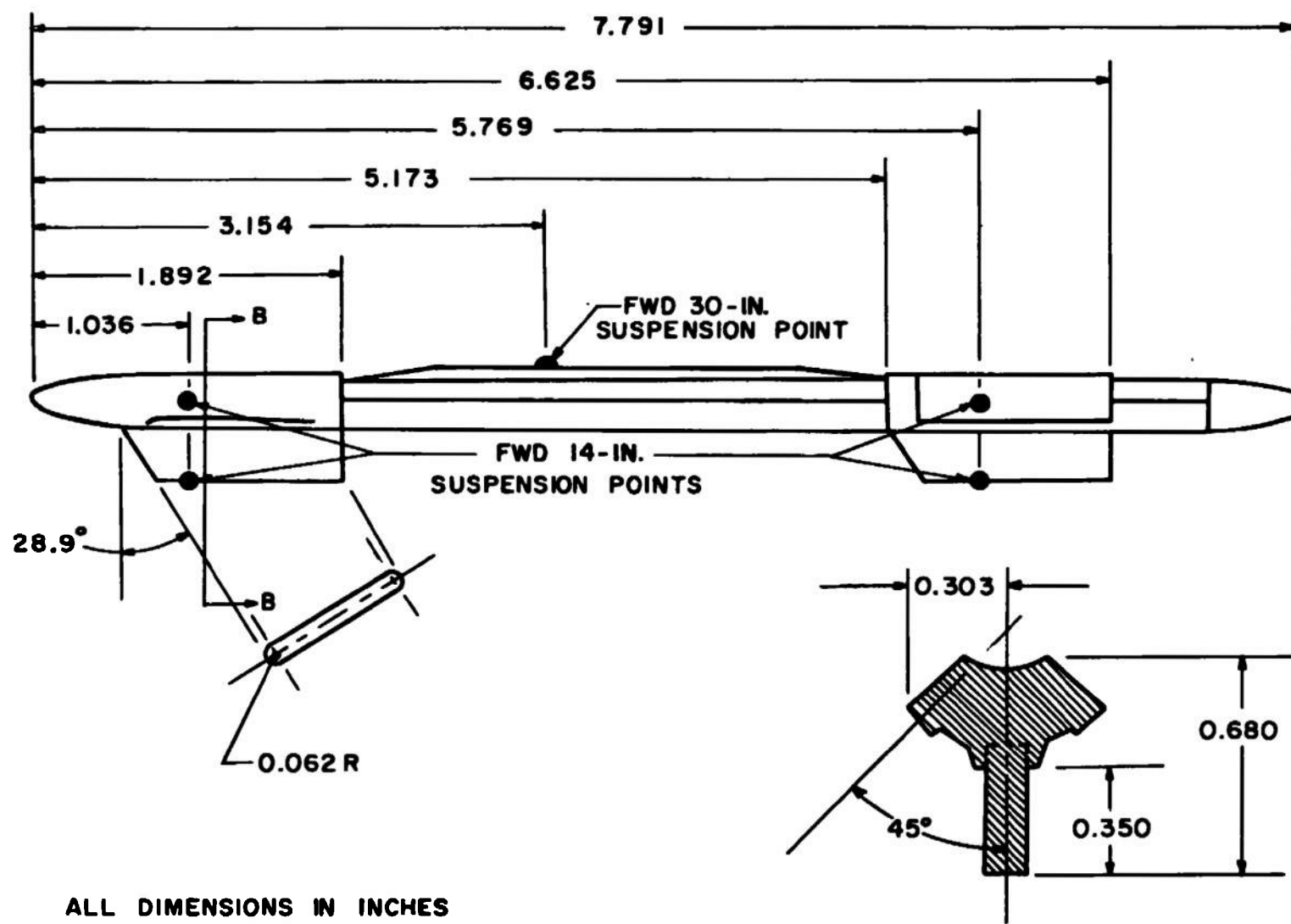
Figure 5. Details and dimensions of the MER model.

a. Basic tail geometry

b. Modified tail geometry
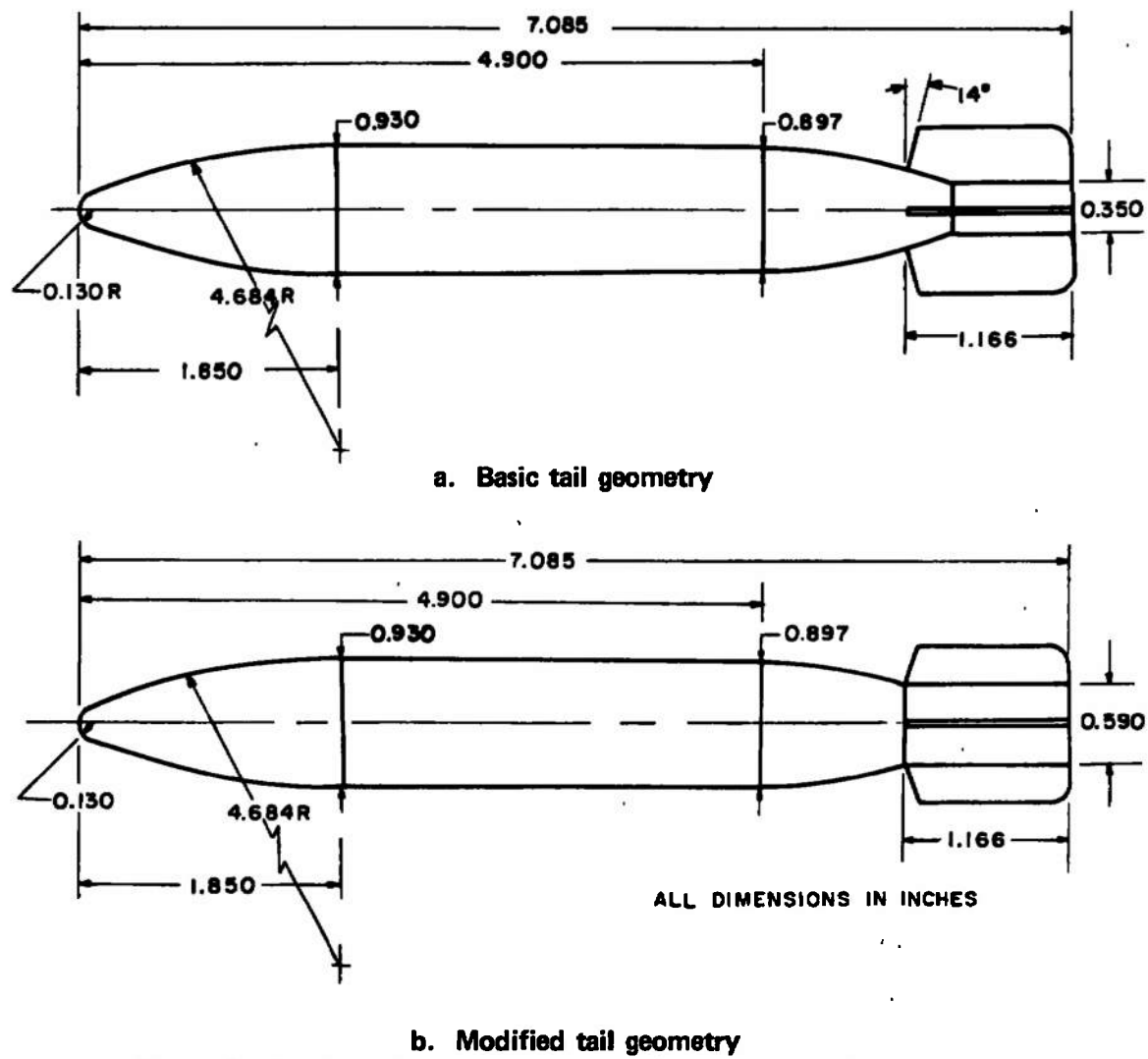
Figure 6. Details and dimensions of the finned BLU-1C/B model with basic and modified tail geometry.
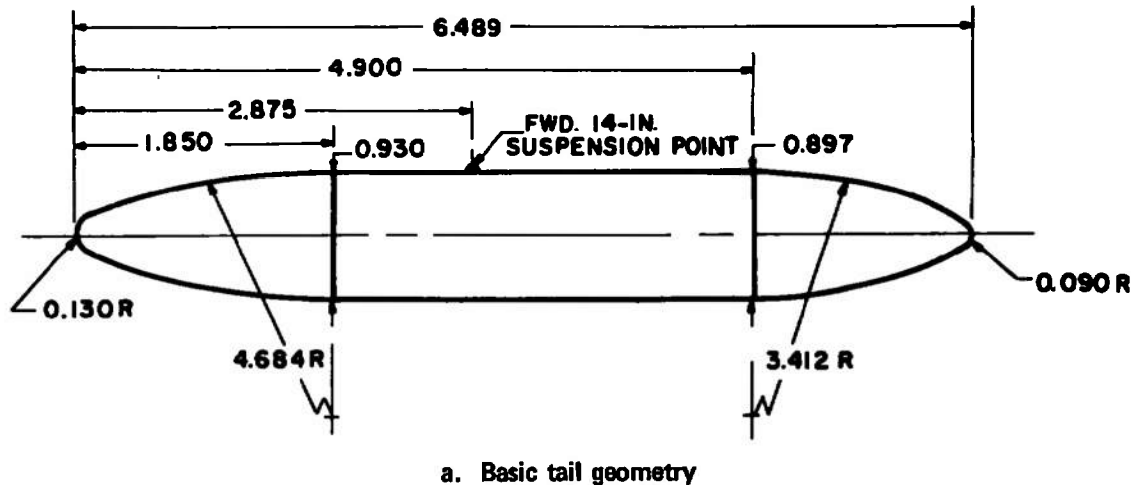
a. Basic tail geometry

ALL DIMENSIONS IN INCHES
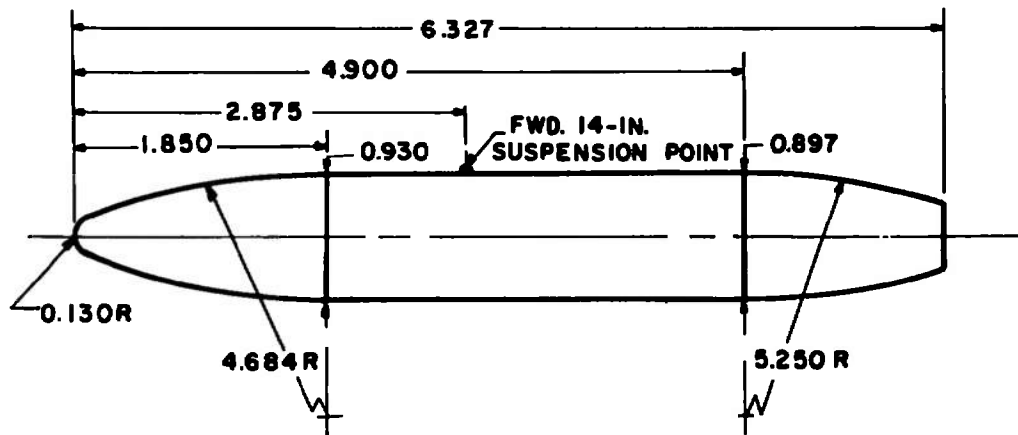
b. Modified tail

Figure 7. Details and dimensions of the unfinned BLU-1C/B with basic and modified tail geometry.

a. Basic geometry

b. Modified tail geometry
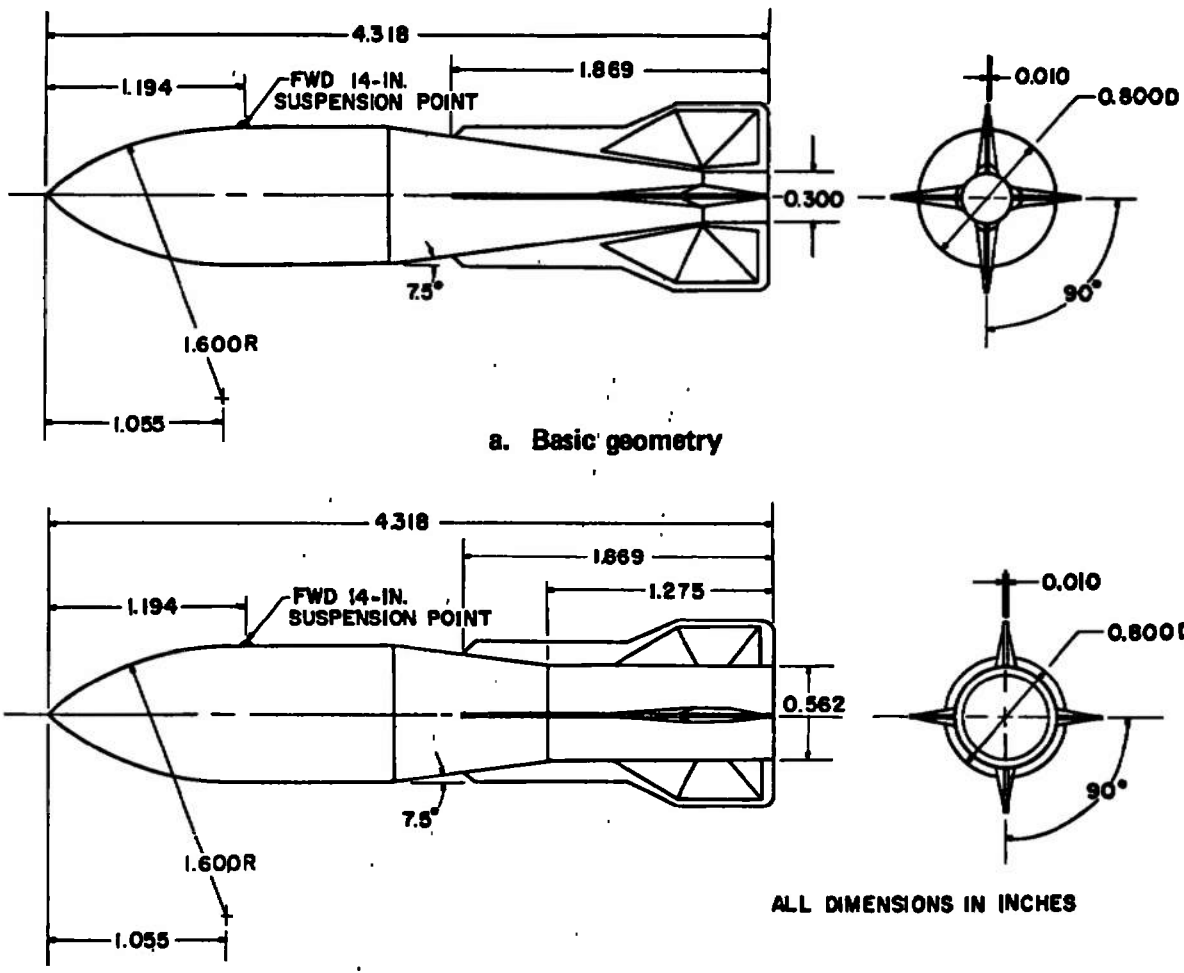
Figure 8. Details and dimensions of the M-117 with basic and
modified tail geometry.

10°   1.000 DIAM

0.400 DIAM

30°

0.500

9.500

29.000

3.755 RIGHT WING
4.361 LEFT WING
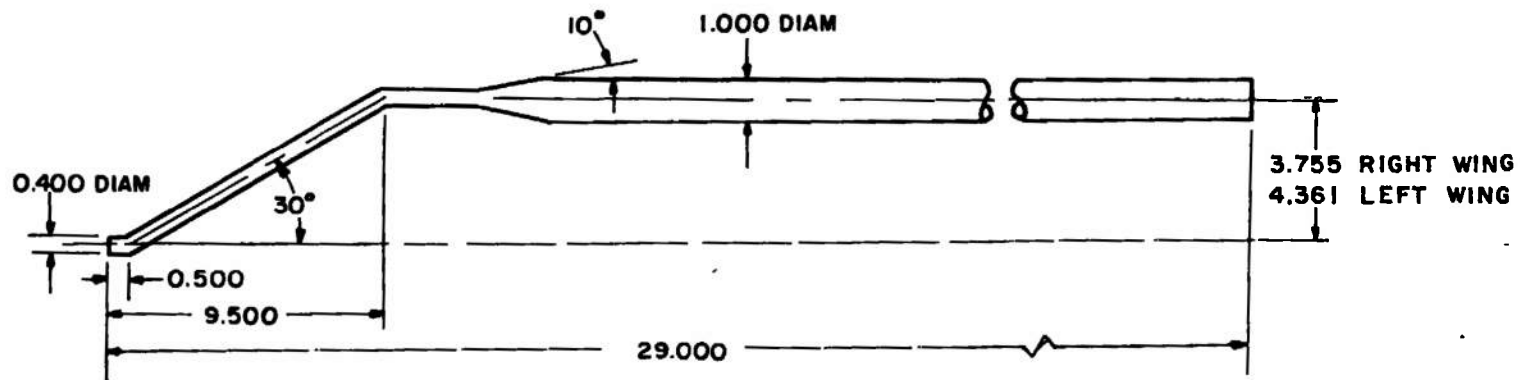
ALL DIMENSIONS IN INCHES

a. 0.4-in.-diam bent dummy sting

0.400 DIAM
0.200 DIAM

10°

1.000 DIAM

8.400

29.000

3.755 RIGHT WING
4.361 LEFT WING
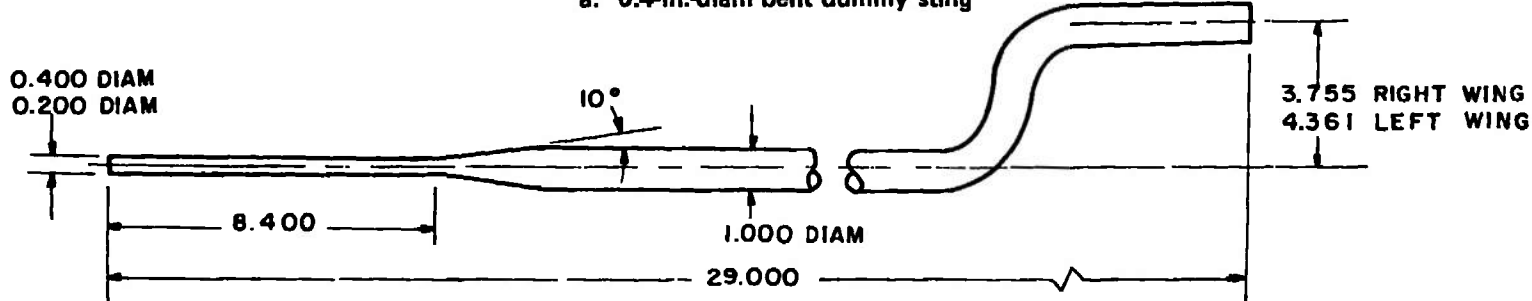
b. 0.2- and 0.4-in.-diam straight dummy sting

Figure 9. Details and dimensions of the 0.4-in.-diam bent dummy sting and 0.2- and 0.4-in.-diam
straight dummy sting.
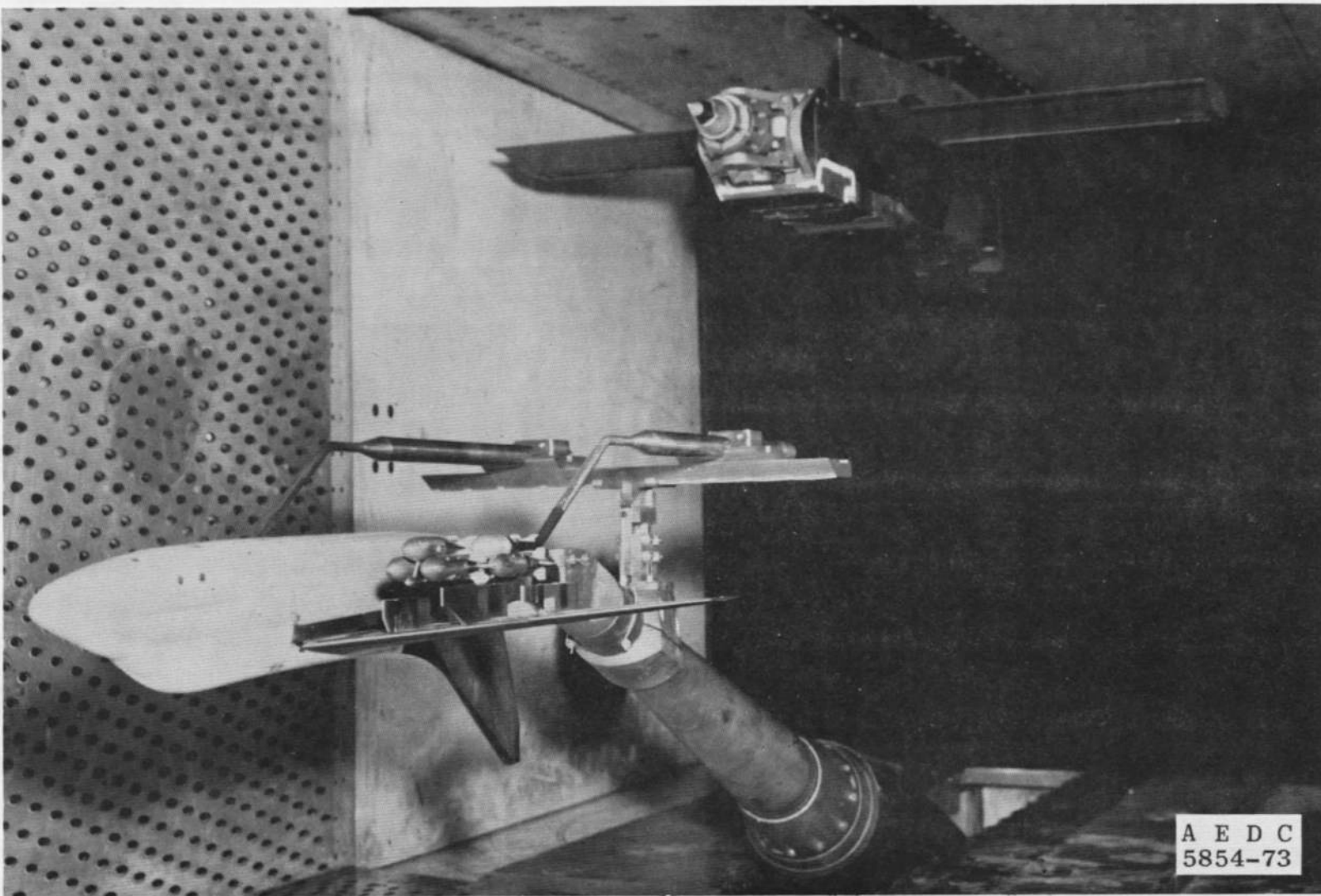
Figure 10. Tunnel installation photograph showing A-7D aircraft, 0.2-in.-diam dummy bent sting, and M-117 stores.

AEDC
6009-73
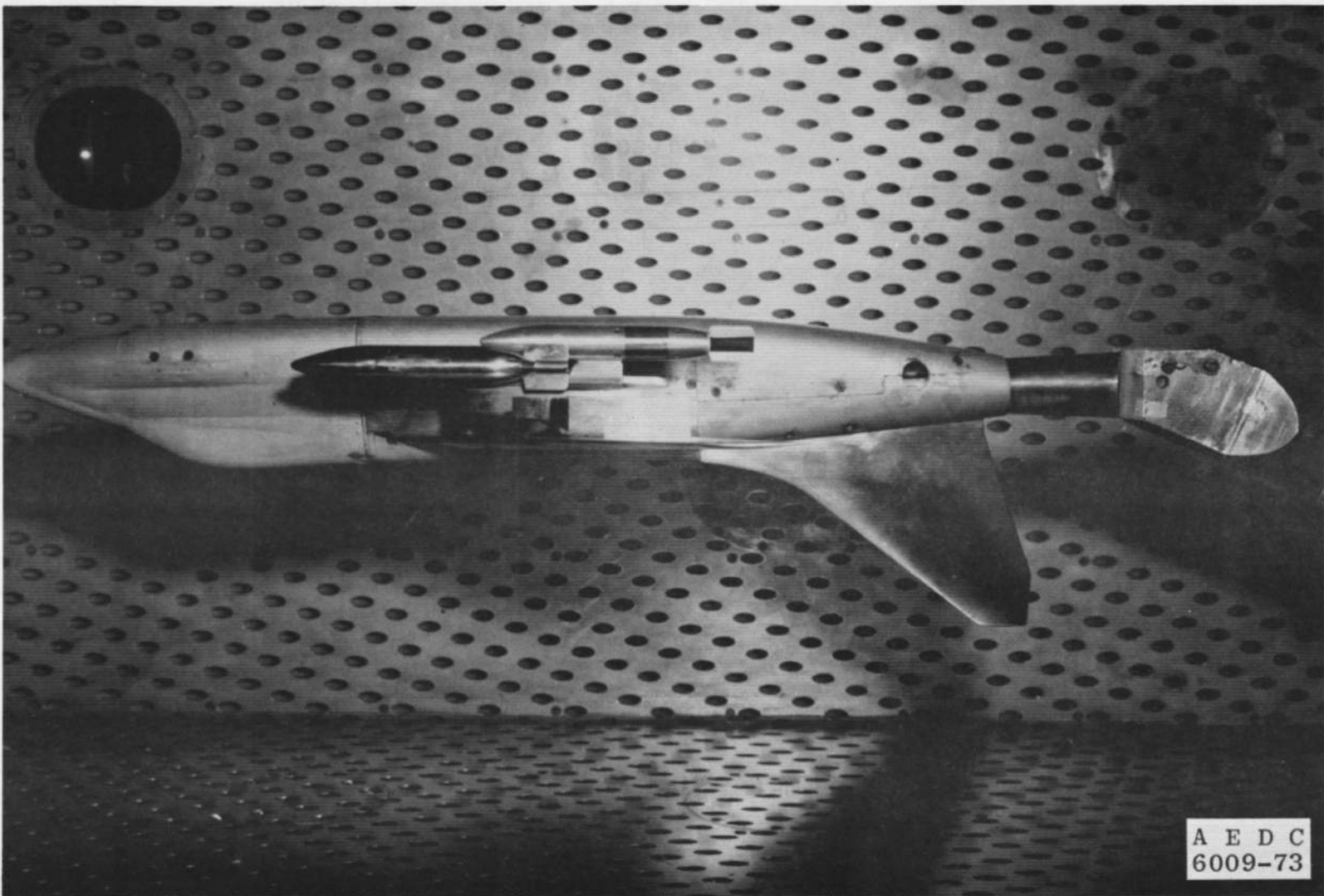
Figure 11. Tunnel installation photograph showing A-7D aircraft and unfinned BLU-1C/B stores.
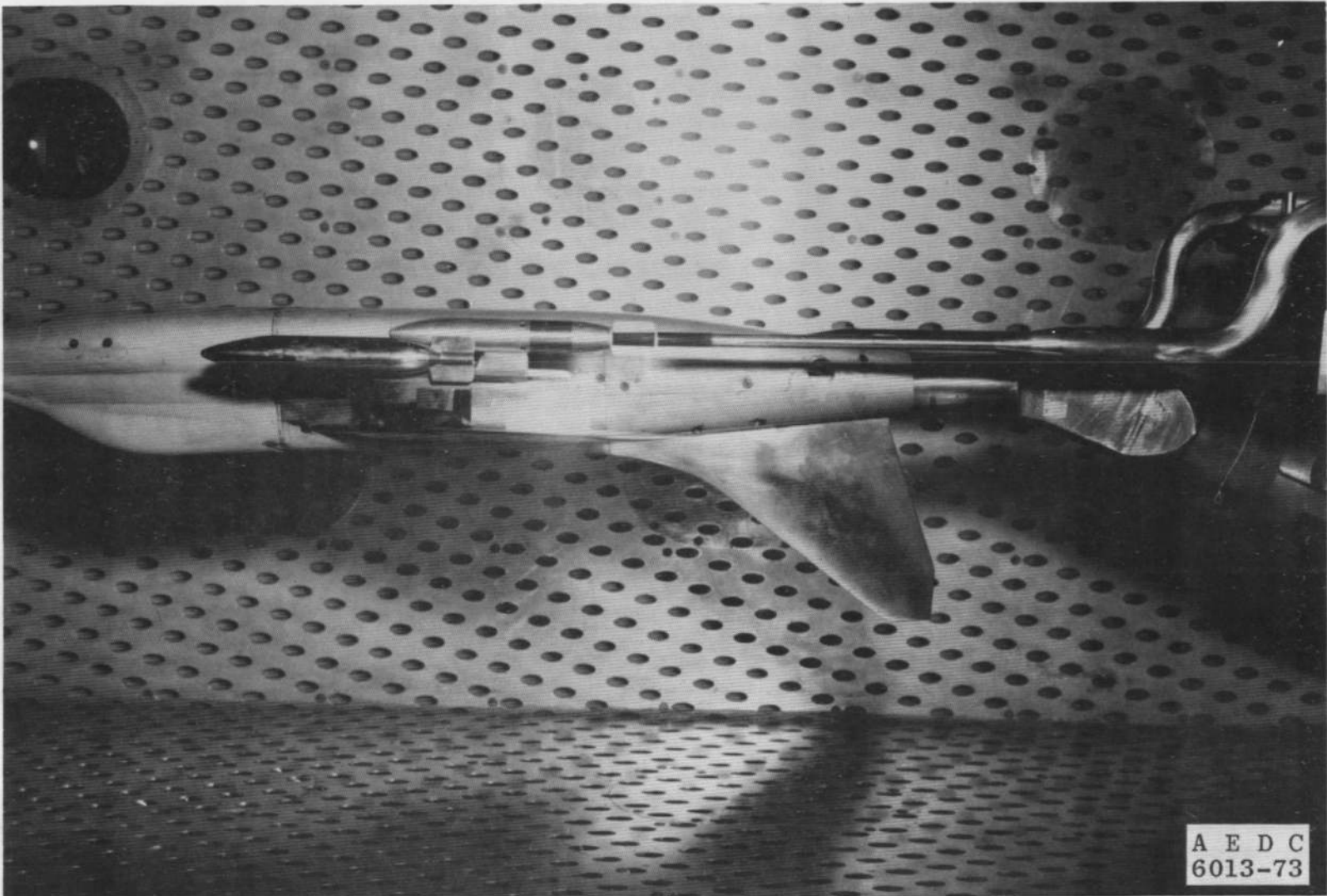
Figure 12. Tunnel installation photograph showing A-7D aircraft, finned BLU-1C/B store, and 0.4-in.-diam straight dummy sting.

CENTERLINE
PYLON LEADING
EDGE

2.204

1.839

4.733

BALANCE
(TYP)

ALL DIMENSIONS IN INCHES
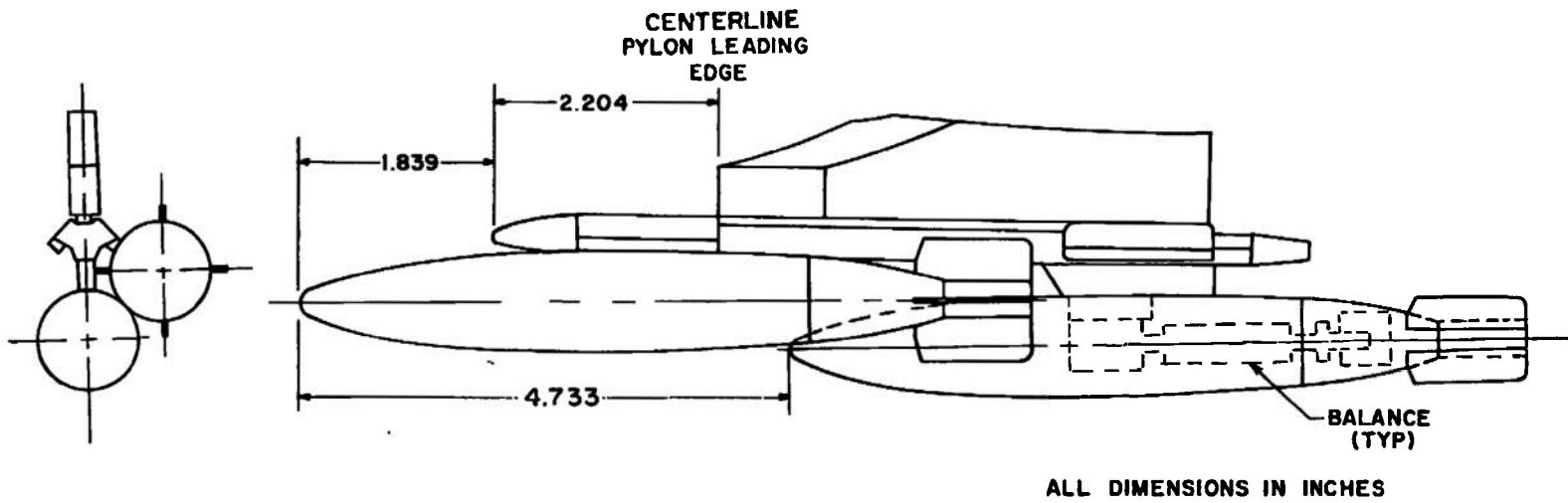
Figure 13. Mounting details of the instrumented finned or unfinned BLU-1C/B store on MER rack.

CENTERLINE
PYLON LEADING
EDGE

2.204

0.158

0.050

ADAPTER
(TYP)

BALANCE
(TYP)

4.730

ALL DIMENSIONS IN INCHES
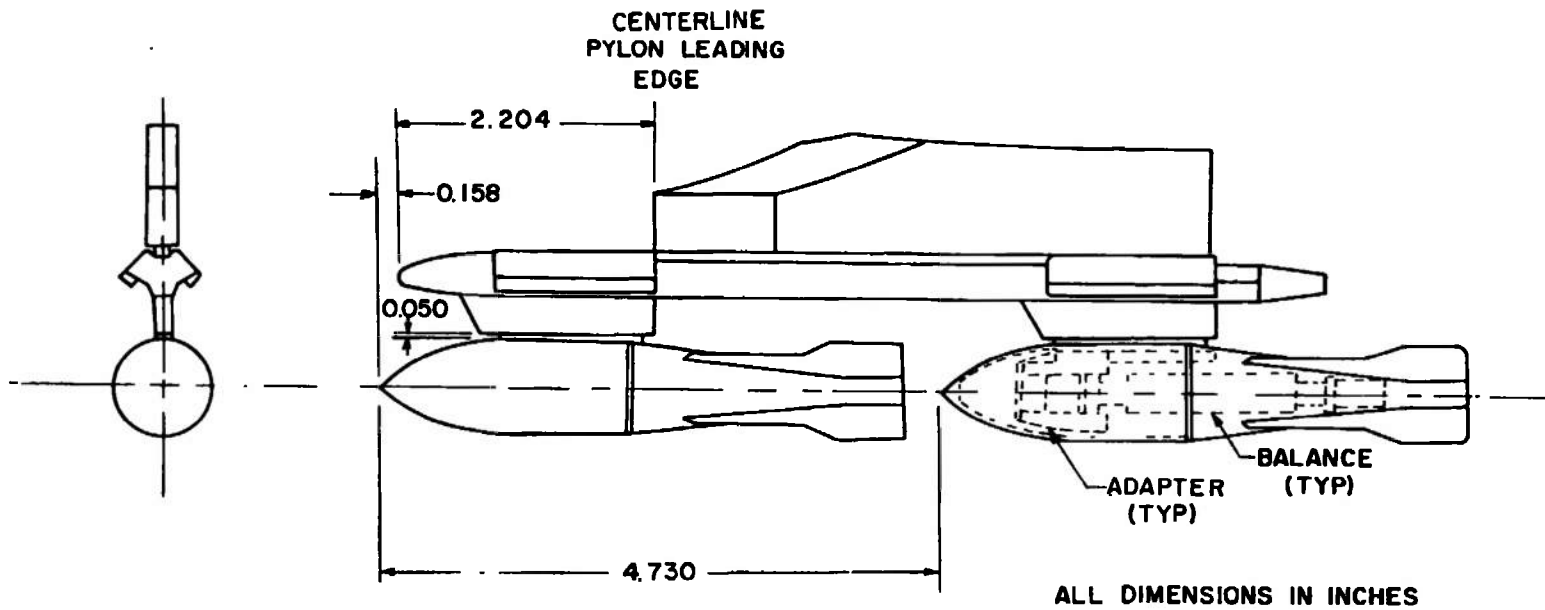
Figure 14. Mounting details of the instrumented M-117GP store on MER rack.

UPSTREAM

MER
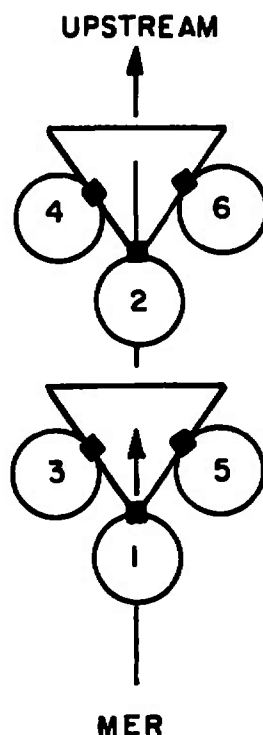
NOTE: The square indicates the orientation of the suspension lugs

TYPE RACK	STATION	ROLL ORIENTATION, deg
MER	1	0
	2	0
	3	45
	4	45
	5	-45
	6	-45

Figure 15. Schematic of the MER store stations and orientations.
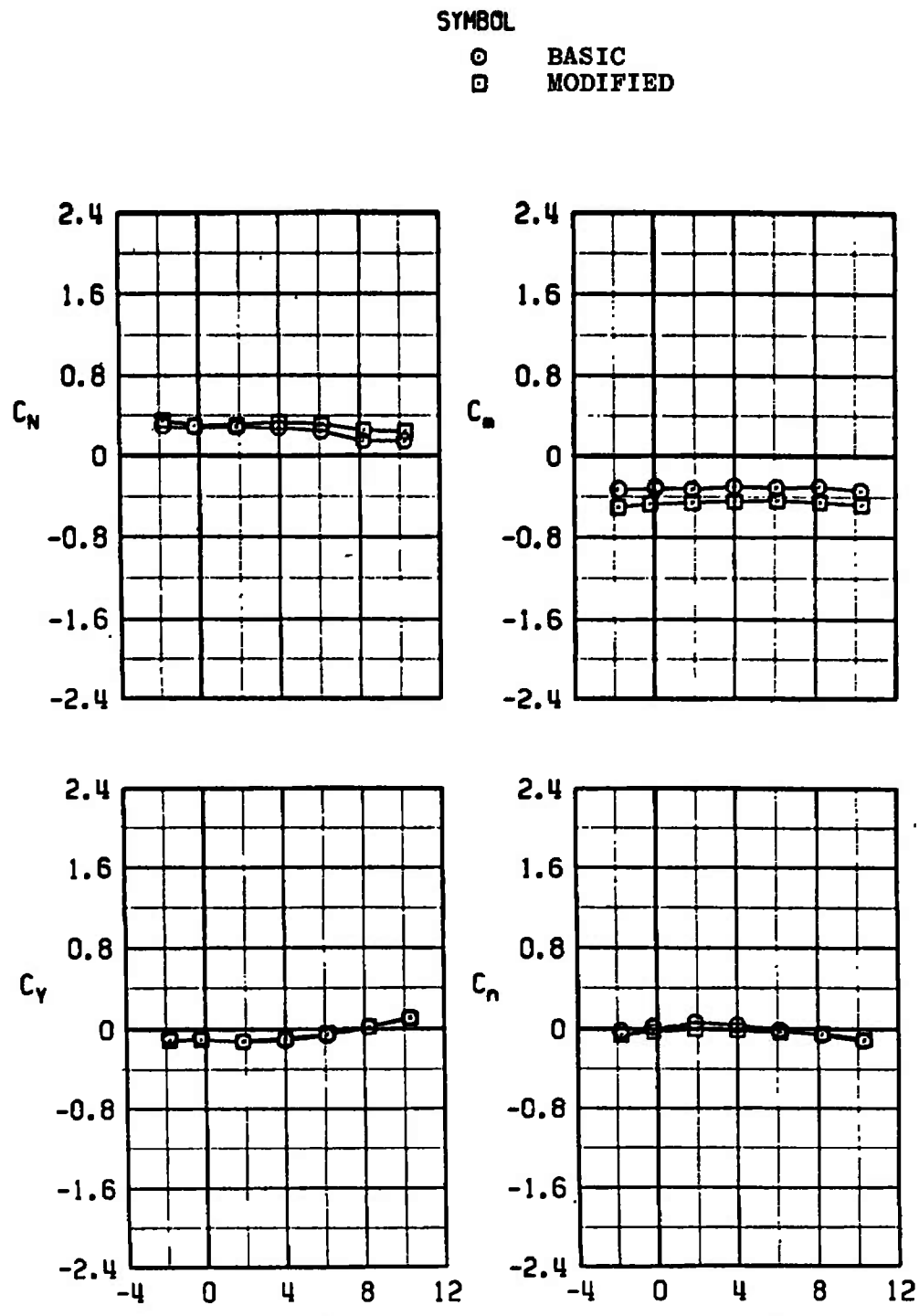
a. $M_\infty = 0.70$

Figure 16. Comparison of basic and modified M-117 store carriage-position
aerodynamic coefficients, configuration 1R.

SYMBOL
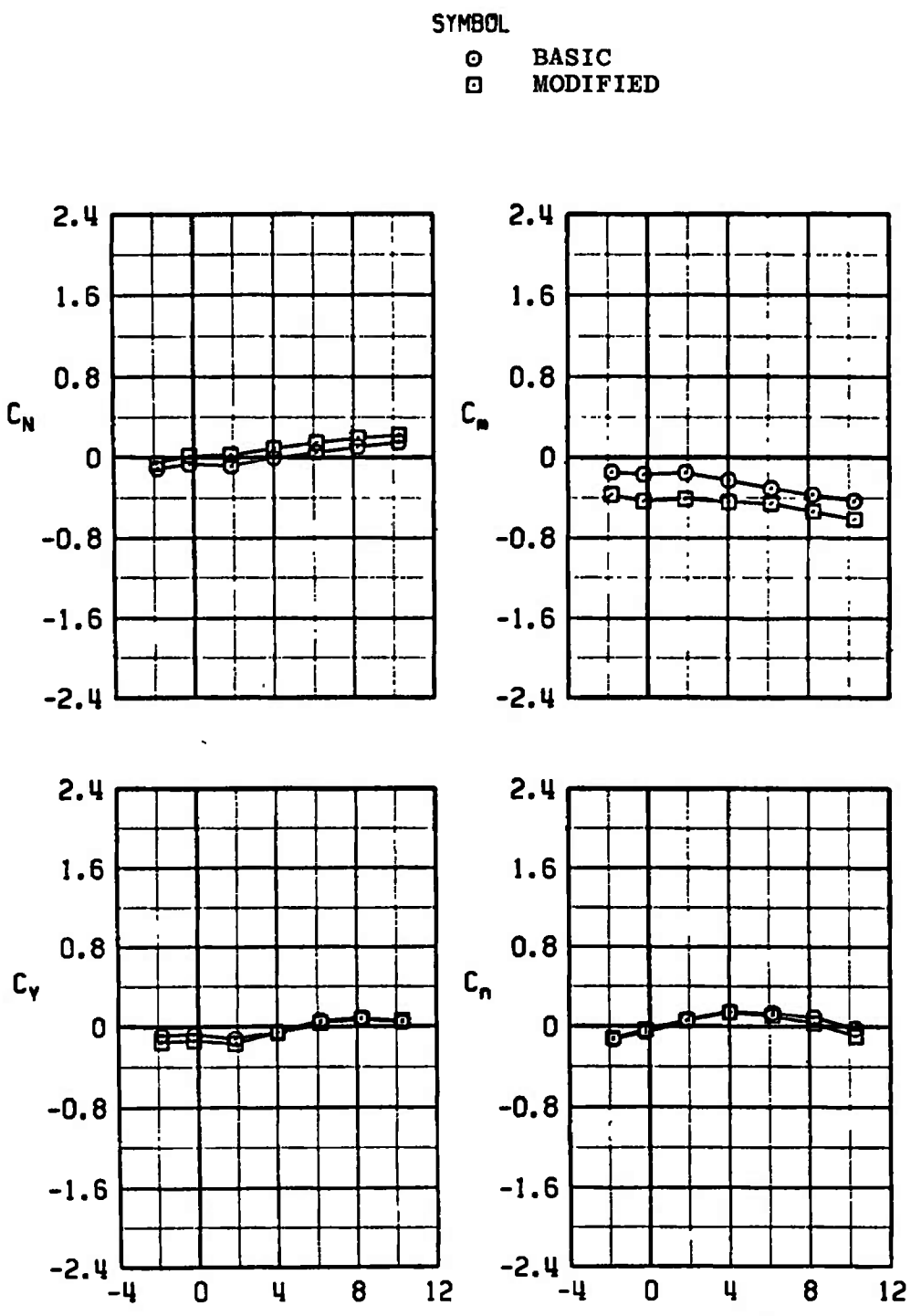
⊙   BASIC
⊡   MODIFIED

b. $M_\infty = 0.90$
Figure 16.   Continued.

SYMBOL

⊙ BASIC
⊡ MODIFIED
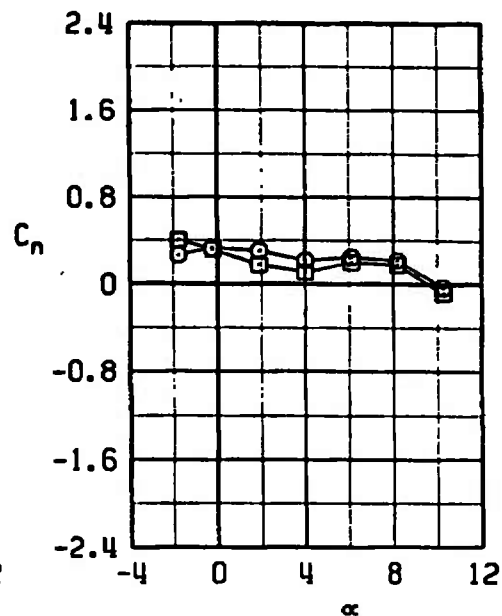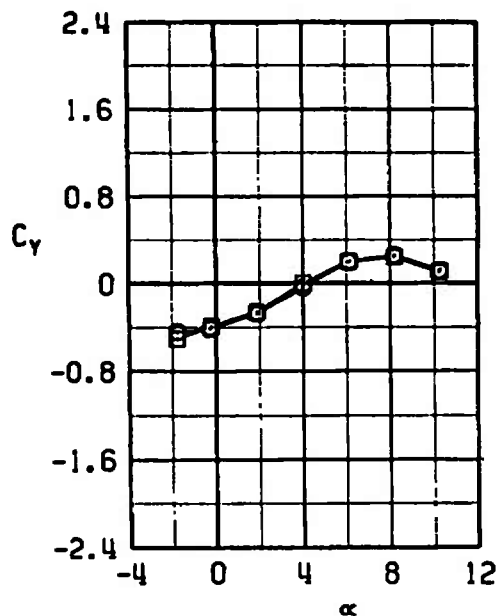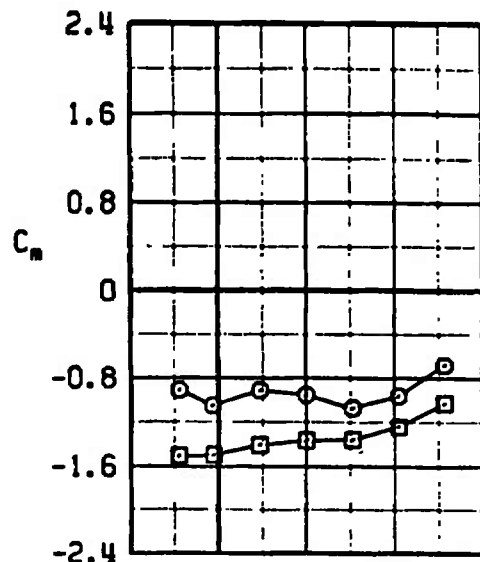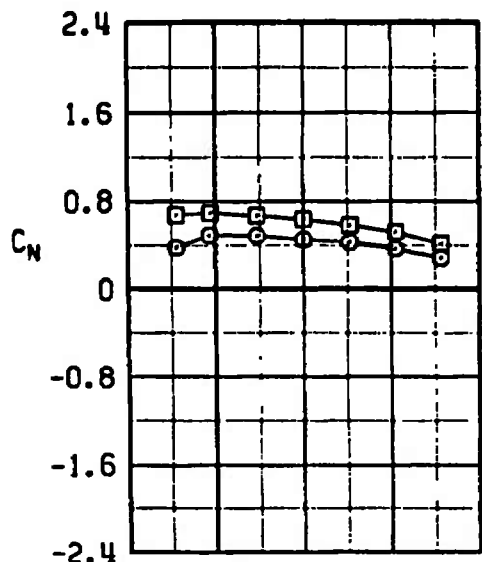
c. M_∞ = 1.05
Figure 16. Concluded.
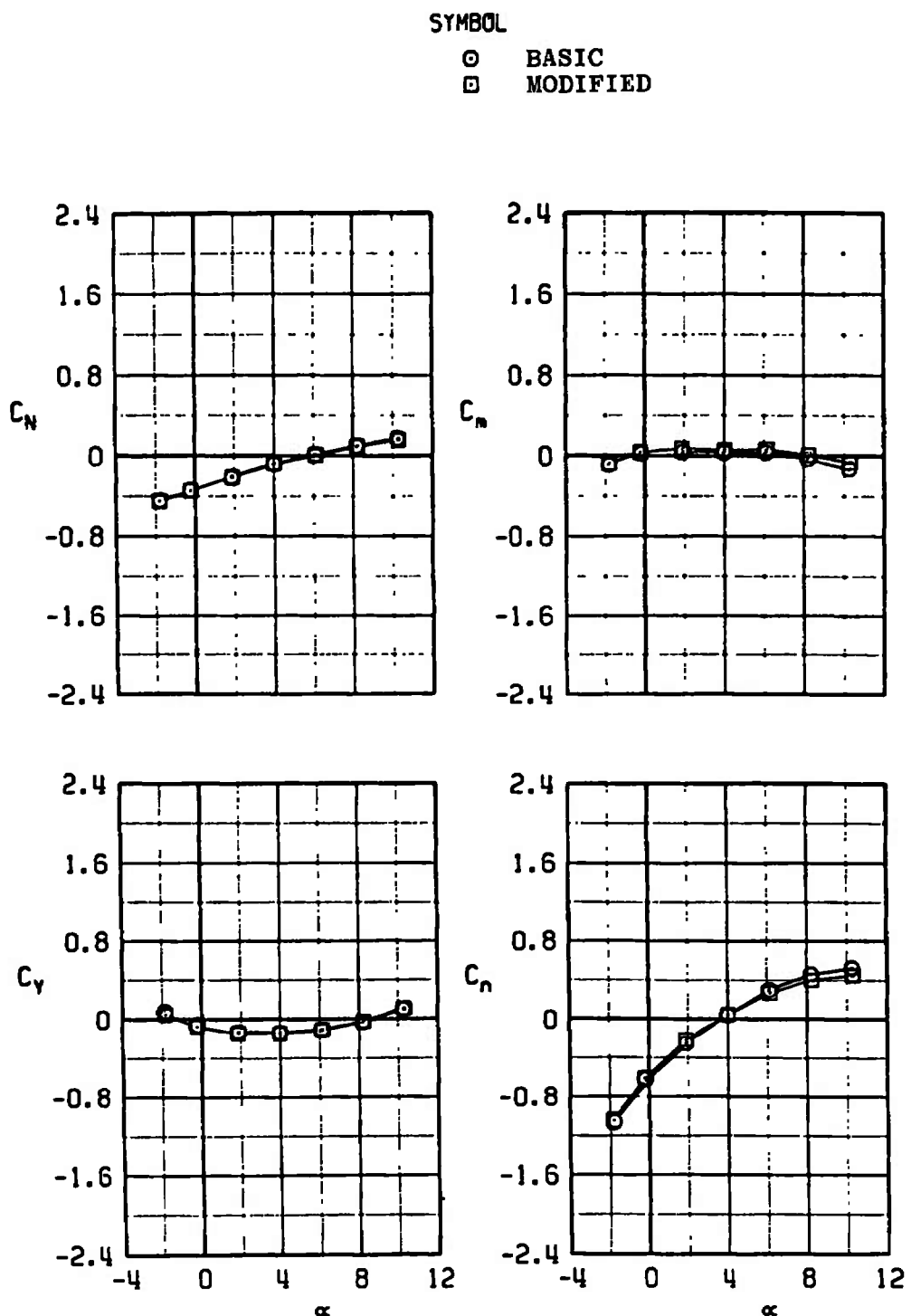
a. $M_\infty = 0.70$

Figure 17. Comparison of basic and modified M-117 store carriage-position aerodynamic coefficients, configuration 1L.

SYMBOL

⊙   BASIC
◻   MODIFIED
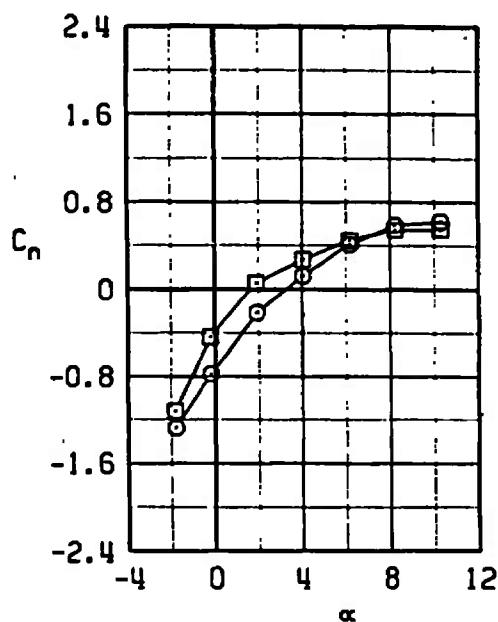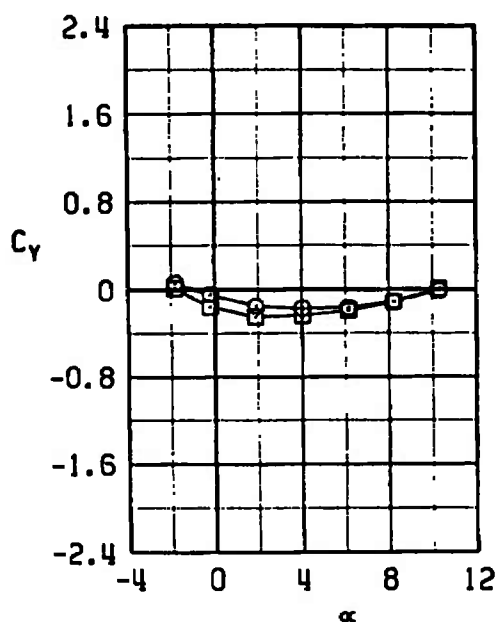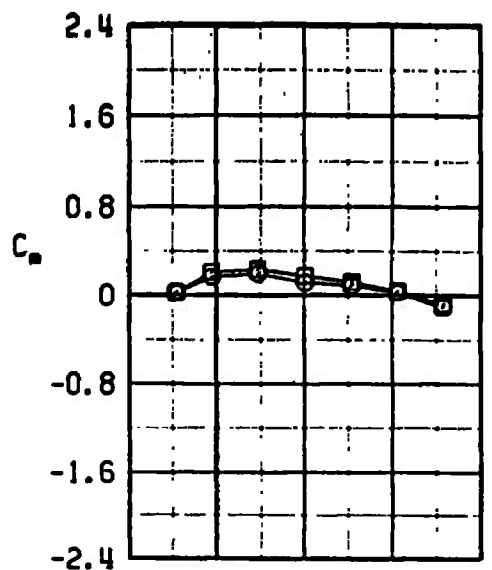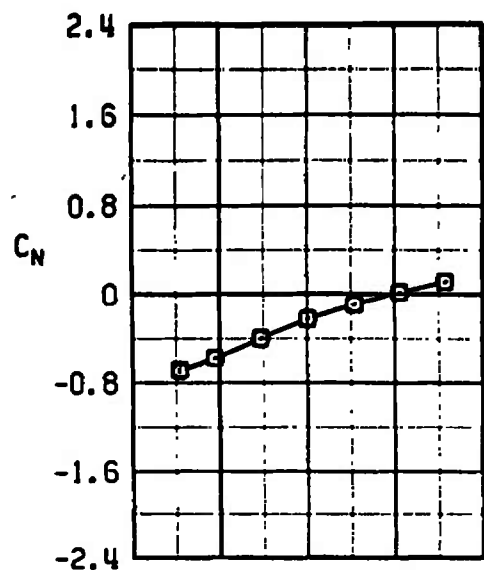
b. $M_\infty = 0.90$
Figure 17. Continued.
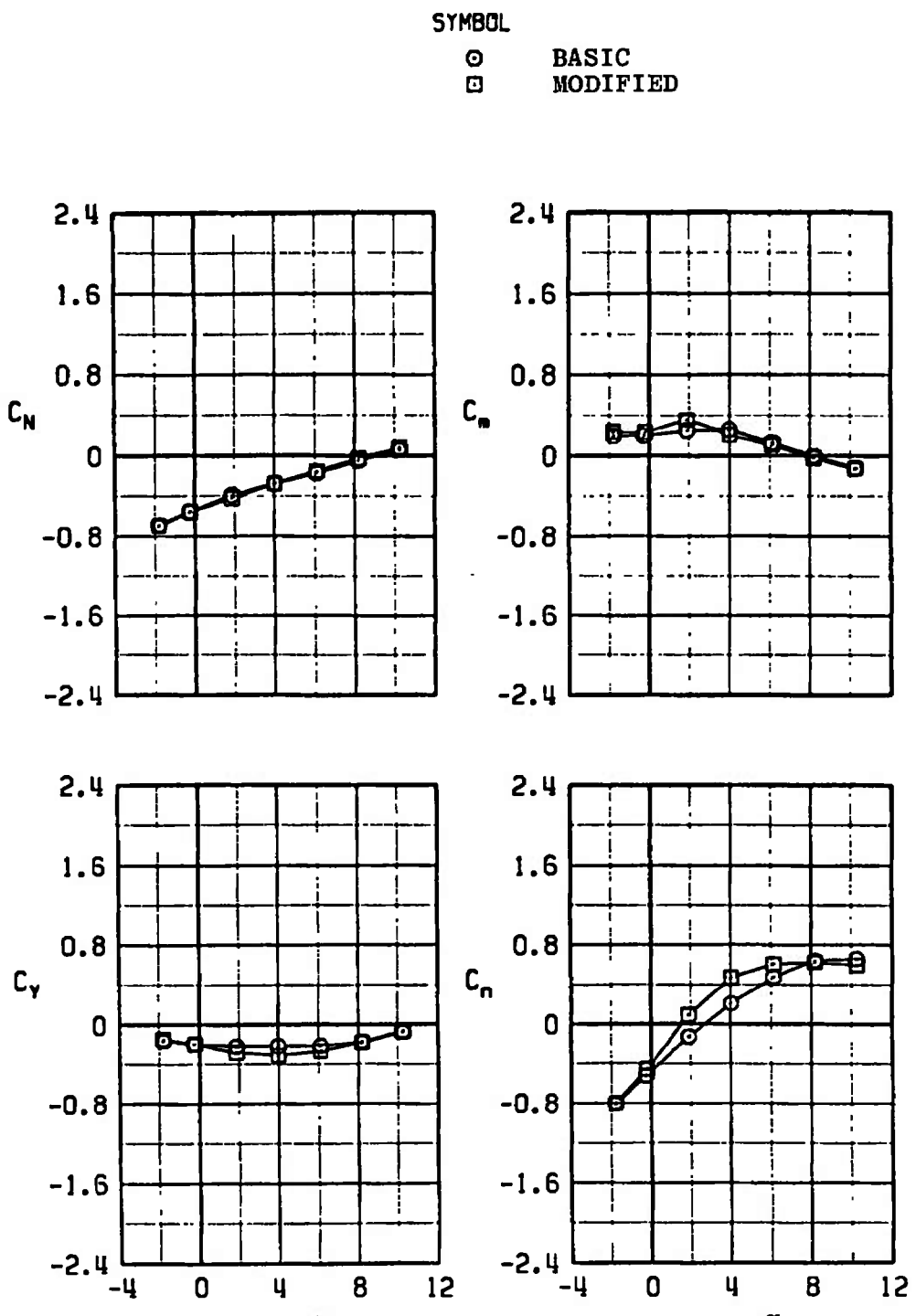
c. $M_\infty = 1.05$
Figure 17. Concluded.
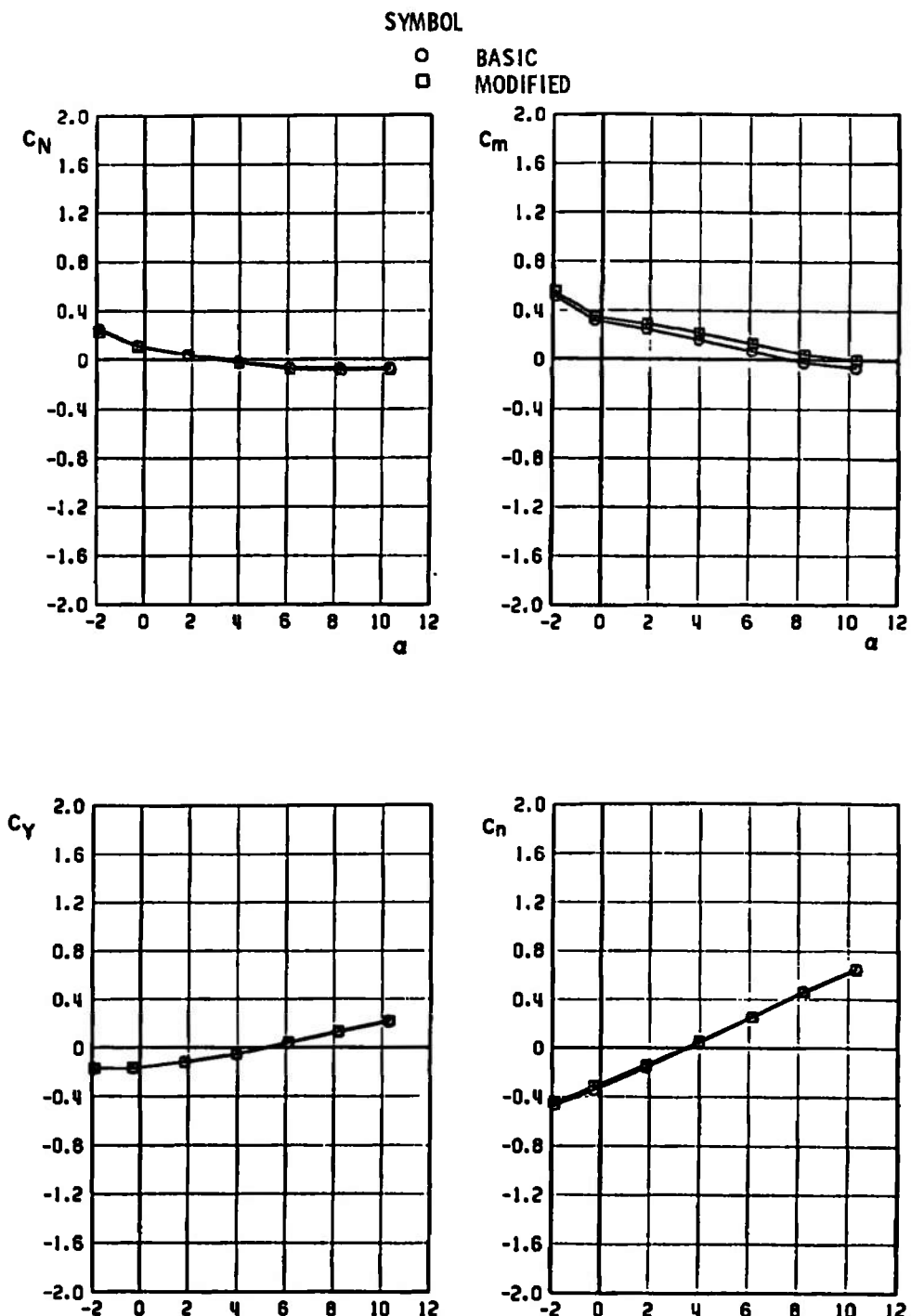
a. $M_\infty = 0.70$

Figure 18. Comparison of basic and modified unfinned BLU-1C/B carriage-position aerodynamic coefficients, configuration 2R.

SYMBOL
○ BASIC
□ MODIFIED
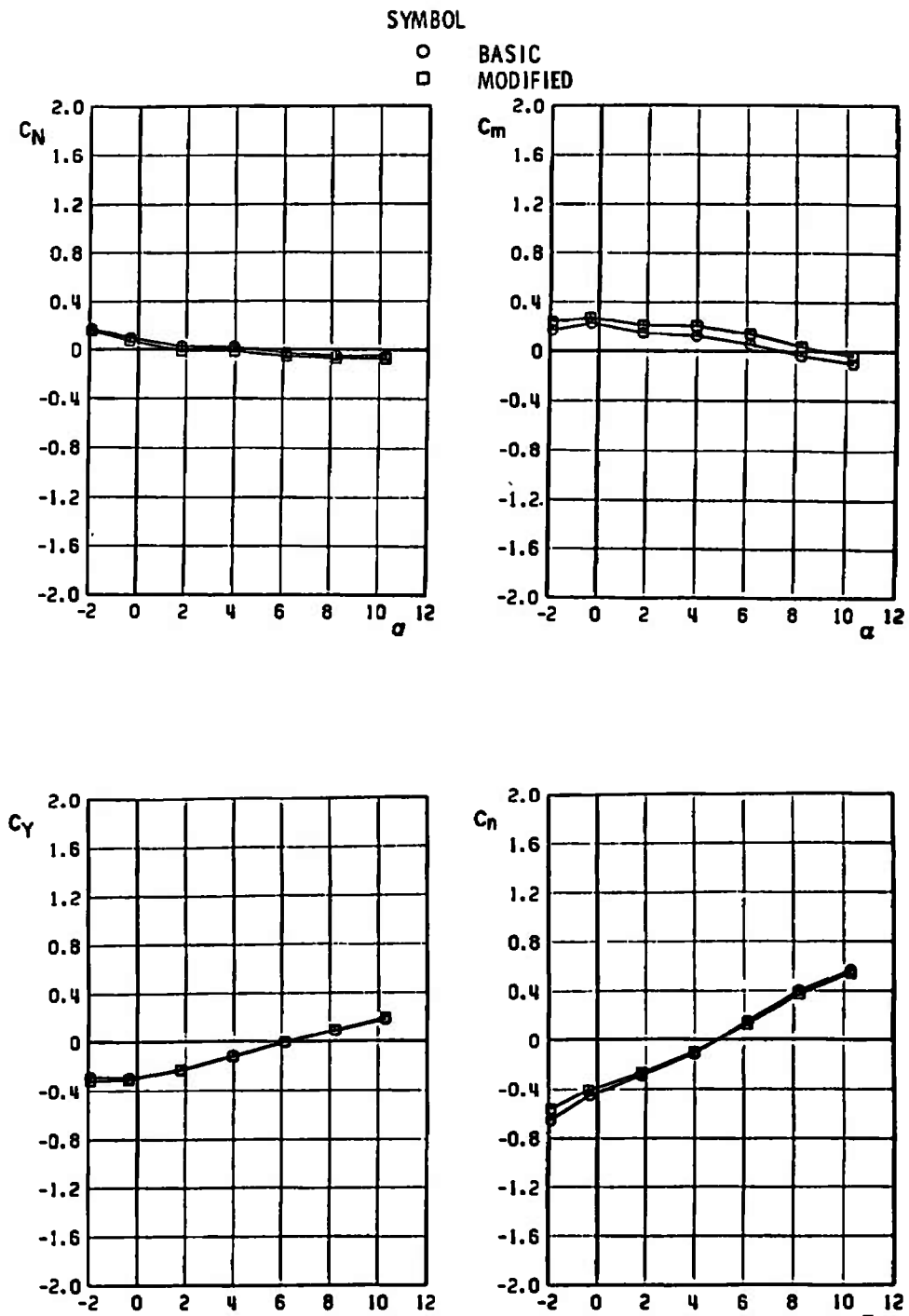
b. $M_\infty = 0.90$
Figure 18. Continued.
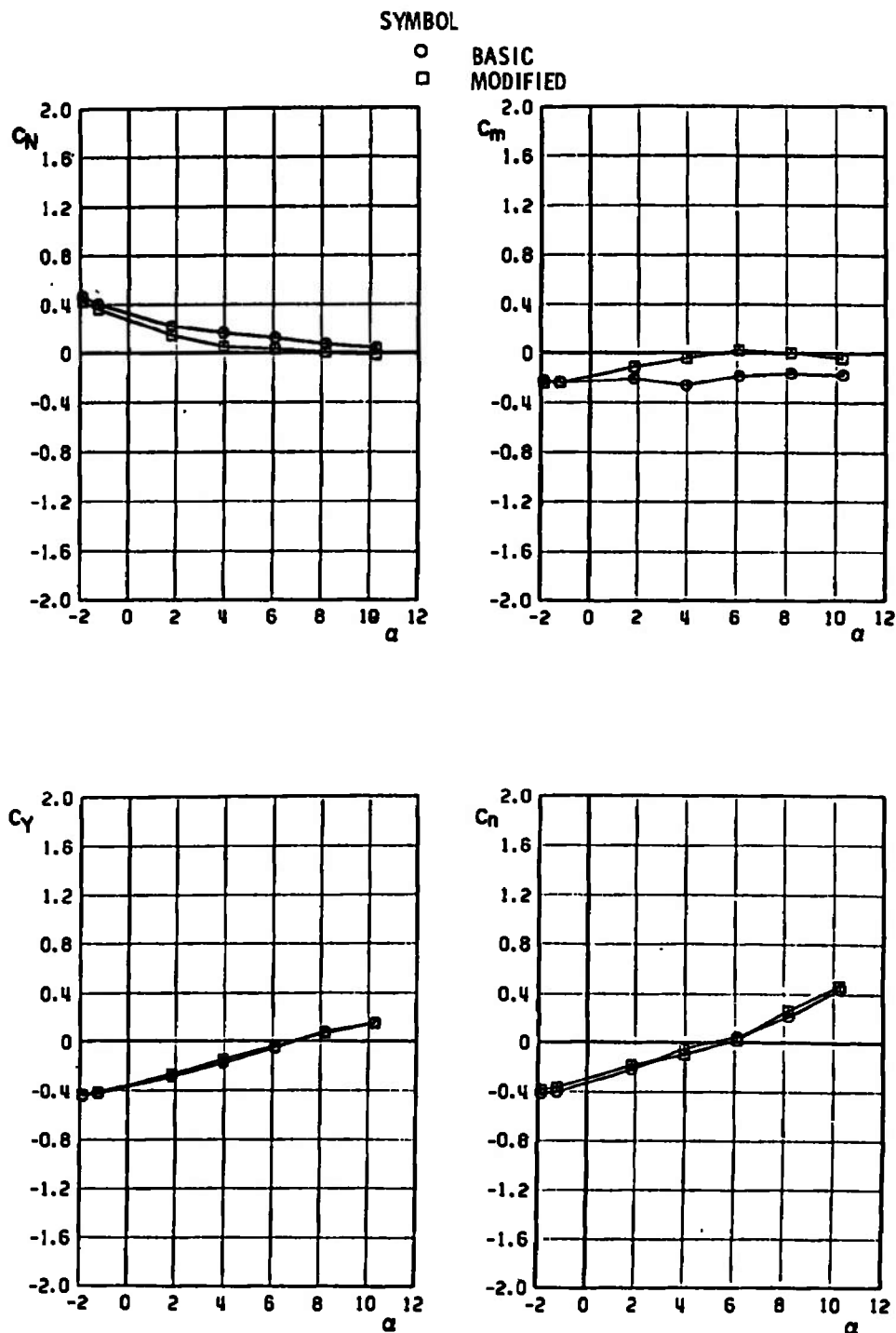
c. $M_\infty = 1.05$
Figure 18. Concluded.
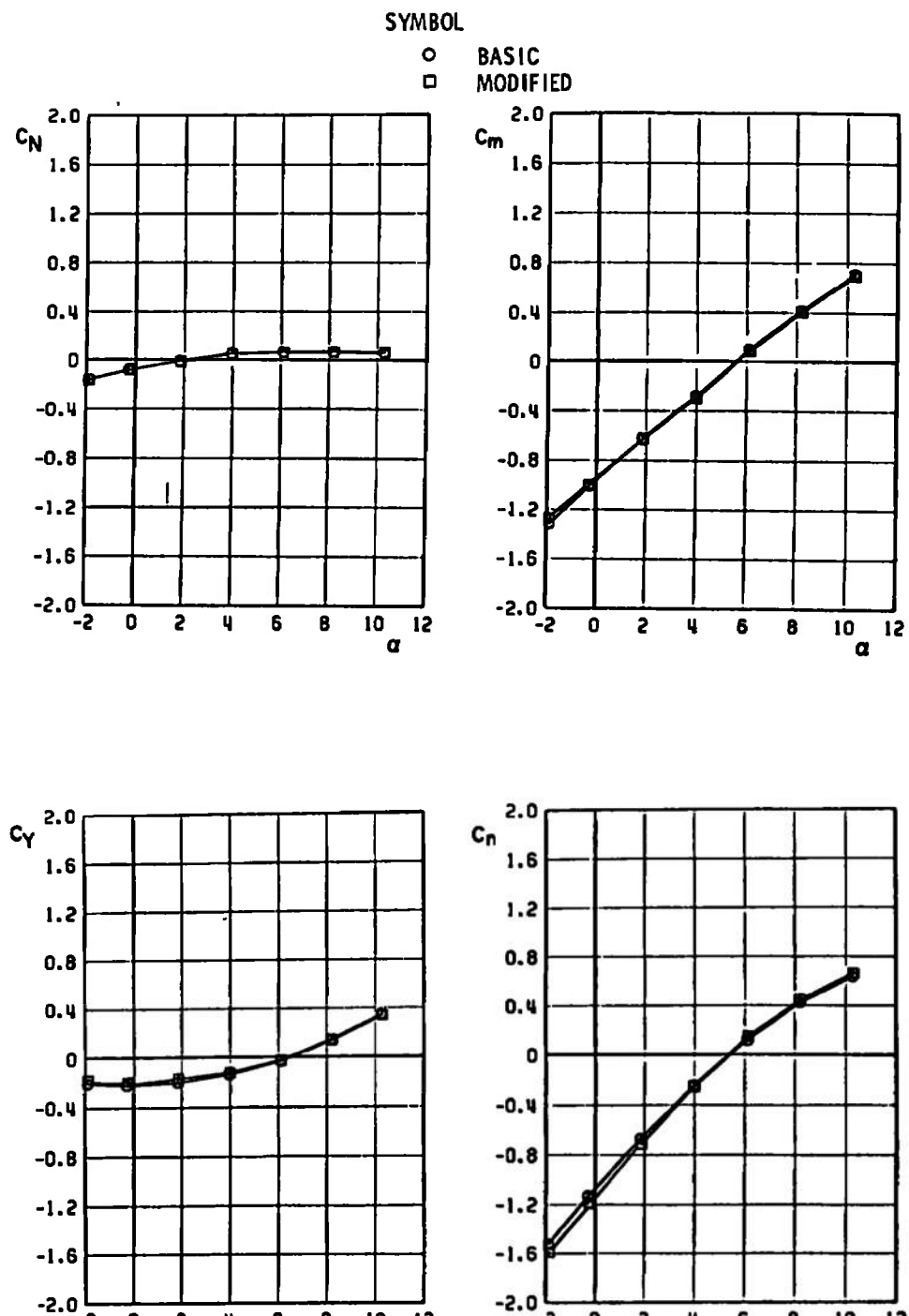
a. $M_\infty = 0.70$

Figure 19. Comparison of basic and modified unfinned BLU-1C/B carriage-
position aerodynamic coefficients, configuration 2L.
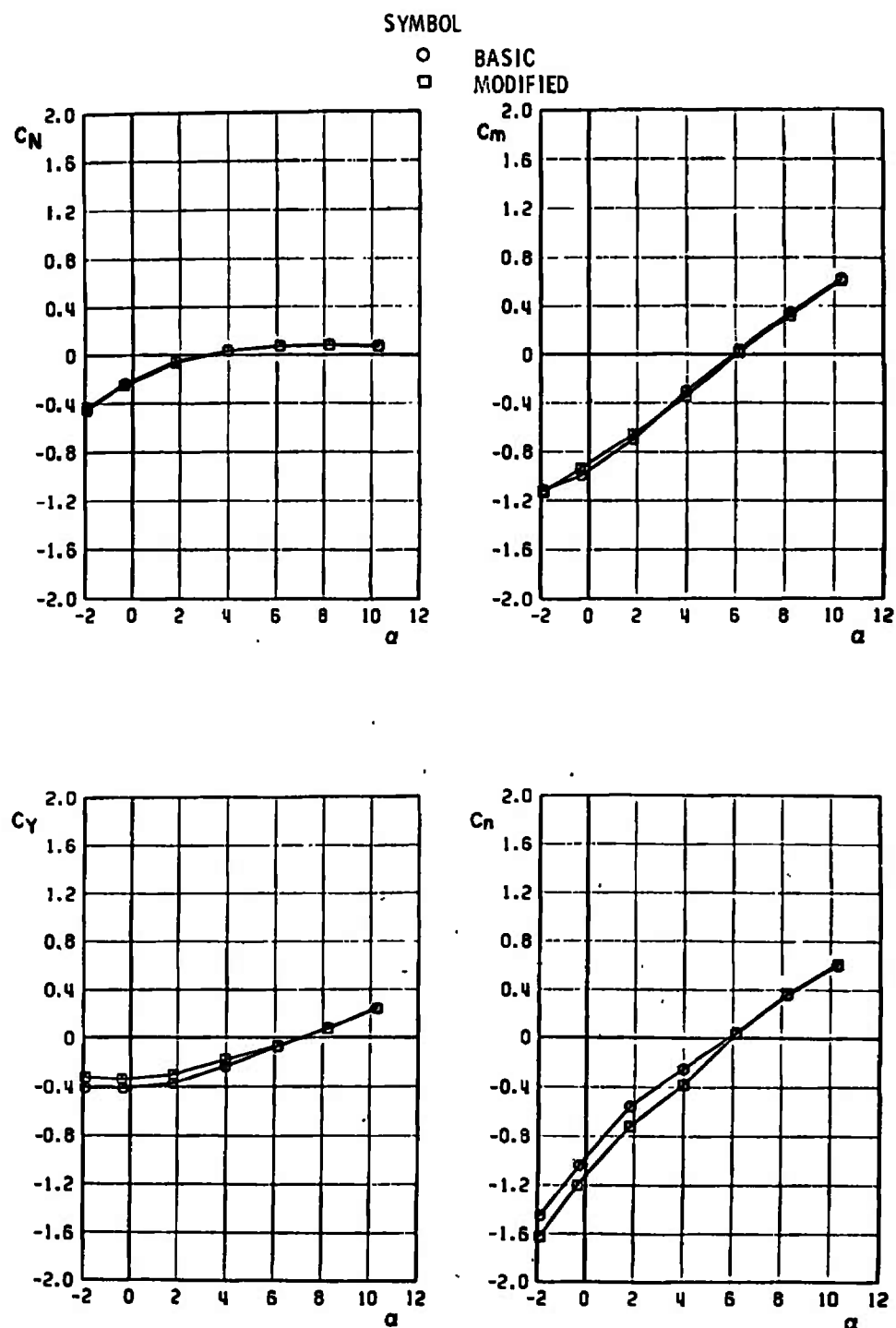
b. $M_\infty = 0.90$
Figure 19. Continued.

40
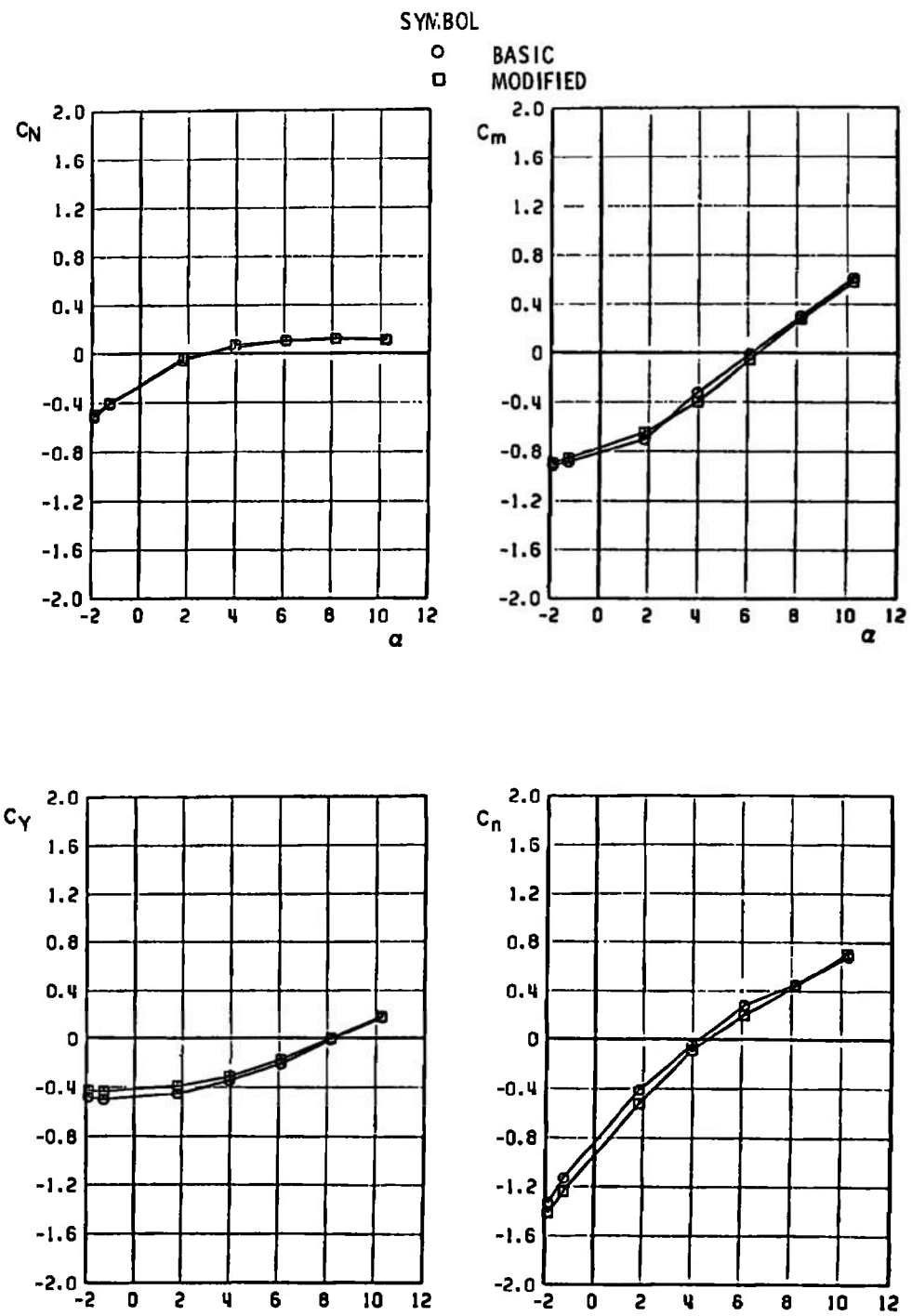
c. $M_\infty = 1.05$
Figure 19. Concluded.

41
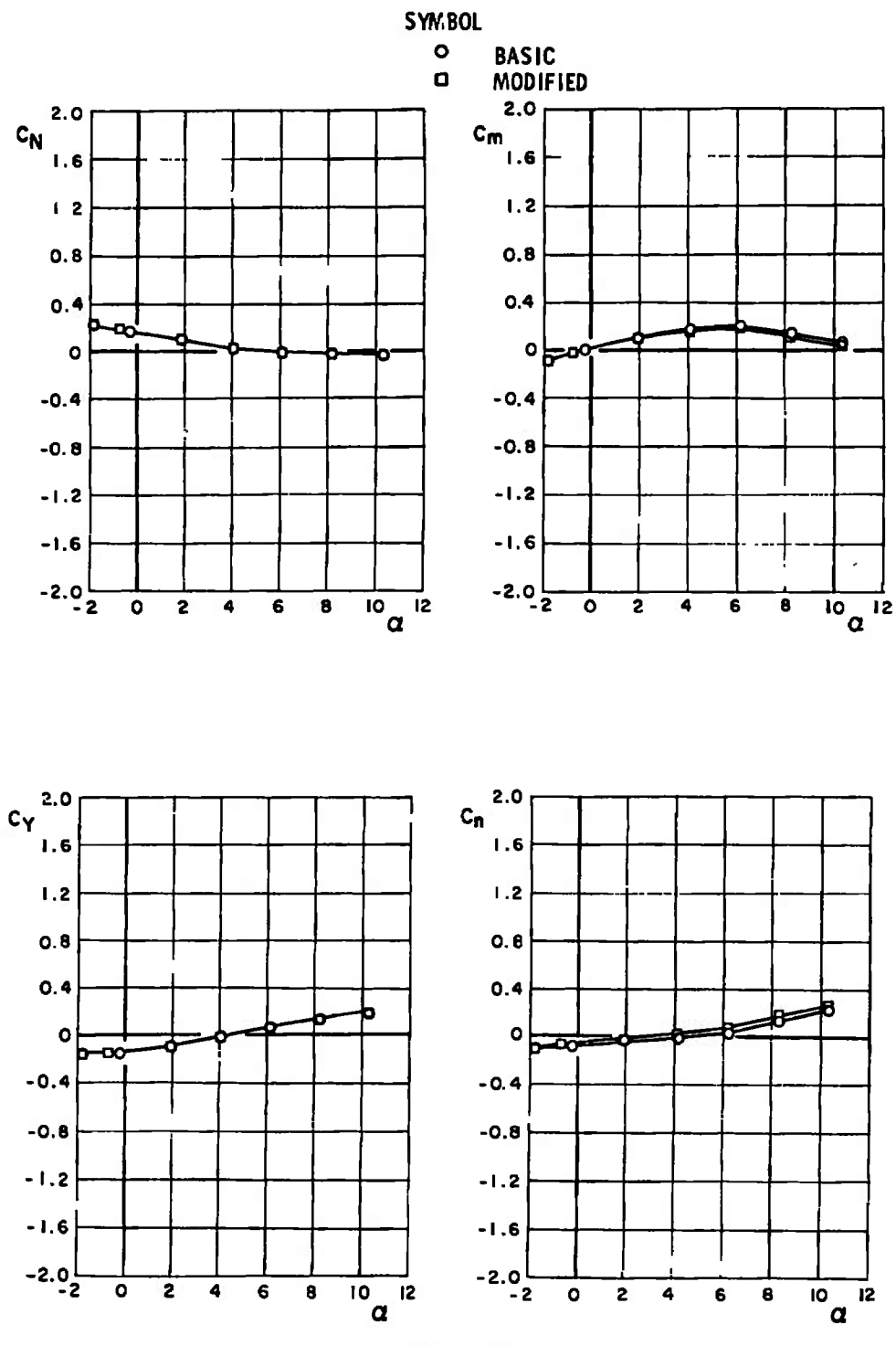
a. $M_\infty = 0.70$

Figure 20. Comparison of basic and modified finned BLU-1C/B carriage-
position aerodynamic coefficients, configuration 3R.
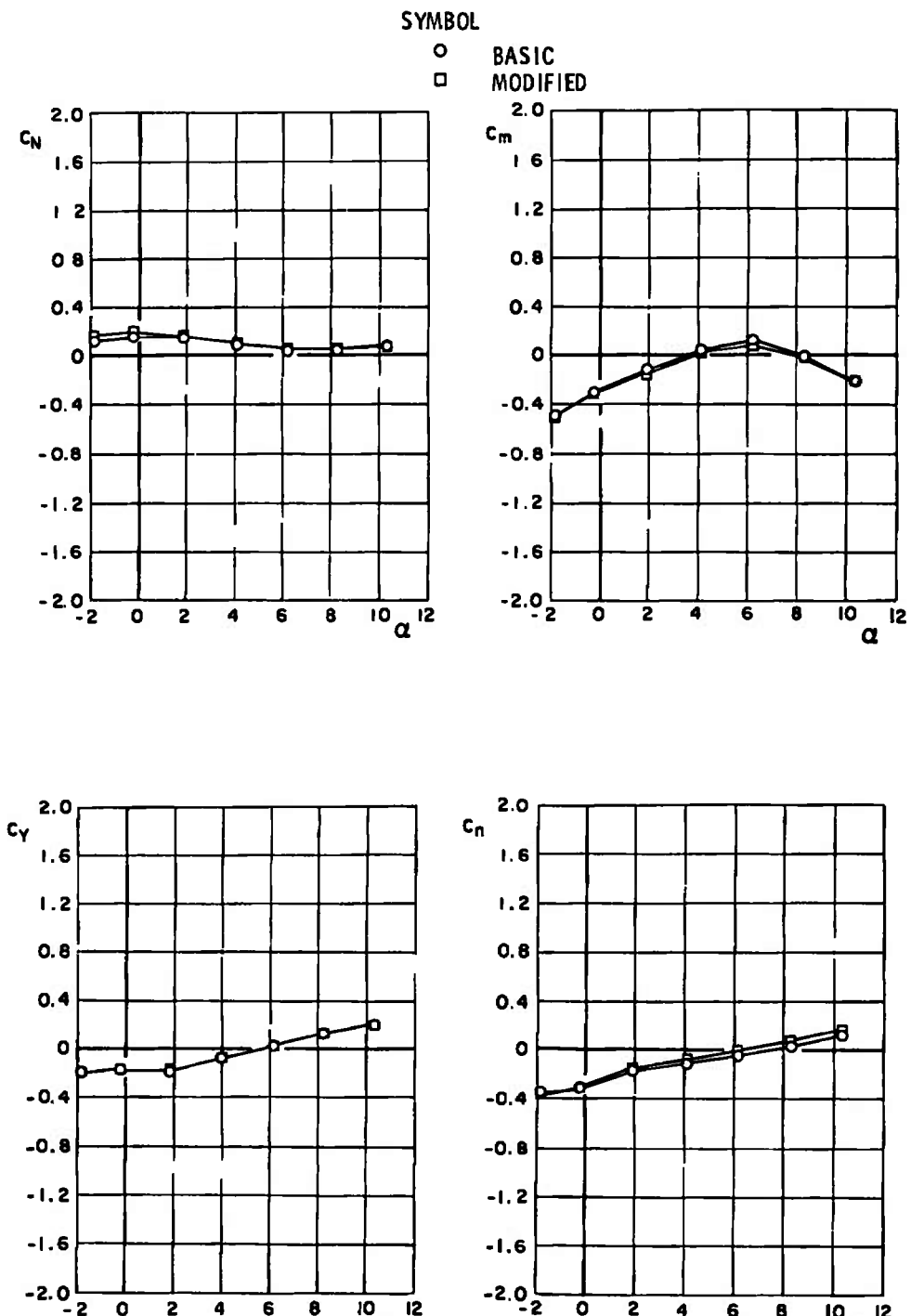
b. $M_\infty = 0.90$
Figure 20. Continued.
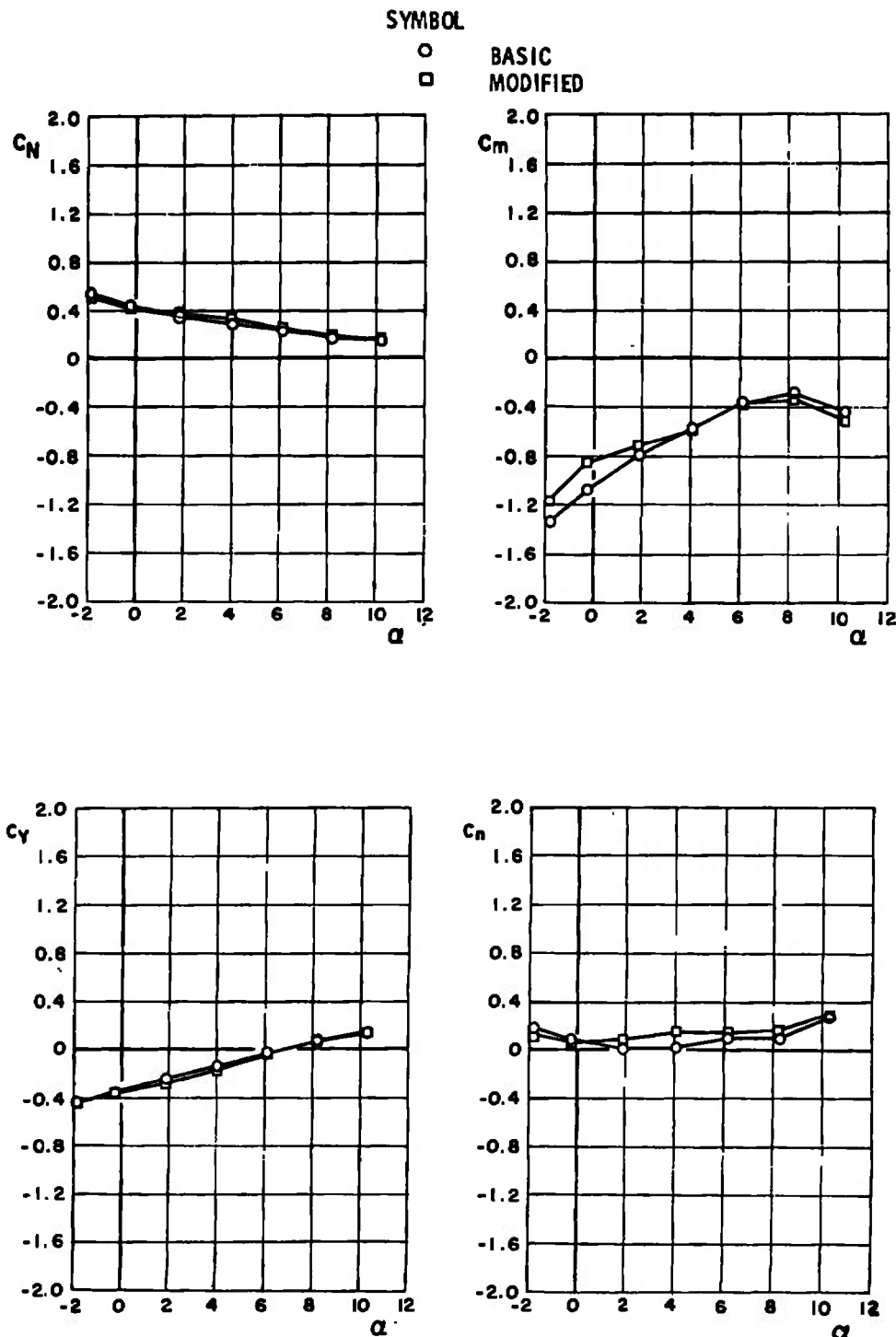
c. $M_\infty = 1.05$
Figure 20. Concluded.
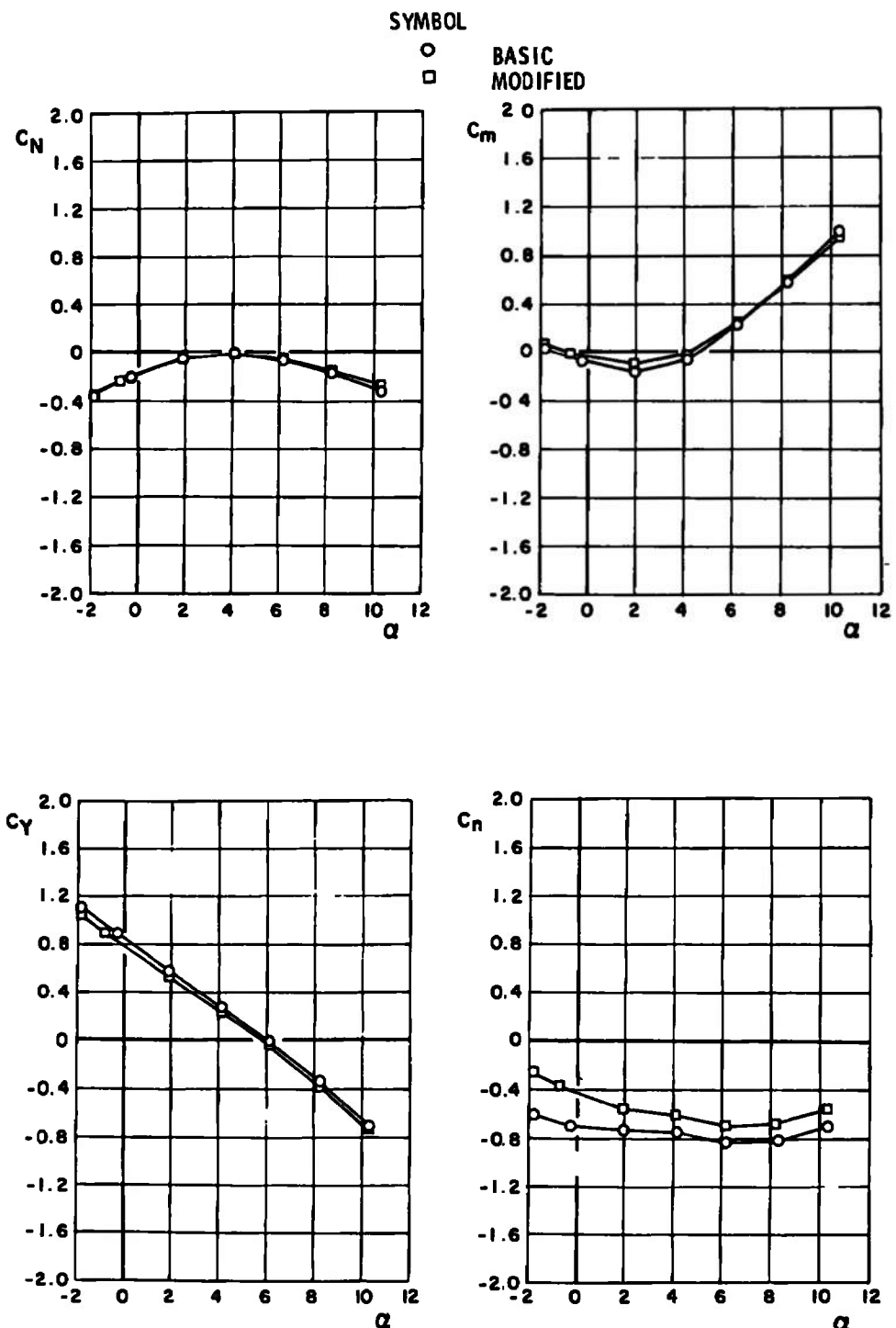
a. $M_\infty = 0.70$

Figure 21. Comparison of basic and modified finned BLU-1C/B carriage-position aerodynamic coefficients, configuration 3L.

45
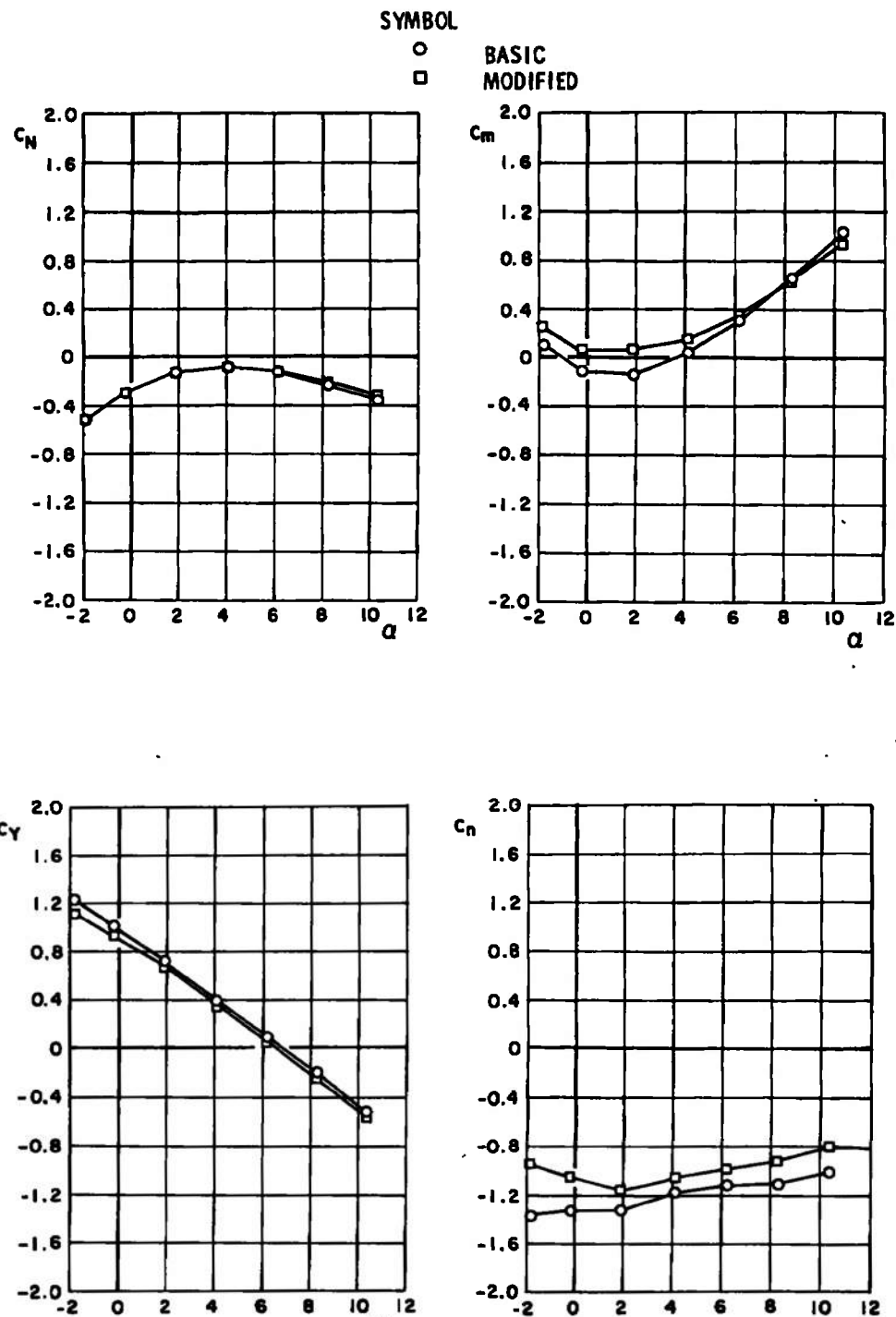
b. $M_\infty = 0.90$
Figure 21. Continued.
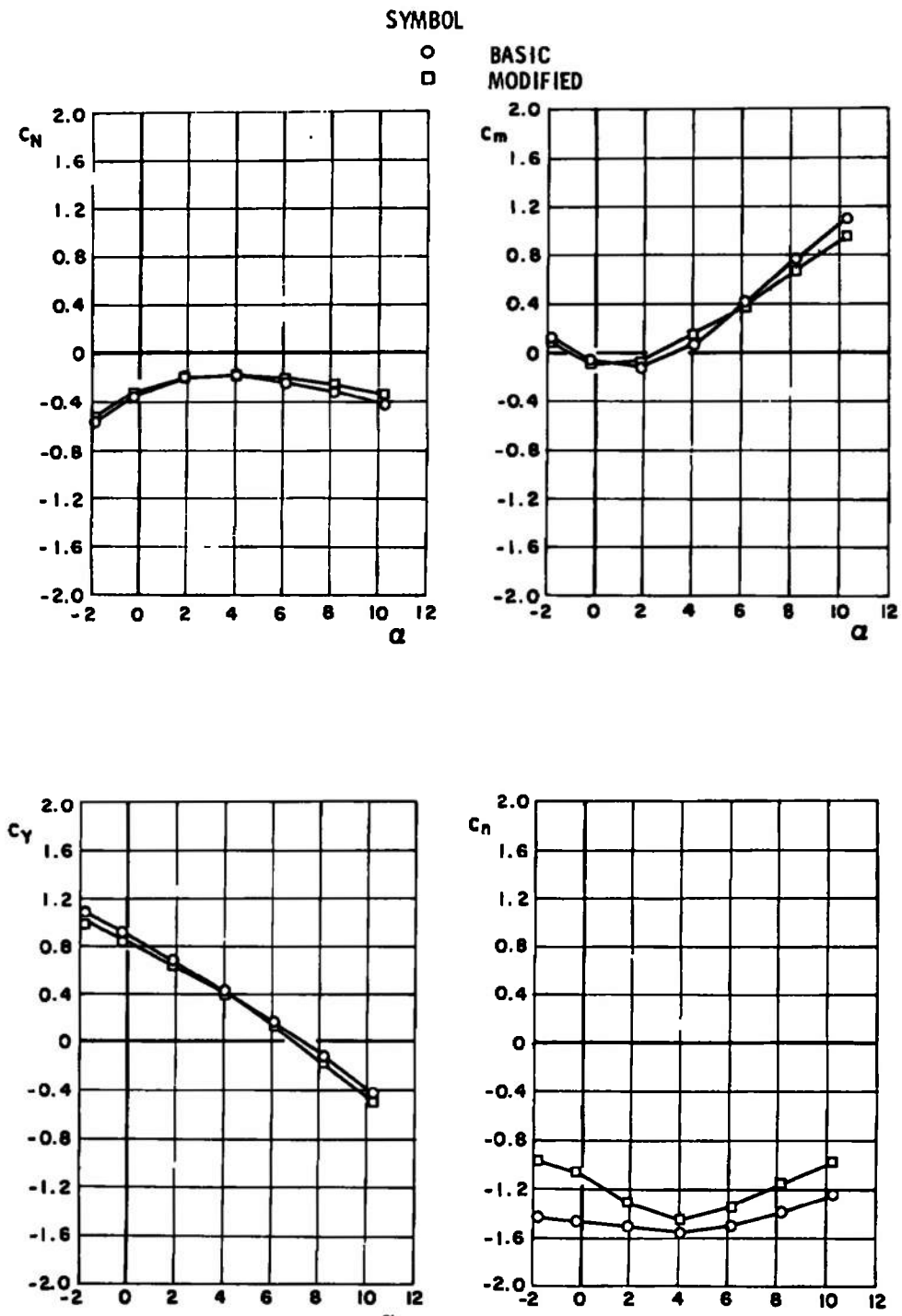
c. $M_\infty = 1.05$
Figure 21. Concluded.

SYMBOL

⊙   NO STING
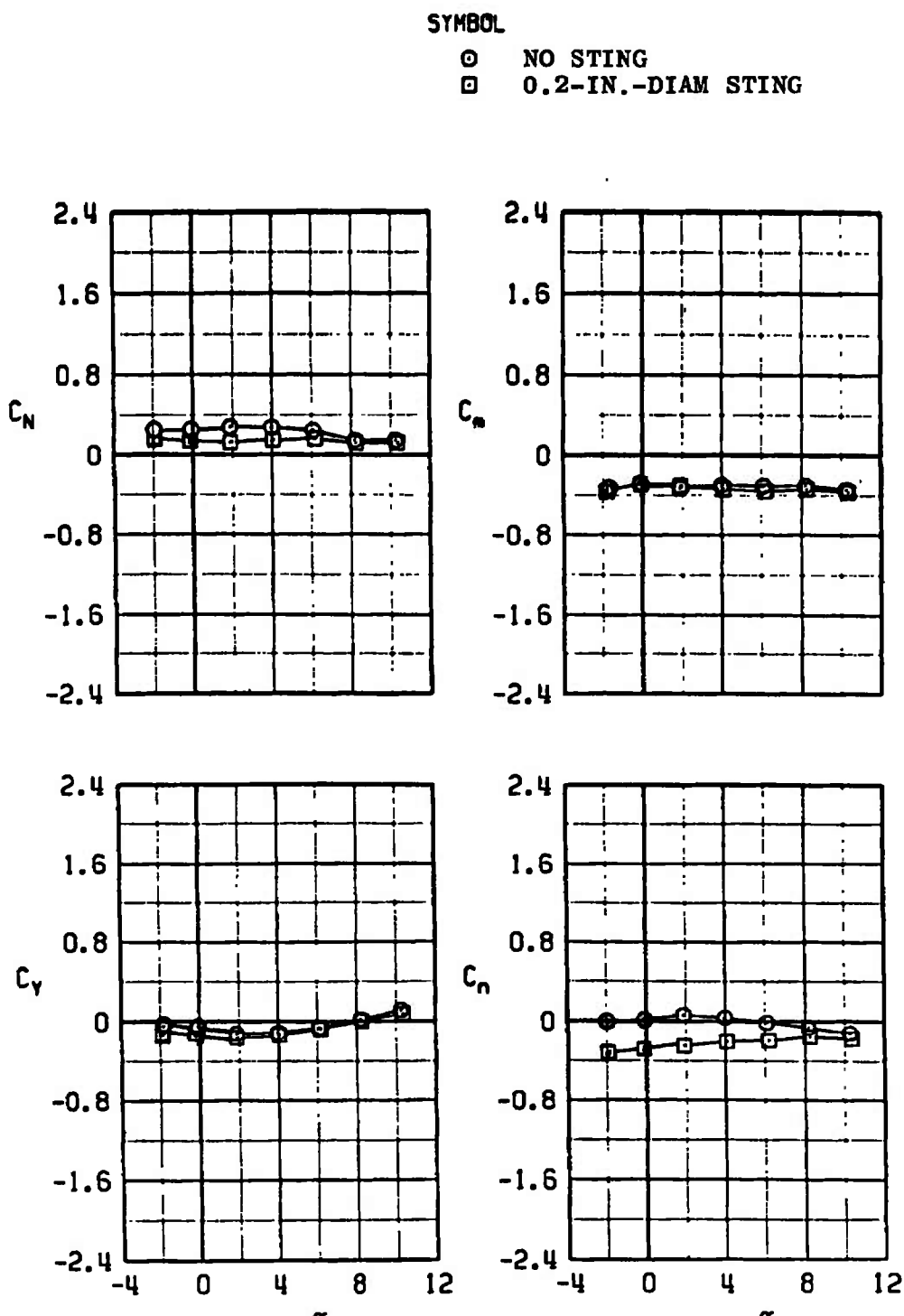
⊡   0.2-IN.-DIAM STING

a. $M_\infty = 0.70$

Figure 22.   Comparison of basic M-117 carriage-position aerodynamic coefficients with and without the presence of the 0.2-in.-diam dummy sting, configuration 1R.

48

SYMBOL

⊙ NO STING
⊡ 0.2-IN.-DIAM STING
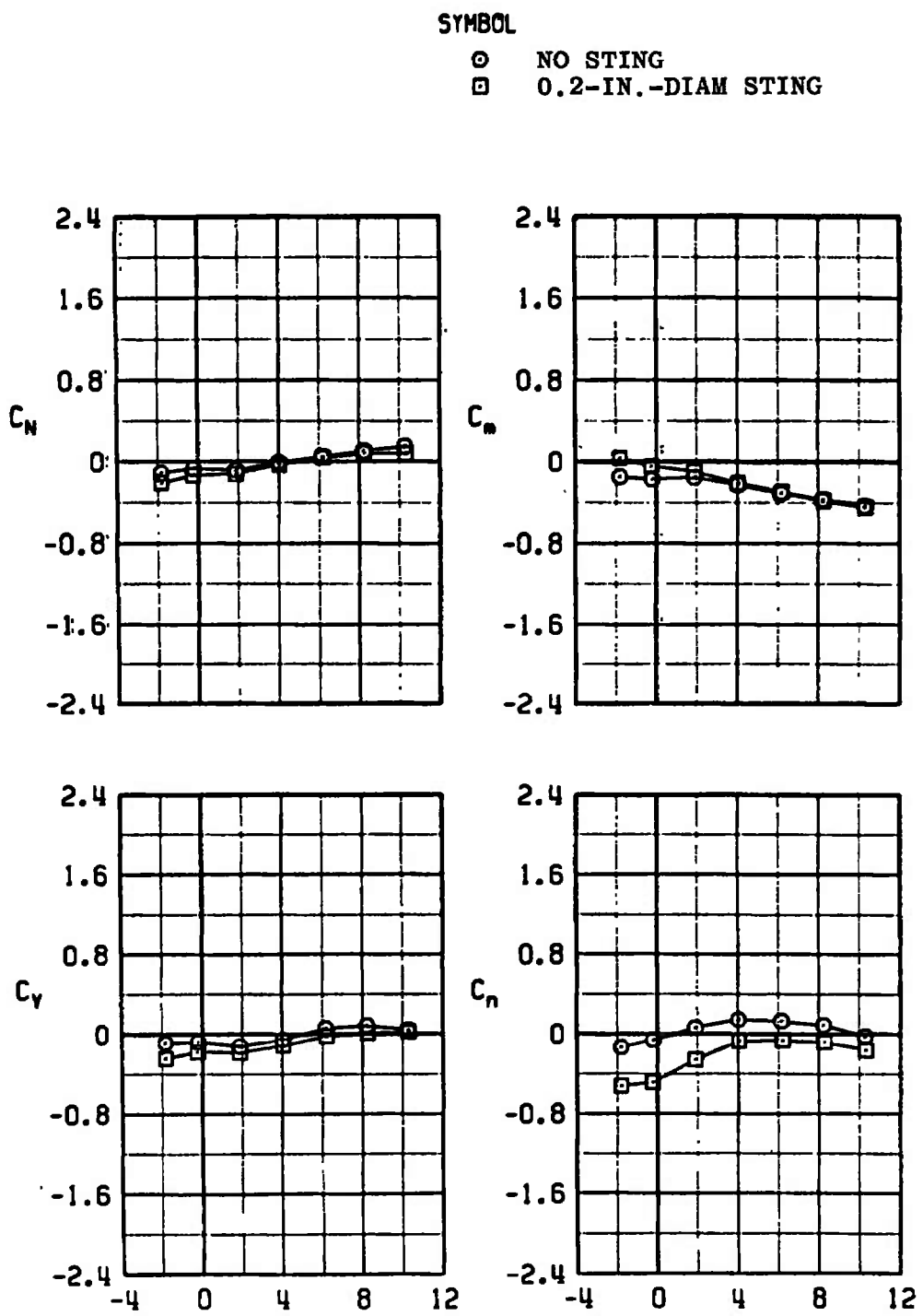
b. $M_\infty = 0.90$
Figure 22. Continued.

SYMBOL

⊙   NO STING
⊡   0.2-IN.-DIAM STING
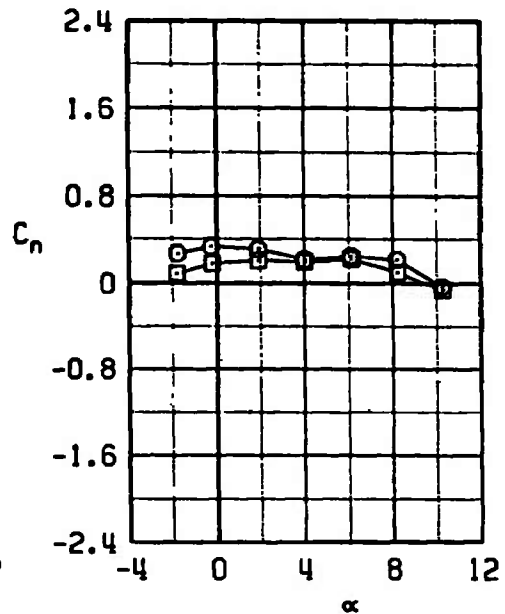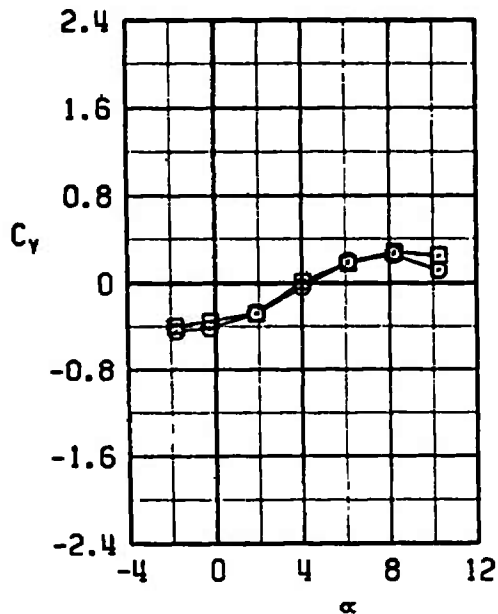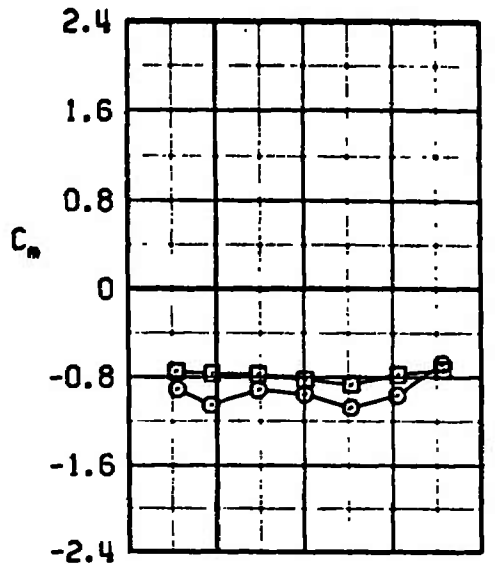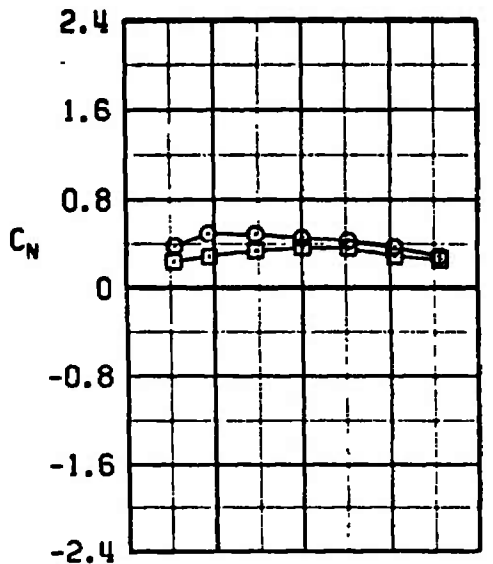
c. $M_\infty = 1.05$
Figure 22. Concluded.

SYMBOL
⊙   NO STING
⊡   0.2-IN.-DIAM STING
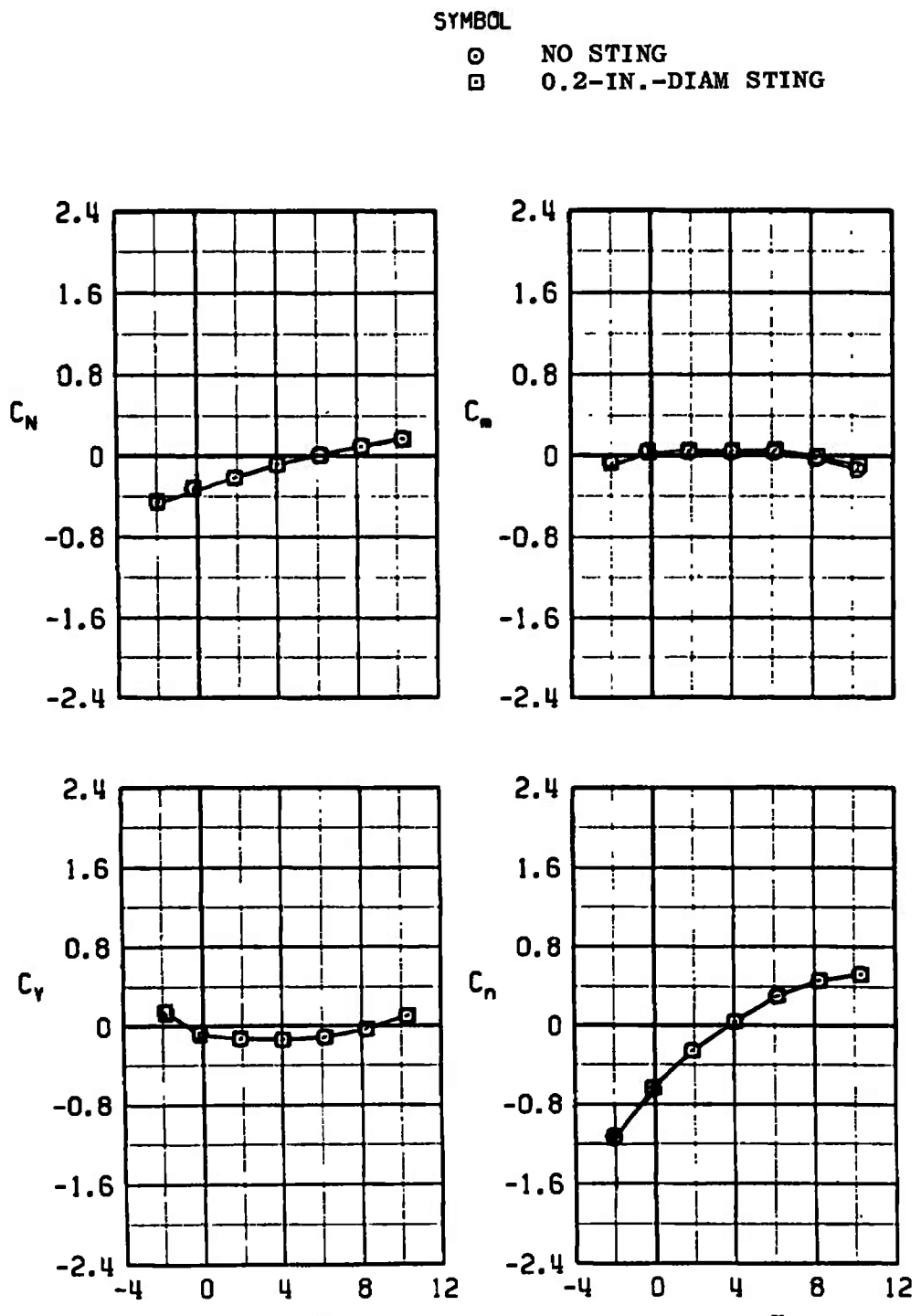
a. $M_\infty = 0.70$
Figure 23. Comparison of basic M-117 carriage-position aerodynamic
coefficients with and without the presence of the 0.2-in.-diam
dummy sting, configuration 1L.

51

SYMBOL

⊙   NO STING
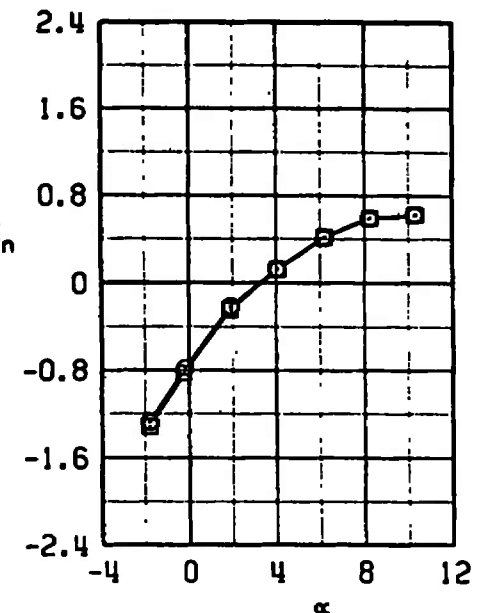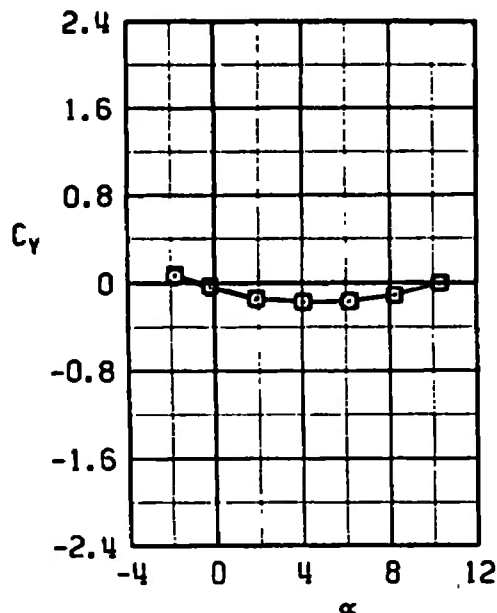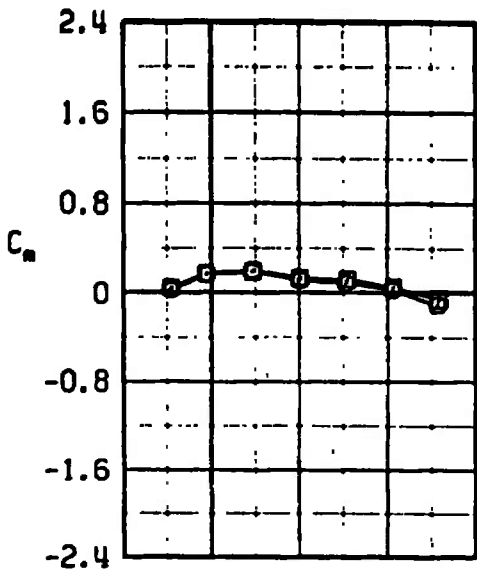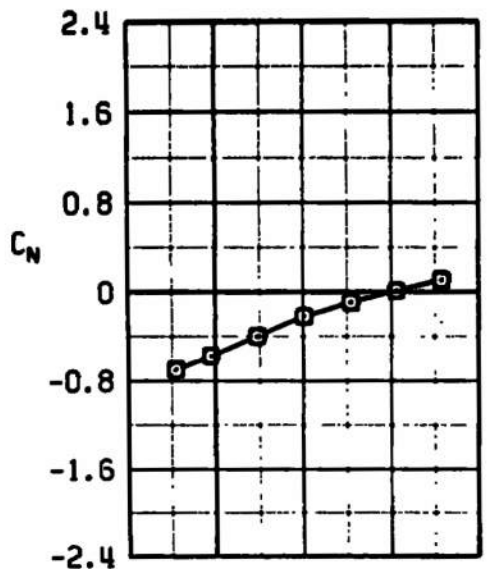
▣   0.2-IN.-DIAM STING

b. $M_\infty = 0.90$

Figure 23. Continued.

SYMBOL
⊙   NO STING
⊟   0.2-IN.-DIAM STING
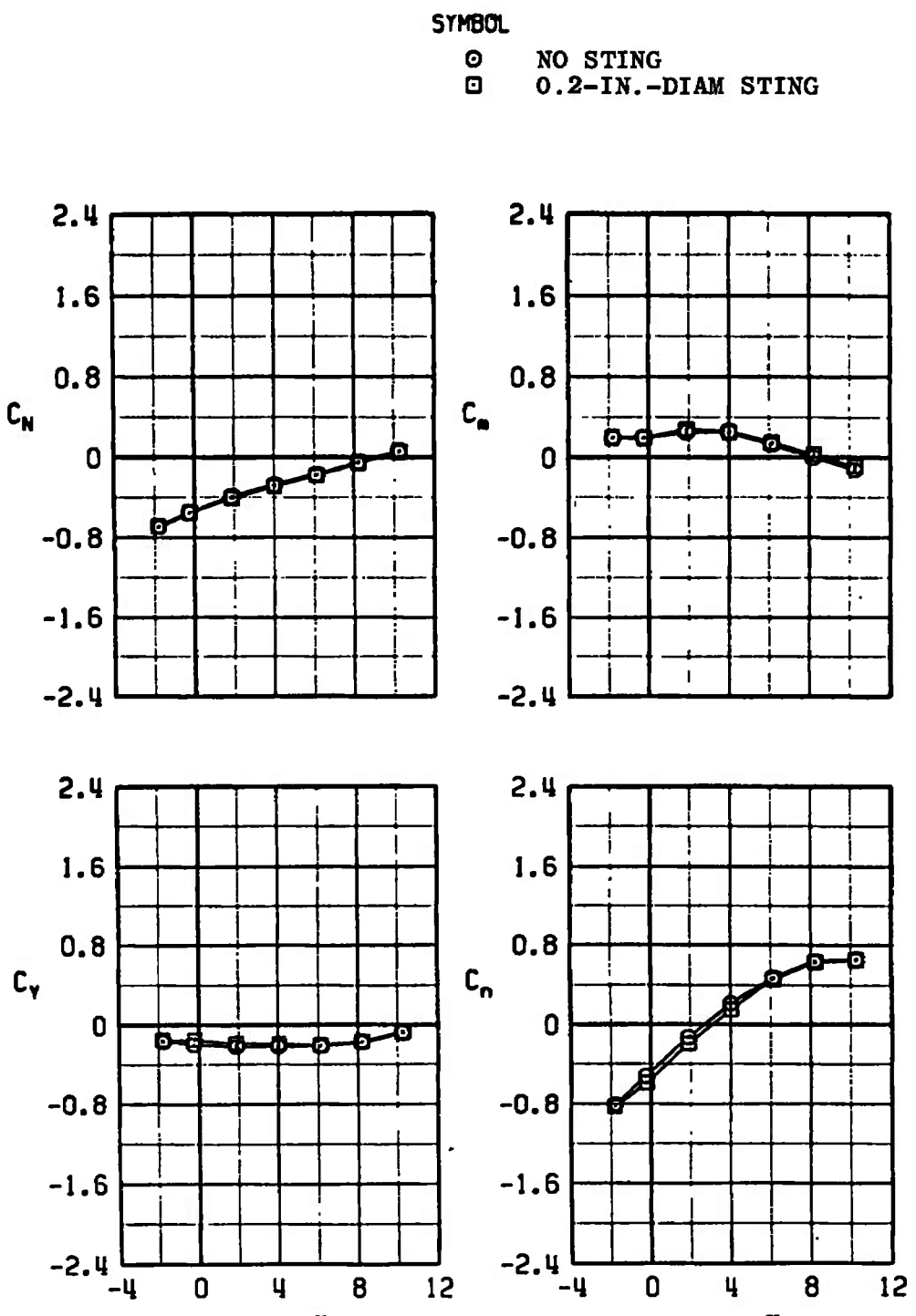
c. $M_\infty = 1.05$
Figure 23. Concluded.

SYMBOL

⊙   NO STING
⊡   0.2-IN.-DIAM STING
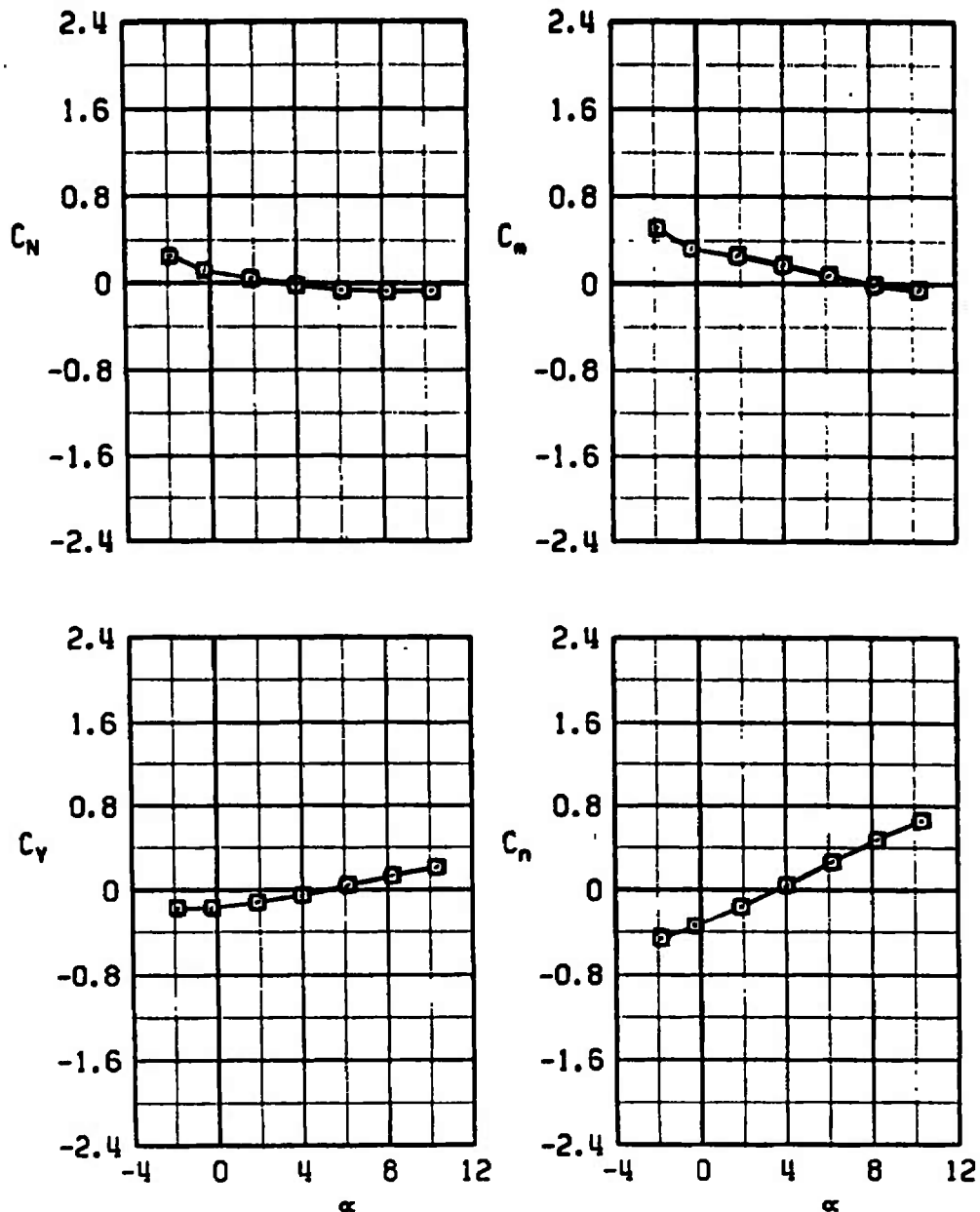
a. $M_\infty = 0.70$

Figure 24. Comparison of basic unfinned BLU-1C/B carriage-position
aerodynamic coefficients with and without the presence of
the 0.2-in.-diam dummy sting, configuration 2R.

SYMBOL
⊙   NO STING
⊡   0.2-IN.-DIAM STING
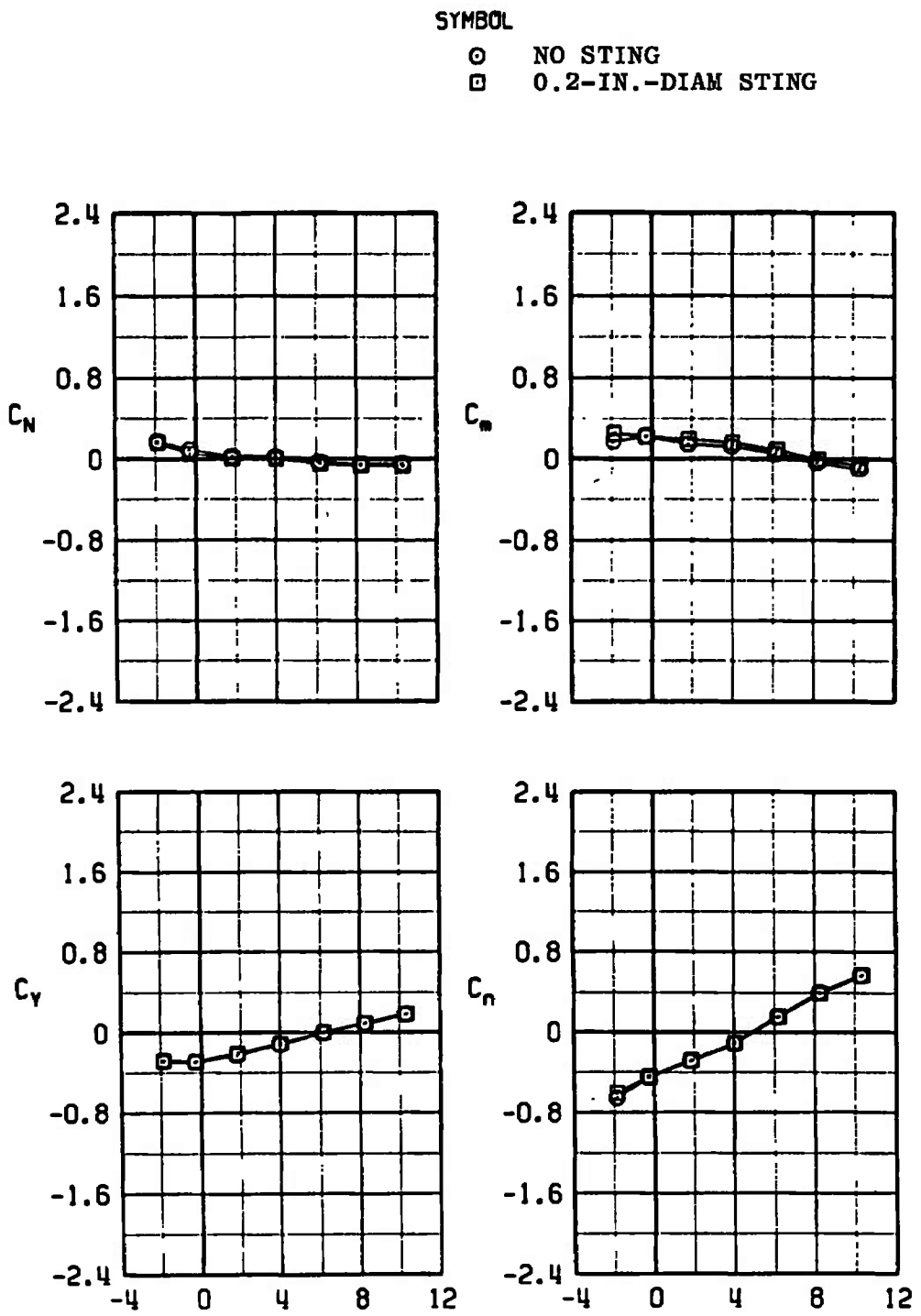
b. M∞ = 0.90
Figure 24. Continued.

SYMBOL

⊙   NO STING
⊡   0.2-IN.-DIAM STING
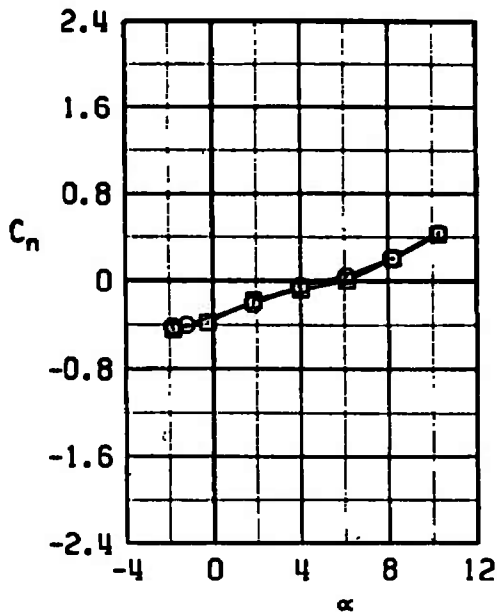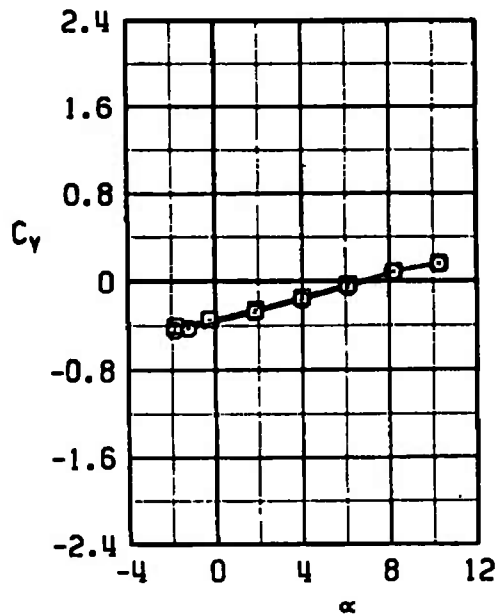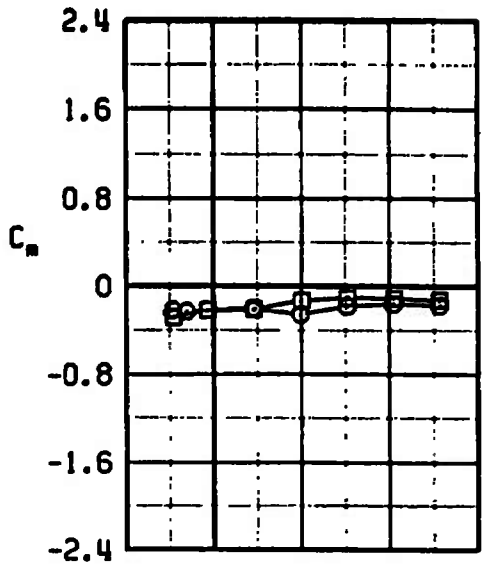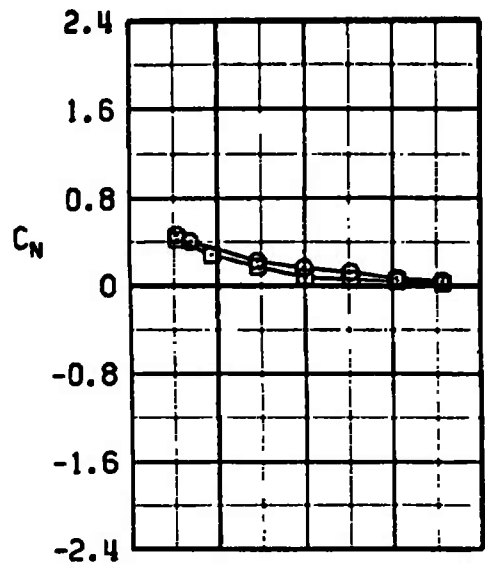
c. $M_\infty = 1.05$
Figure 24. Concluded.

SYMBOL

⊙   NO STING
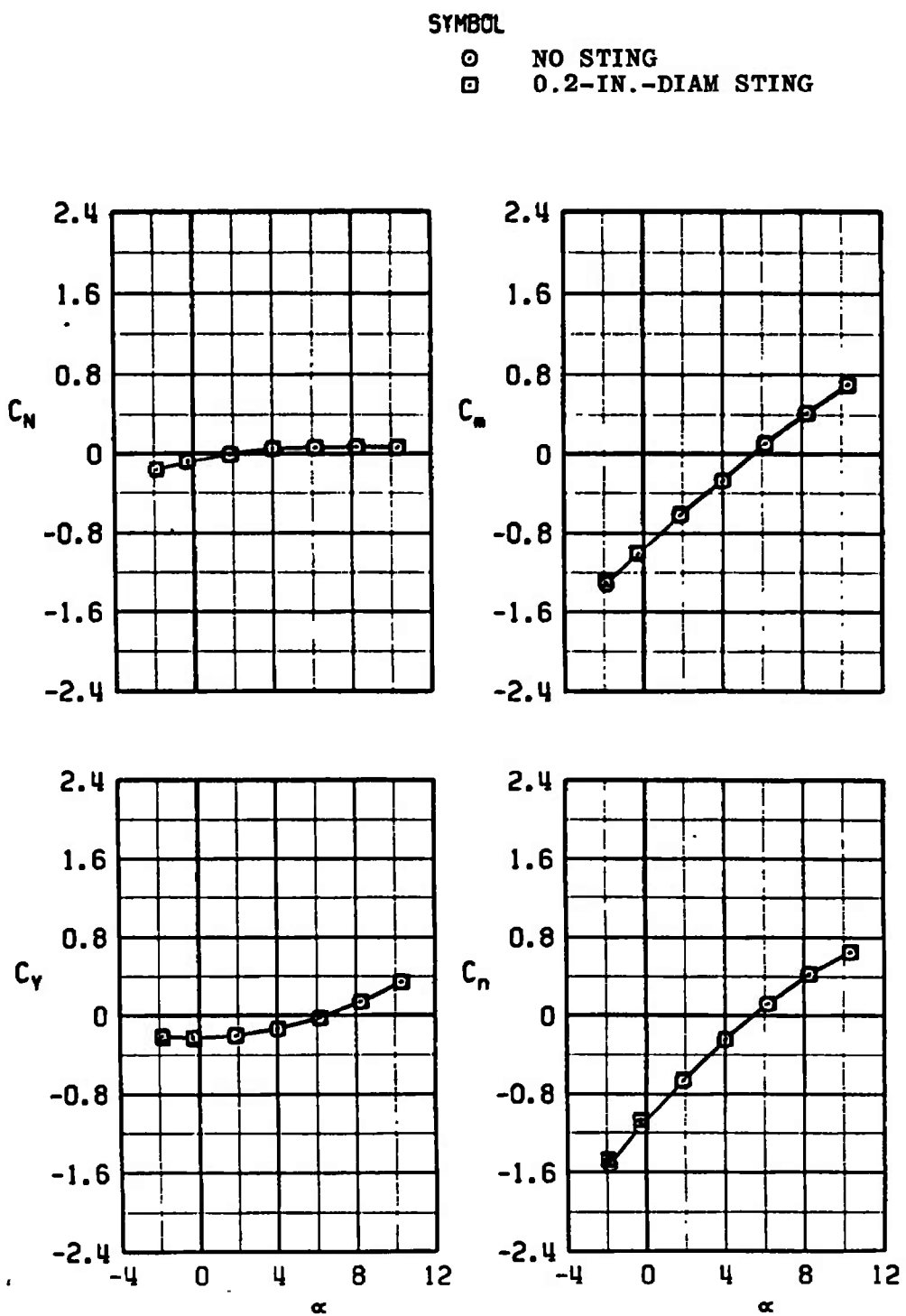
□   0.2-IN.-DIAM STING

a. M$_\infty$ = 0.70

Figure 25. Comparison of basic unfinned BLU-1C/B carriage-position
aerodynamic coefficients with and without the presence of
the 0.2-in.-diam dummy sting, configuration 2L.

SYMBOL

⊙   NO STING
⊡   0.2-IN.-DIAM STING
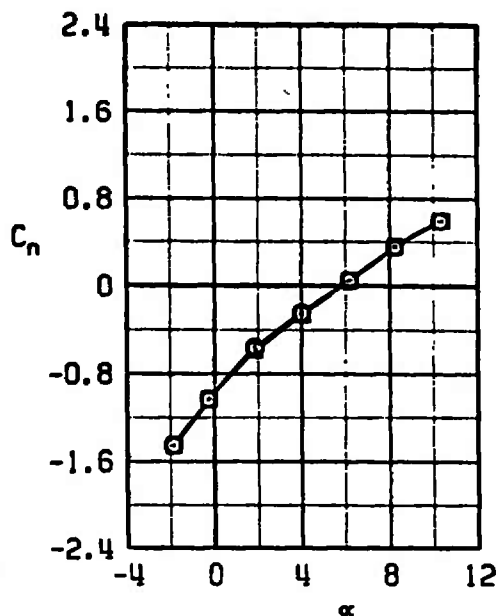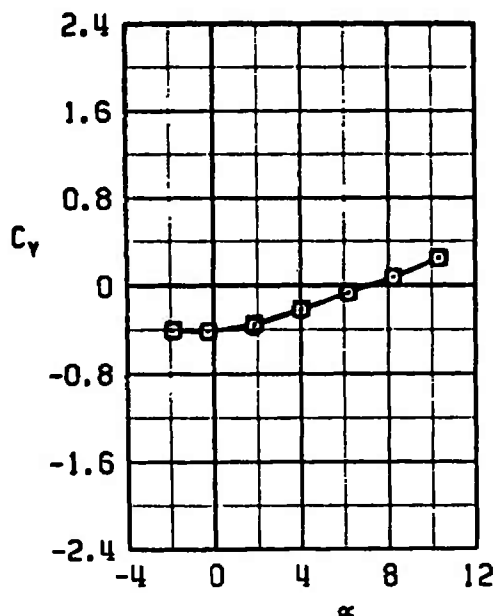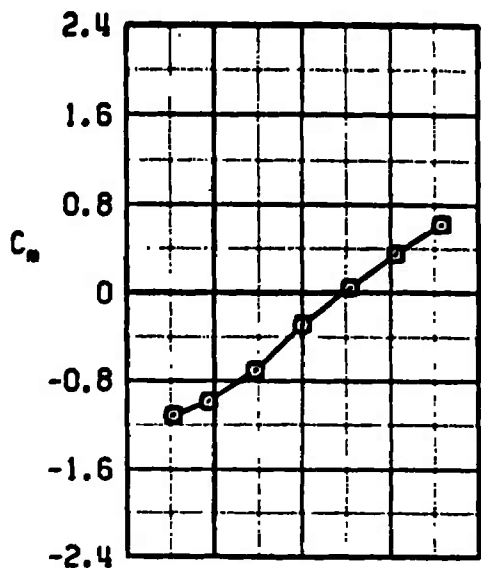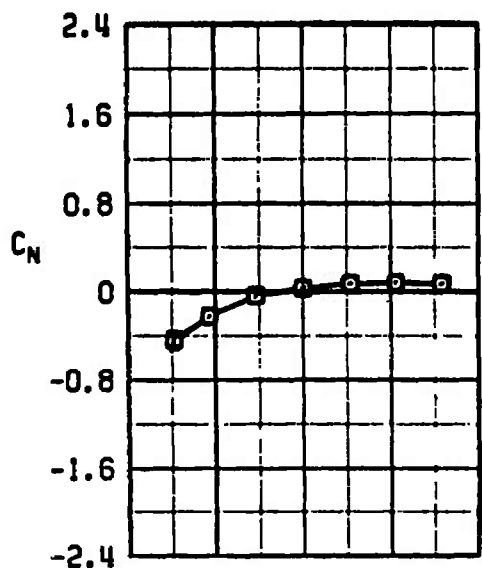

b. $M_\infty \approx 0.90$
Figure 25. Continued.

SYMBOL
⊙   NO STING
⊡   0.2-IN.-DIAM STING
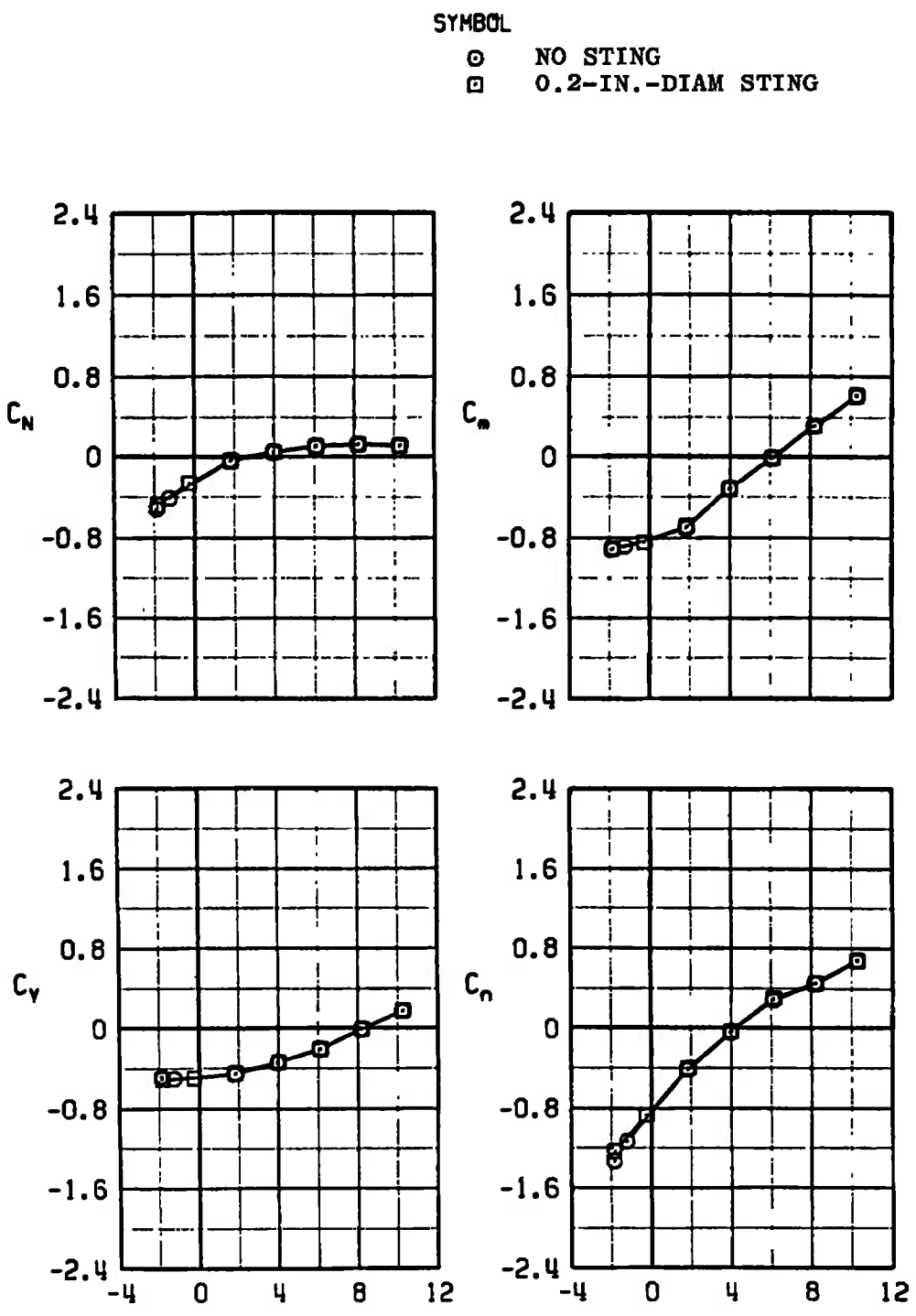
c. $M_\infty = 1.05$
Figure 25. Concluded.

SYMBOL

⊙ NO STING
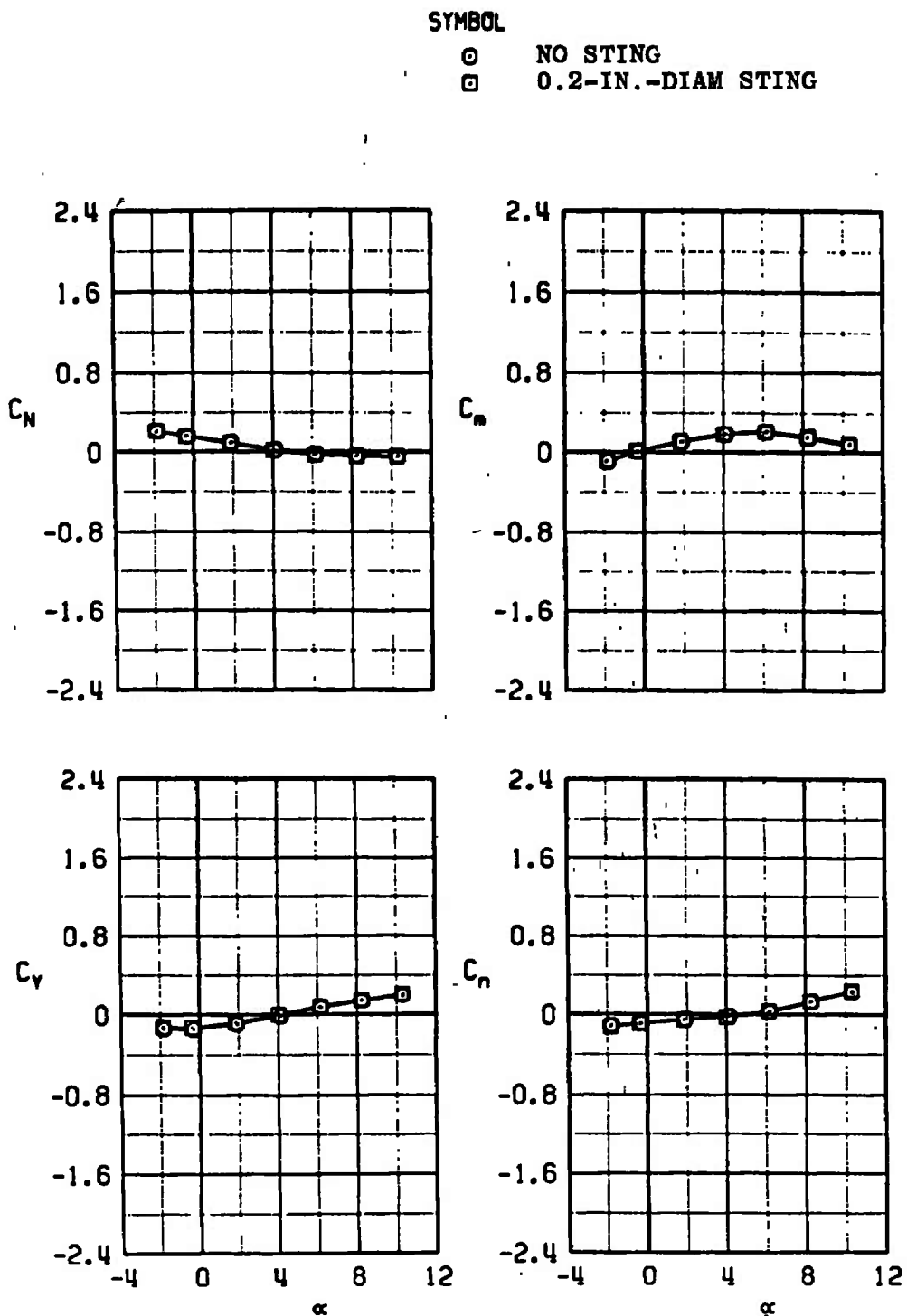
⊡ 0.2-IN.-DIAM STING

a. $M_\infty = 0.70$

Figure 26. Comparison of basic finned BLU-1C/B carriage-position
aerodynamic coefficients with and without the presence
of the 0.2-in.-diam dummy sting, configuration 3R.

SYMBOL
⊙   NO STING
⊡   0.2-IN.-DIAM STING
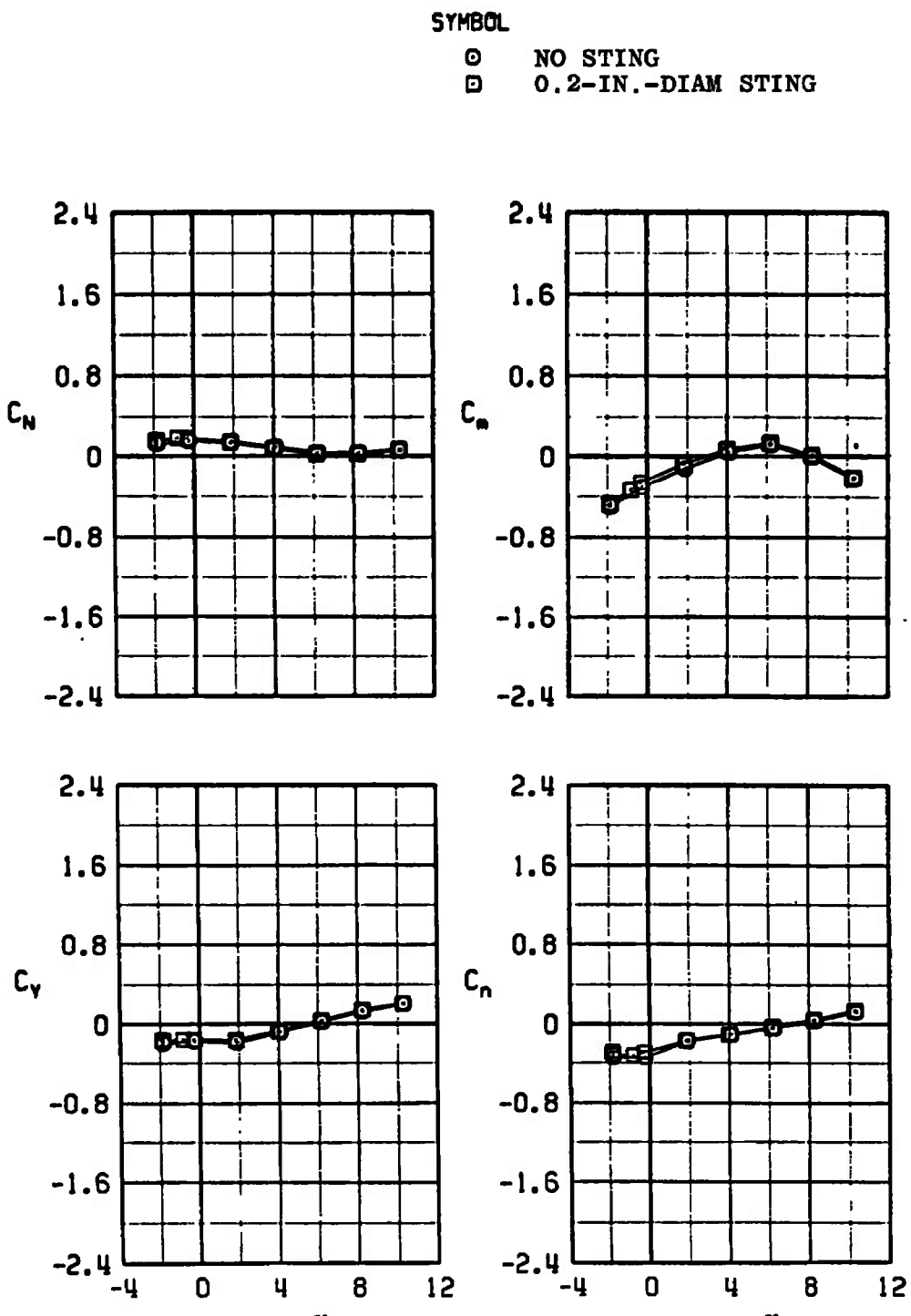
b. $M_\infty = 0.90$
Figure 26. Continued.

SYMBOL

⊙   NO STING
⊡   0.2-IN.-DIAM STING
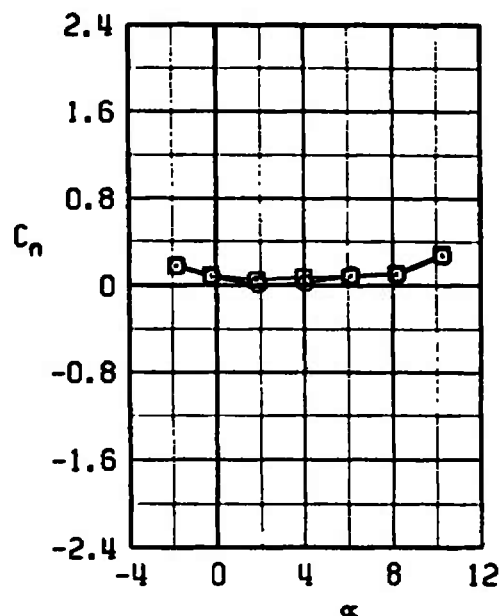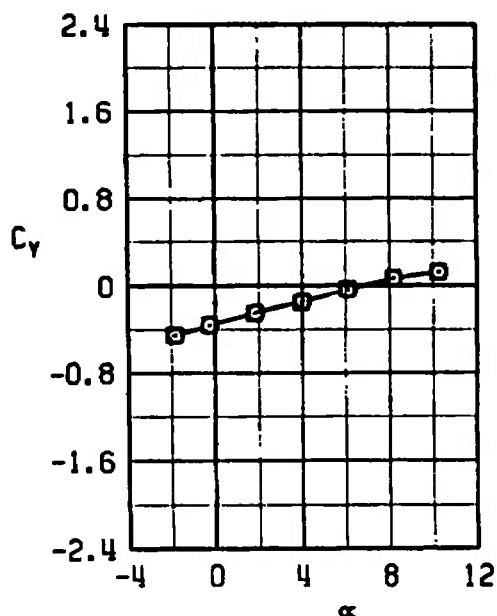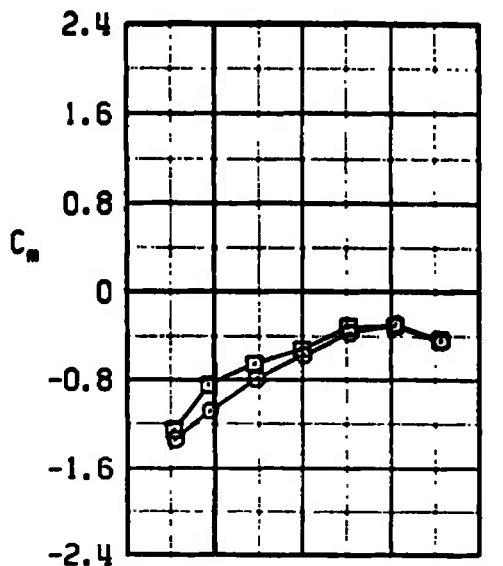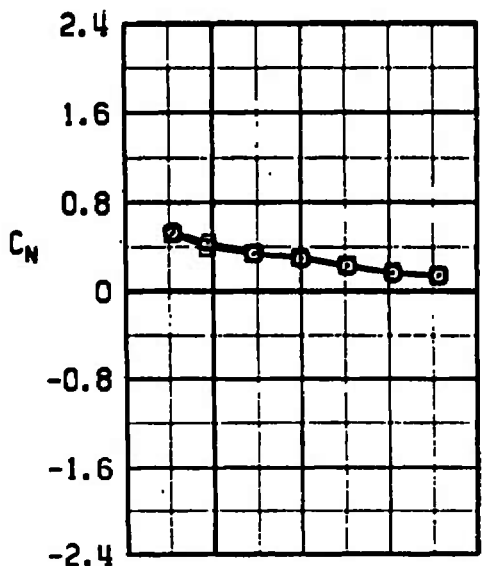
c. M_∞ = 1.05
Figure 26. Concluded.
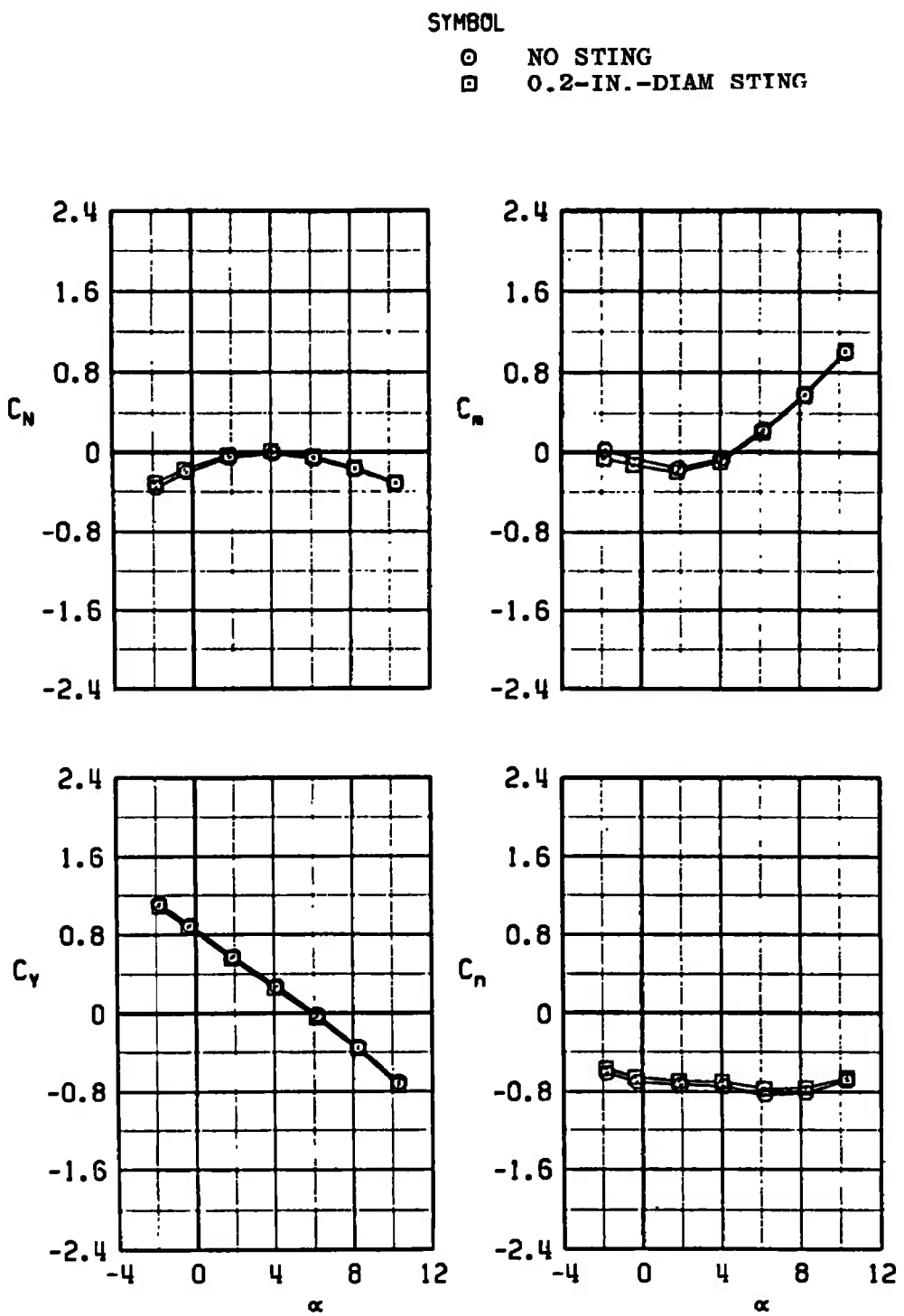
a. $M_\infty = 0.70$

Figure 27. Comparison of basic finned BLU-1C/B carriage-position
aerodynamic coefficients with and without the presence of
the 0.2-in.-diam dummy sting, configuration 3L.

SYMBOL

⊙   NO STING
⊡   0.2-IN.-DIAM STING
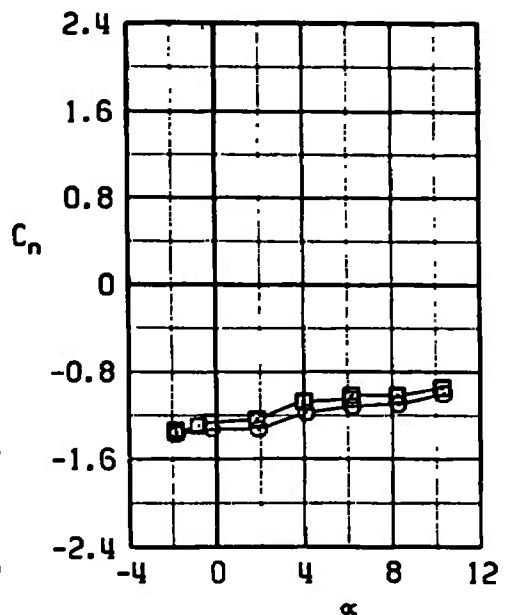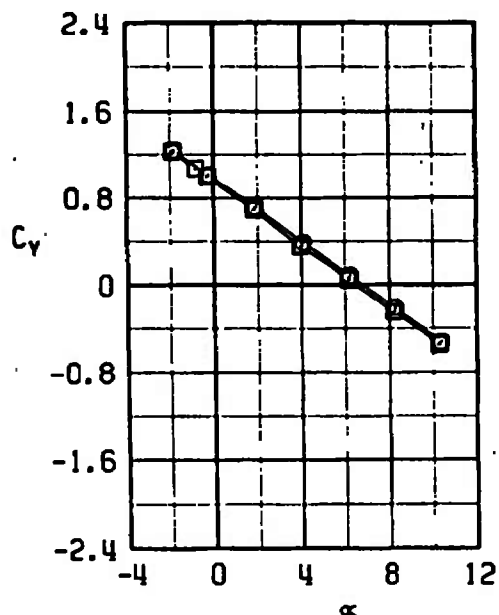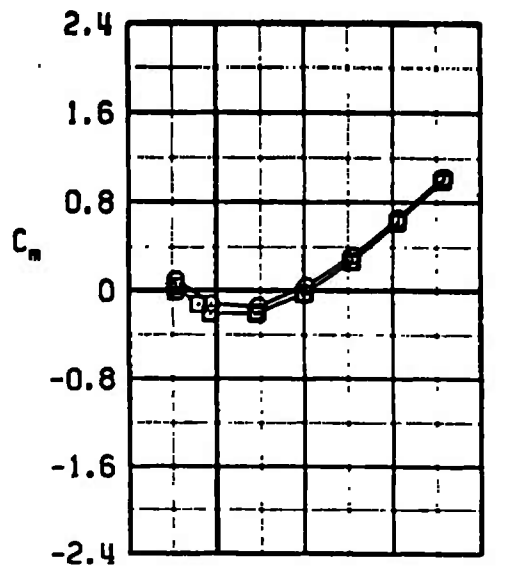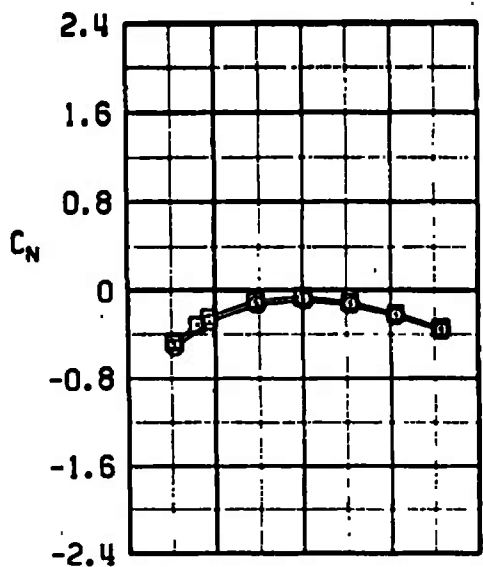
b. $M_\infty = 0.90$
Figure 27. Continued.

SYMBOL

⊙   NO STING

⊡   0.2-IN.-DIAM STING
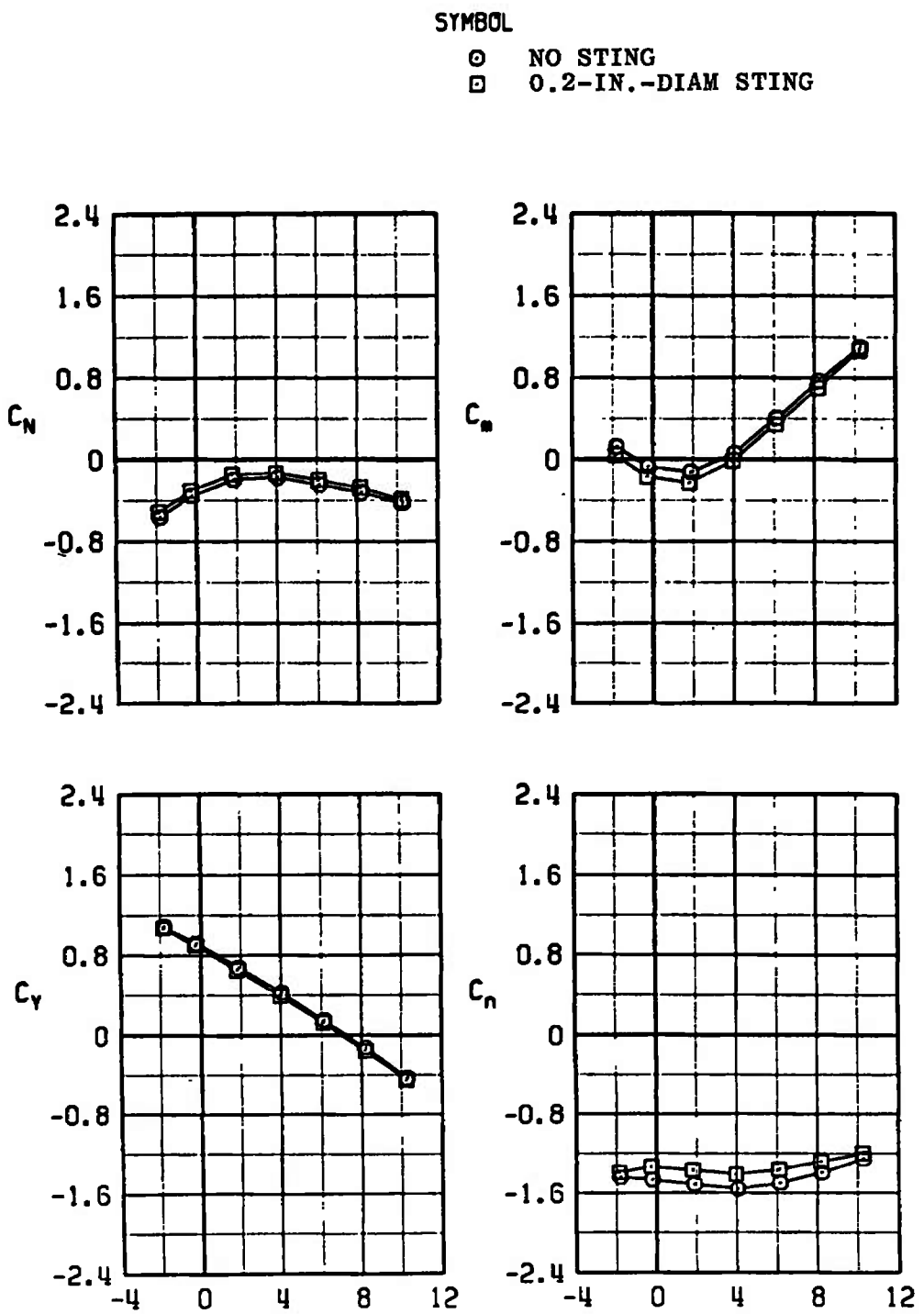
c. $M_\infty = 1.05$
Figure 27. Concluded.

SYMBOL
⊙ NO STING
⊡ 0.4-IN.-DIAM STRAIGHT STING
△ 0.4-IN.-DIAM BENT STING
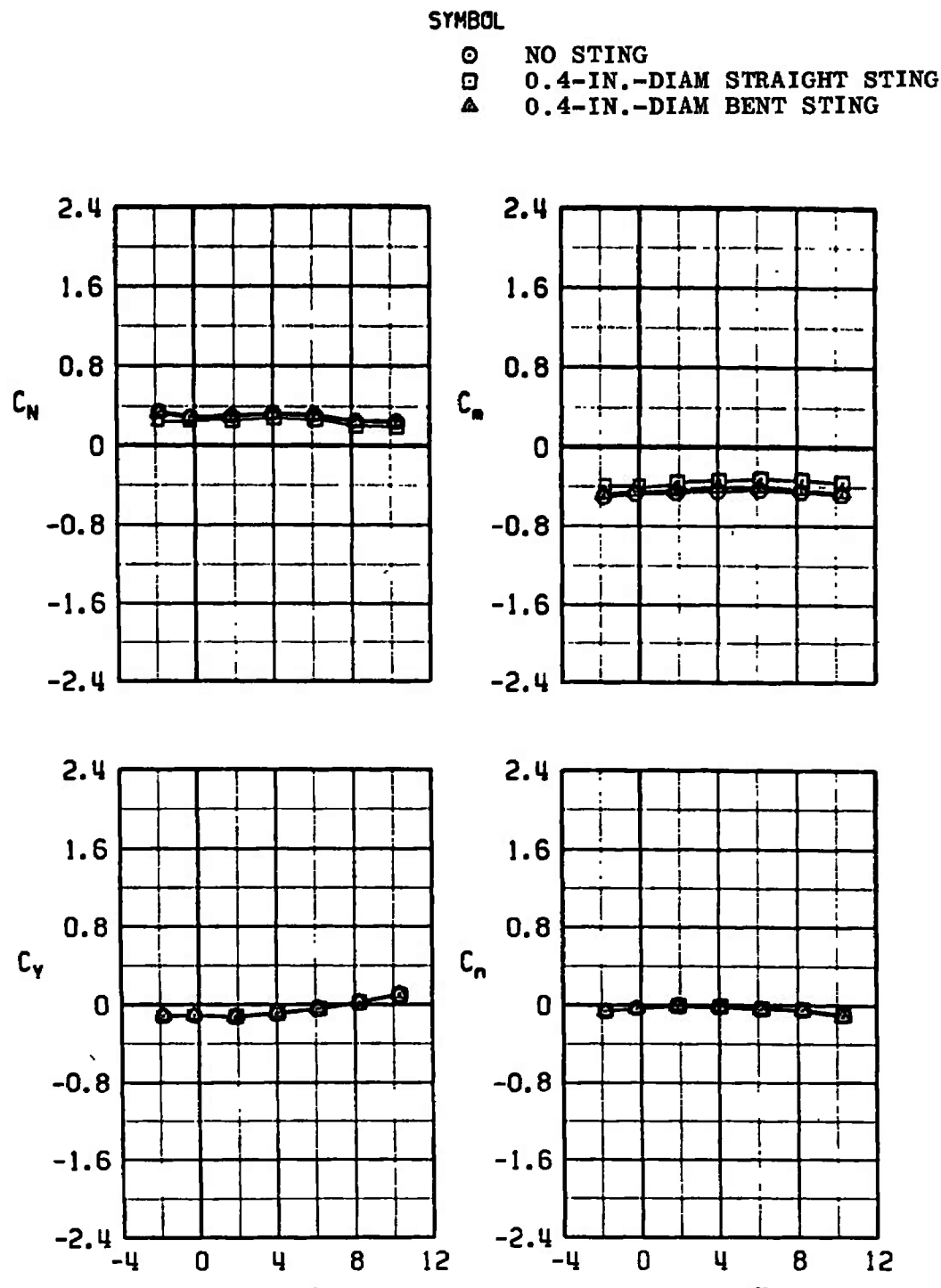
a. $M_\infty = 0.70$

Figure 28. Comparison of modified M-117 carriage-position aerodynamic coefficients with and without the presence of the 0.4-in.-diam dummy sting, configuration 1R.

66

SYMBOL

⊙ NO STING
▣ 0.4-IN.-DIAM STRAIGHT STING
△ 0.4-IN.-DIAM BENT STING
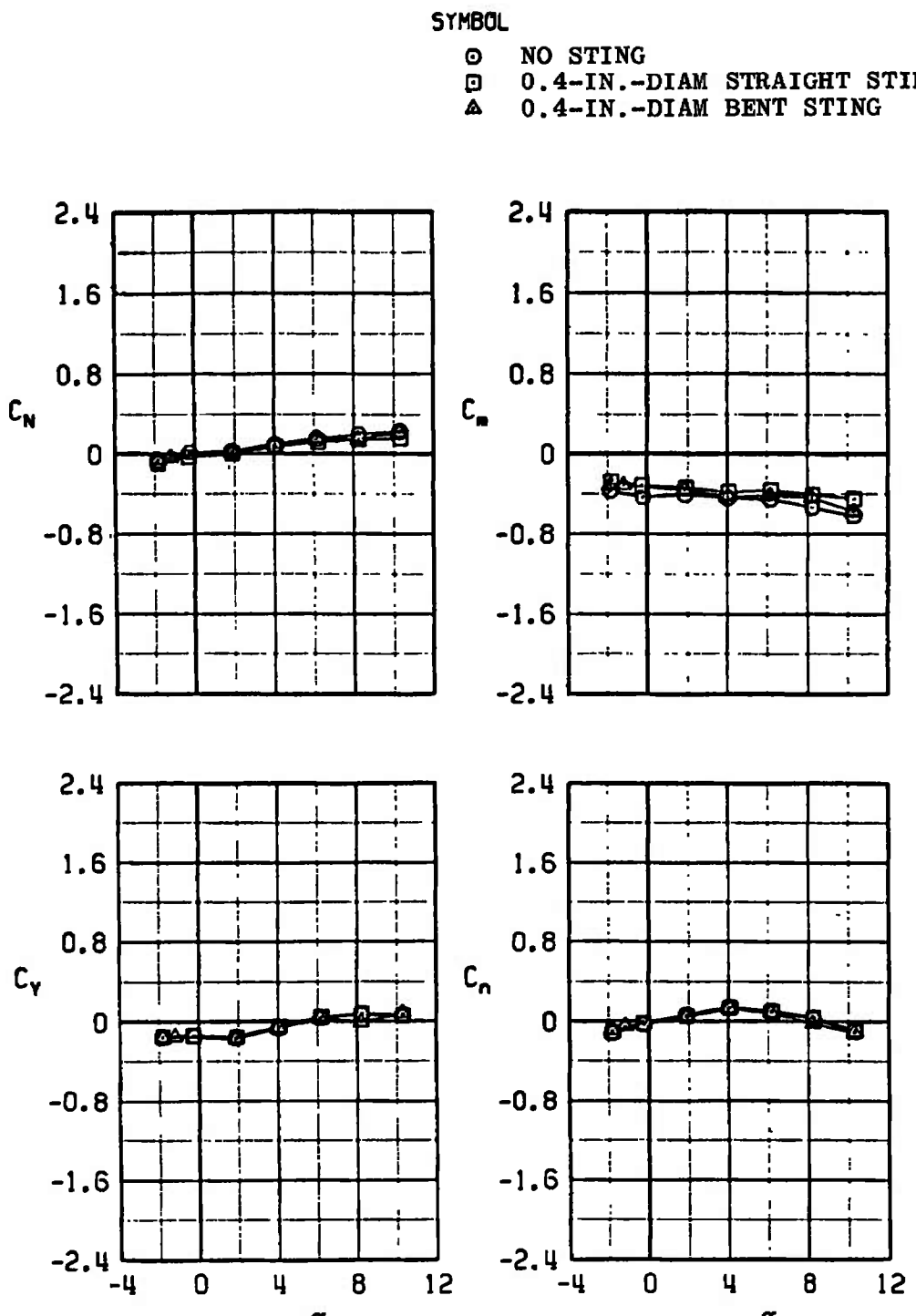
b. $M_\infty = 0.90$
Figure 28. Continued.

67

SYMBOL

⊙   NO STING
⊡   0.4-IN.-DIAM STRAIGHT STING
△   0.4-IN.-DIAM BENT STING
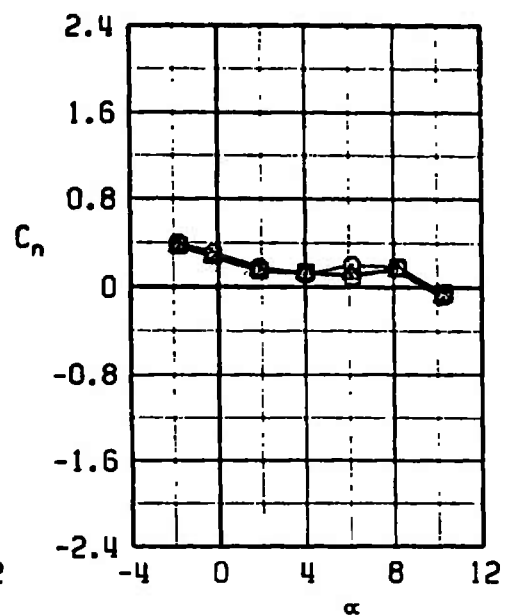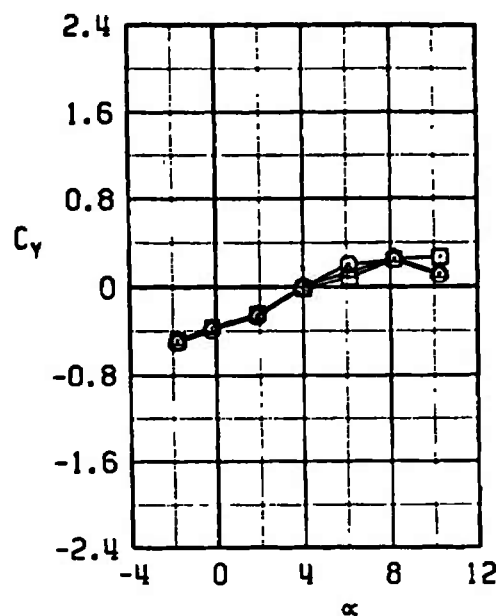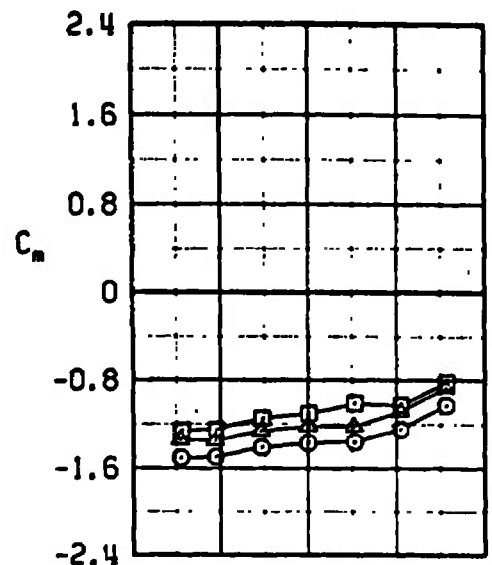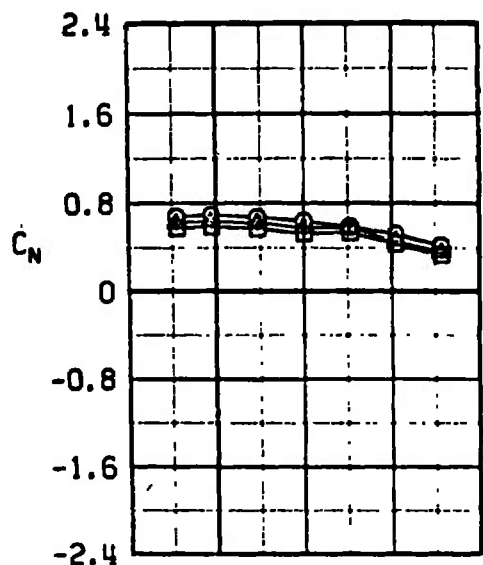
c. M_∞ = 1.05
Figure 28. Concluded.

SYMBOL

⊙ NO STING
▣ 0.4-IN.-DIAM STRAIGHT STING
△ 0.4-IN.-DIAM BENT STING
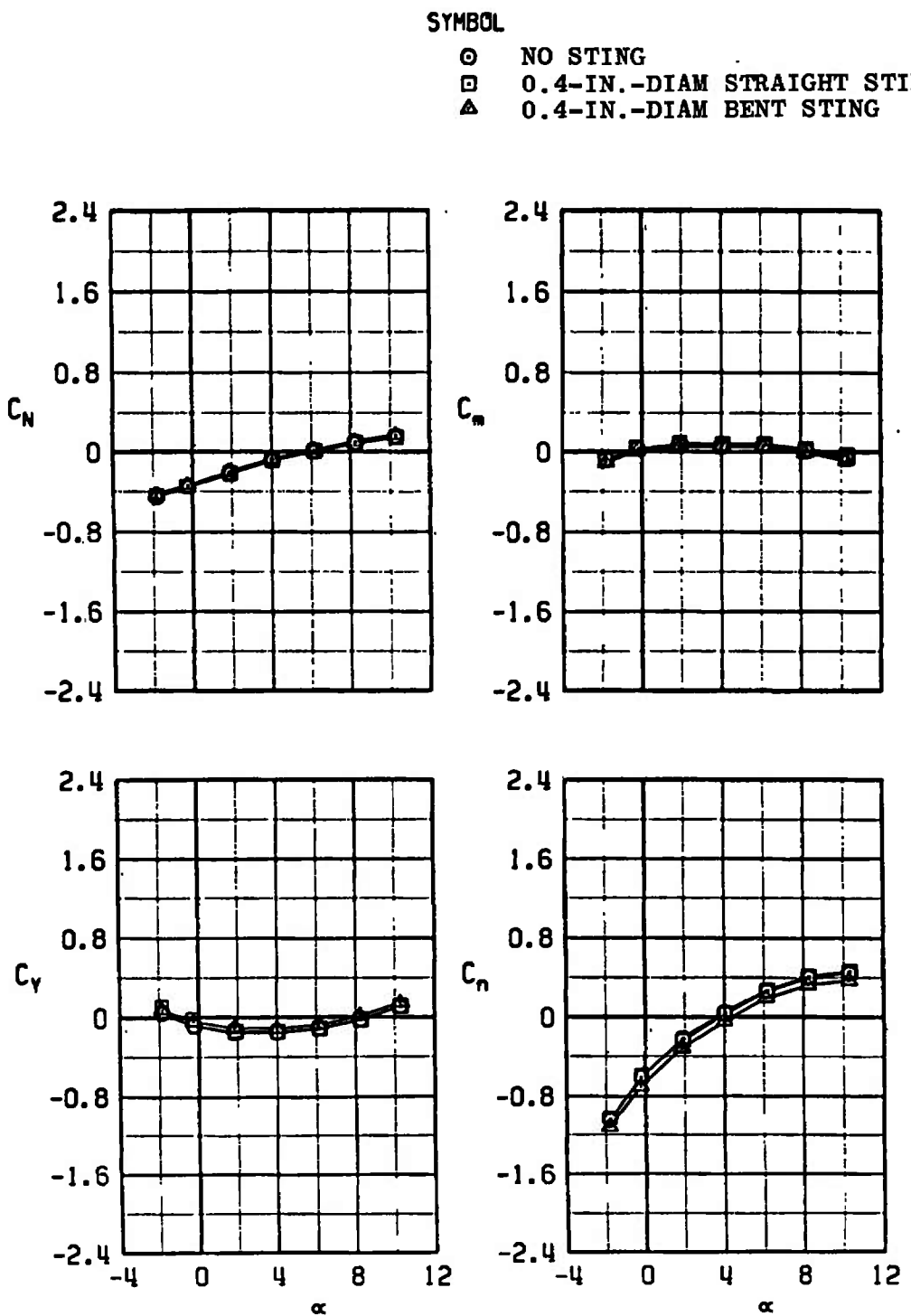
a. $M_\infty = 0.70$

Figure 29. Comparison of modified M-117 carriage-position aerodynamic
coefficients with and without the presence of the 0.4-in.-diam
dummy sting, configuration 1L.

69

SYMBOL

⊙ NO STING
⊡ 0.4-IN.-DIAM STRAIGHT STING
△ 0.4-IN.-DIAM BENT STING
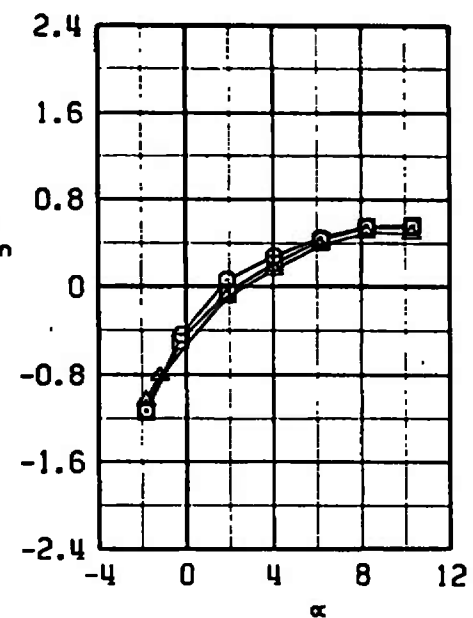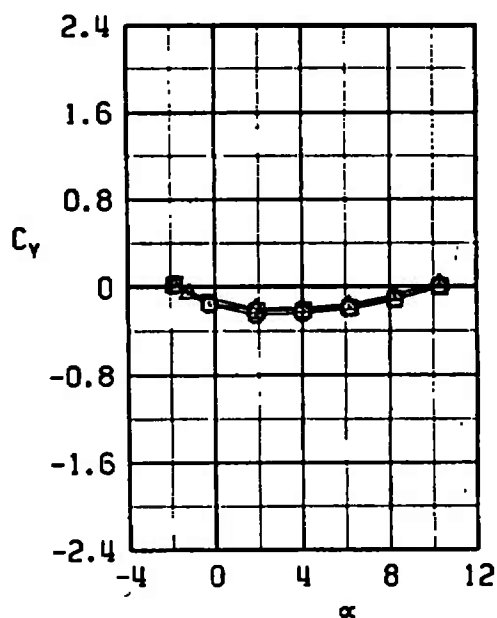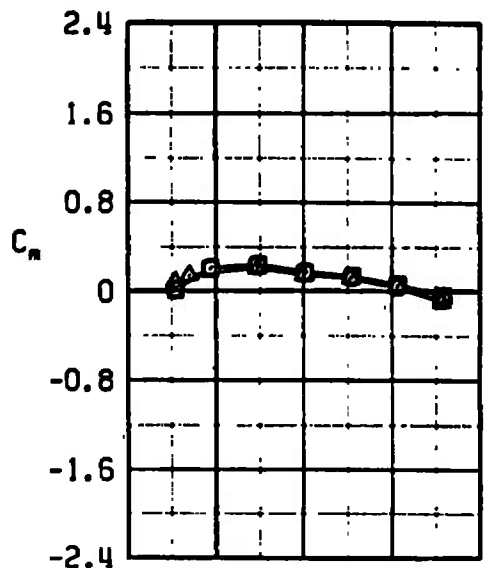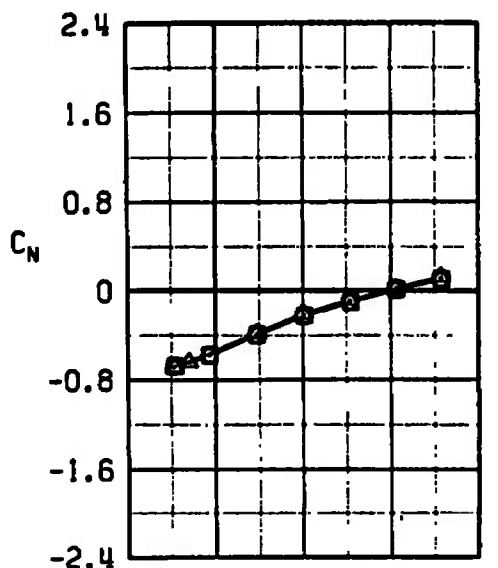
b. $M_\infty = 0.90$
Figure 29. Continued.

SYMBOL
⊙   NO STING
▣   0.4-IN.-DIAM STRAIGHT STING
△   0.4-IN.-DIAM BENT STING
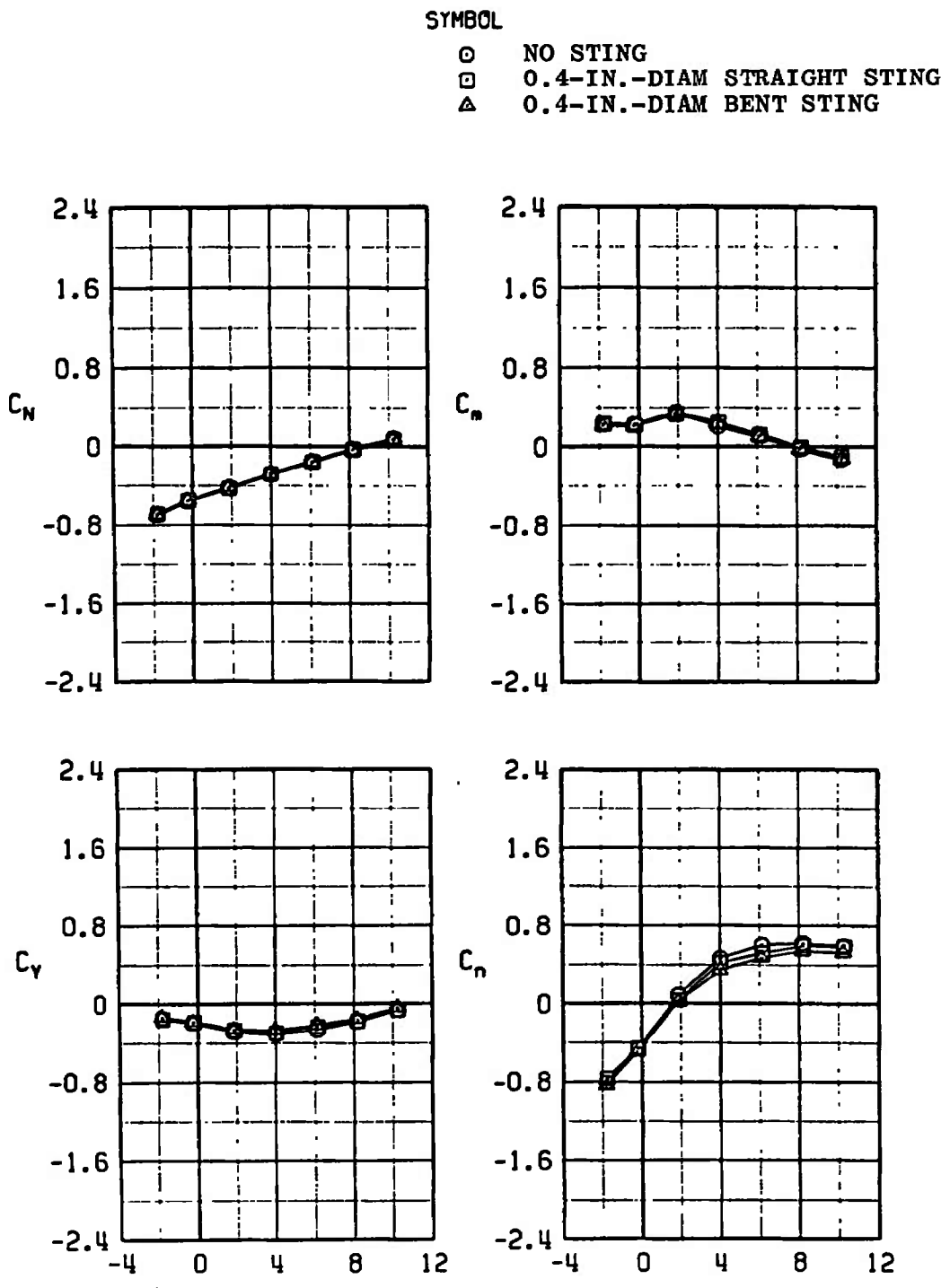
c. M_∞ = 1.05
Figure 29. Concluded.

SYMBOL
⊙   NO STING
⊡   0.4-IN.-DIAM STRAIGHT STING
△   0.4-IN.-DIAM BENT STING
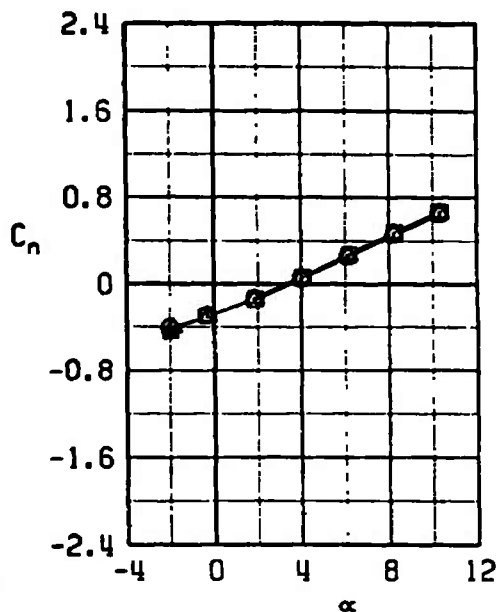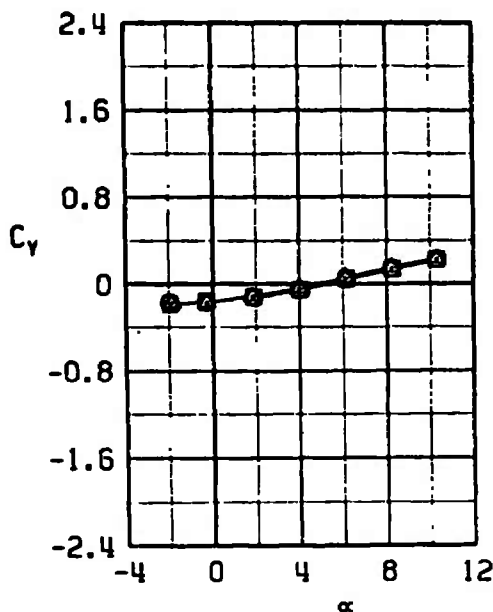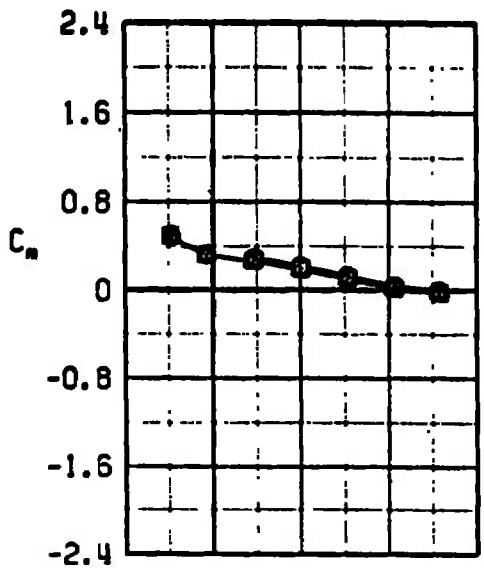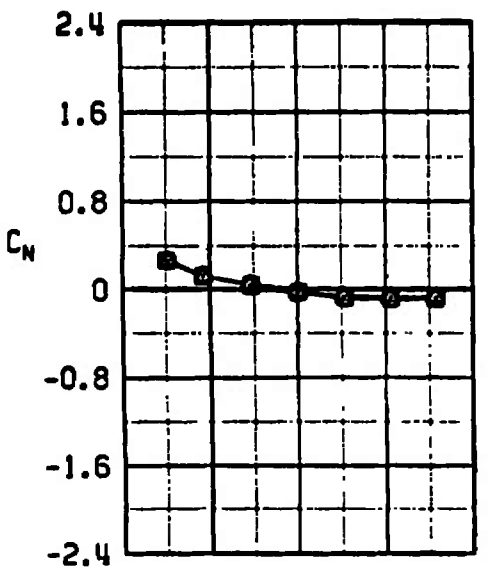
a. $M_\infty = 0.70$

Figure 30. Comparison of modified unfinned BLU-1C/B carriage-position aerodynamic coefficients with and without the presence of the 0.4-in.-diam dummy sting, configuration 2R.

SYMBOL

⊙ NO STING
⊡ 0.4-IN.-DIAM STRAIGHT STING
△ 0.4-IN.-DIAM BENT STING
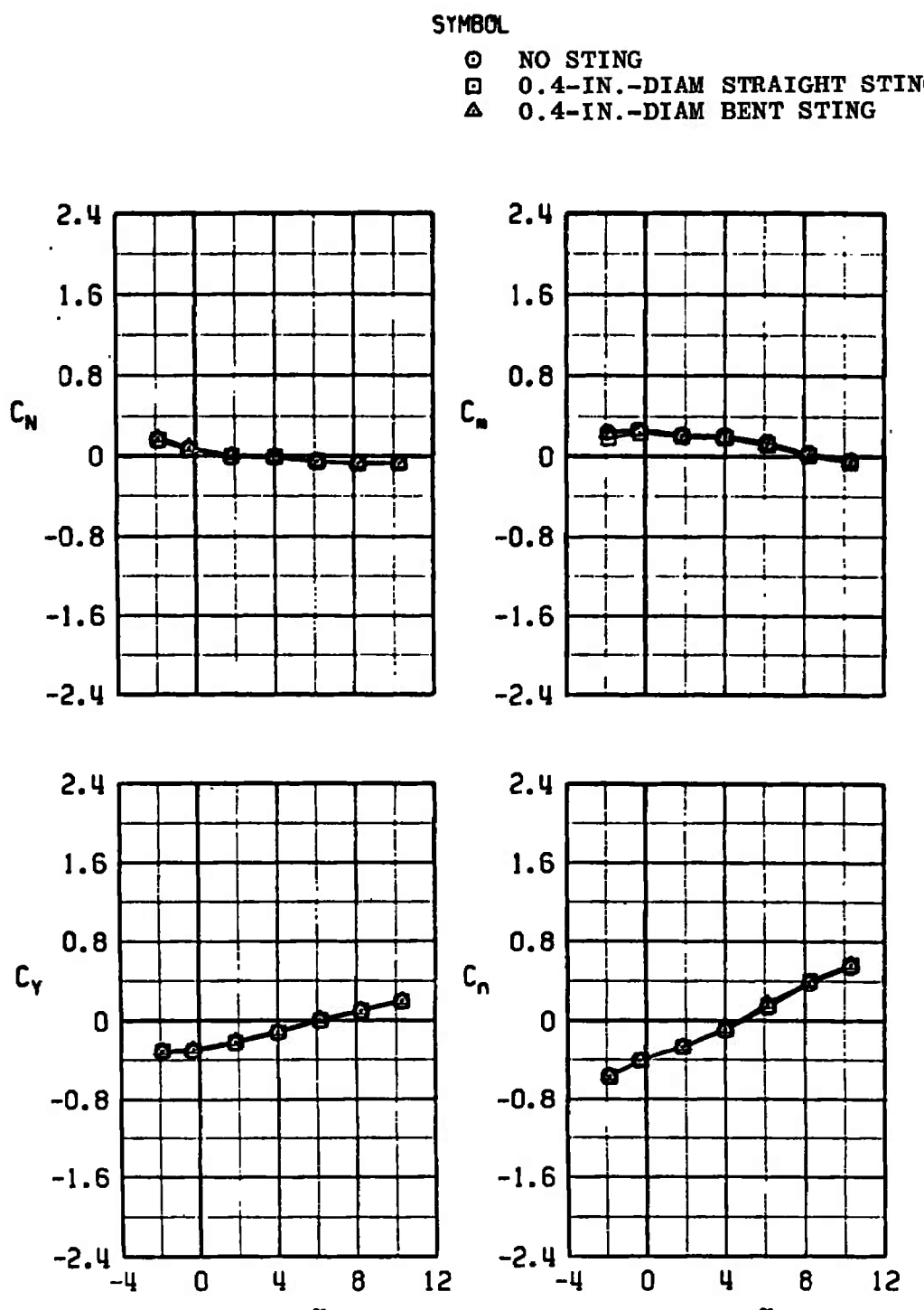
b. $M_\infty = 0.90$
Figure 30. Continued.

SYMBOL
⊙   NO STING
▣   0.4–IN.–DIAM STRAIGHT STING
△   0.4–IN.–DIAM BENT STING
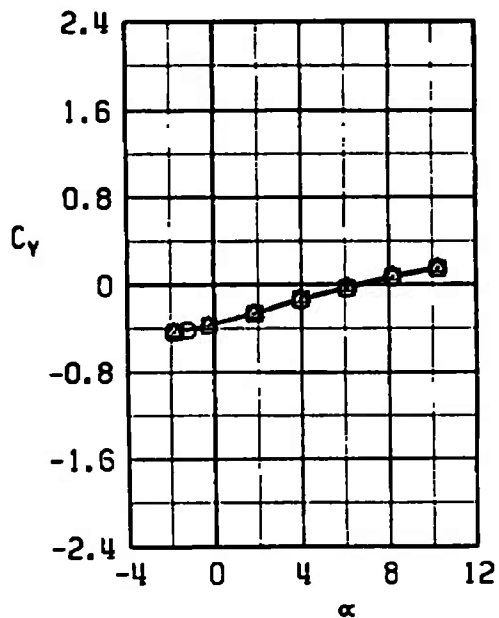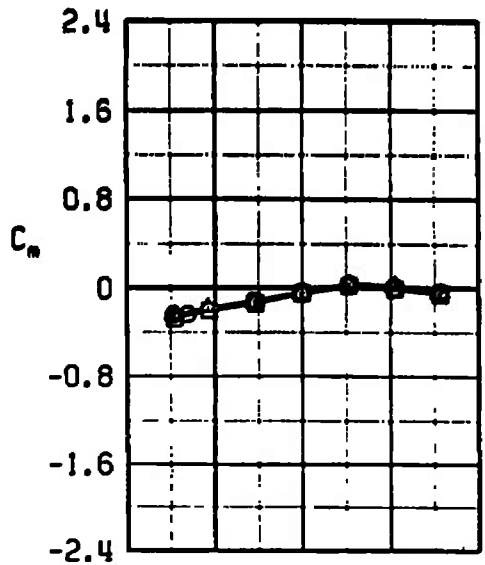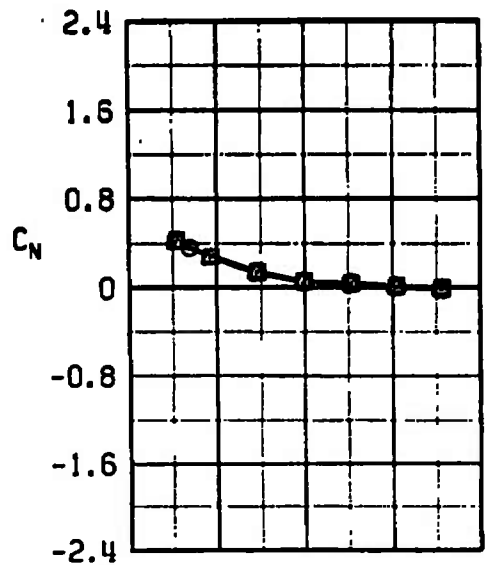
c. M_∞ = 1.05
Figure 30. Concluded.

SYMBOL

⊙ NO STING
▣ 0.4-IN.-DIAM STRAIGHT STING
△ 0.4-IN.-DIAM BENT STING
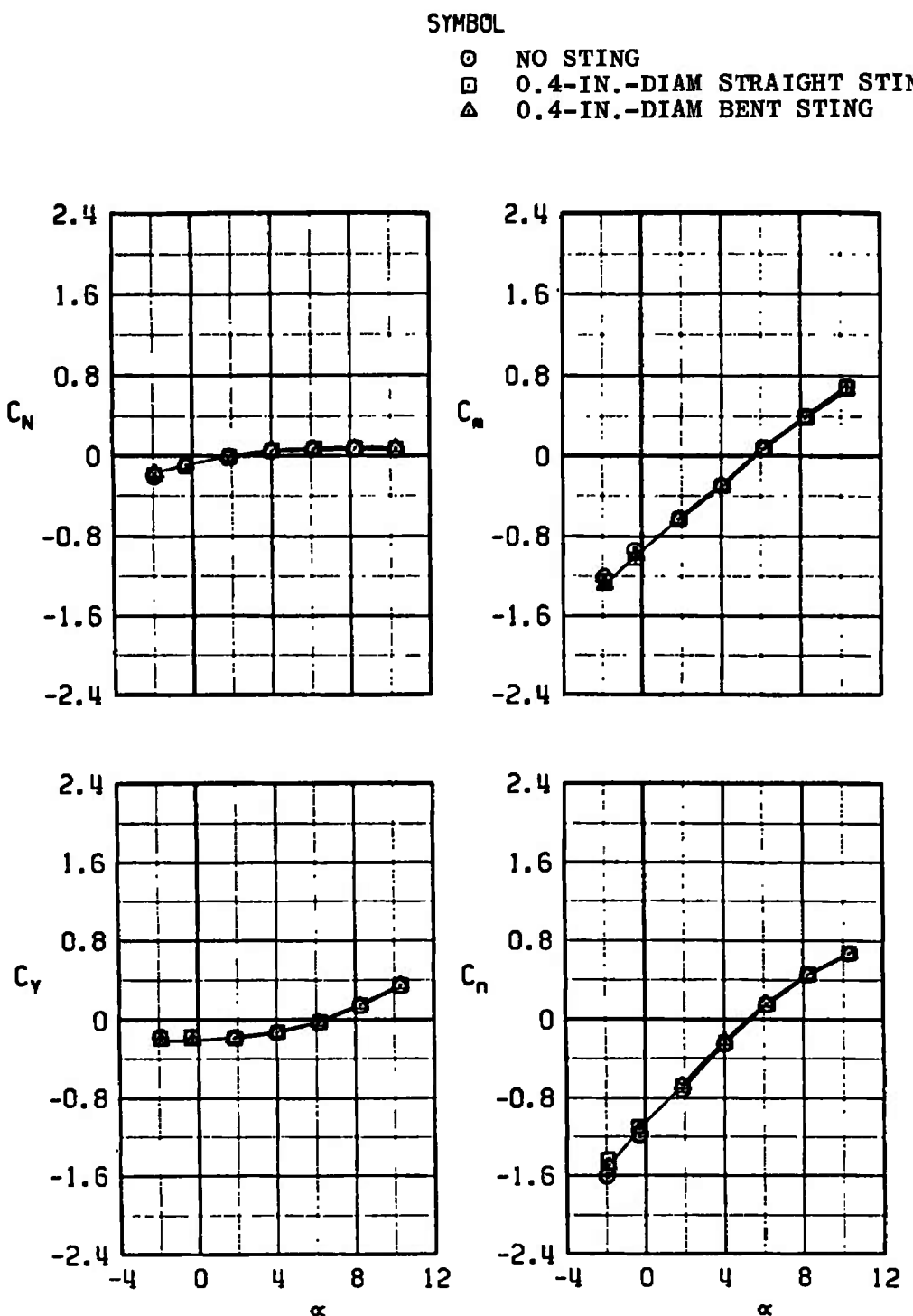
a. $M_\infty = 0.70$

Figure 31. Comparison of modified unfinned BLU-1C/B carriage-position aerodynamic coefficients with and without the presence of the 0.4-in.-diam dummy sting, configuration 2L.

SYMBOL
⊙   NO STING
▣   0.4-IN.-DIAM STRAIGHT STING
△   0.4-IN.-DIAM BENT STING
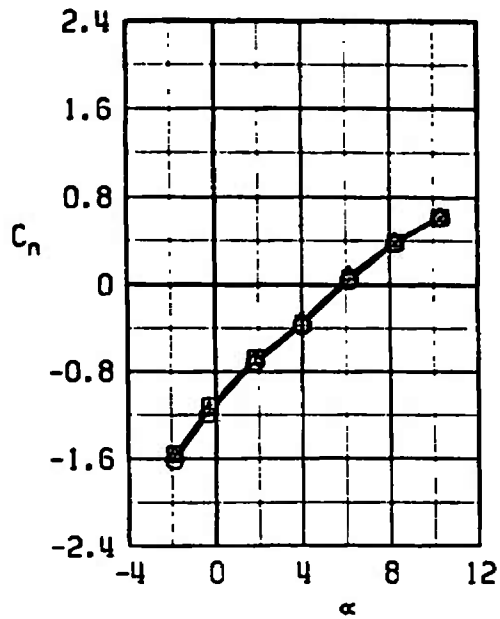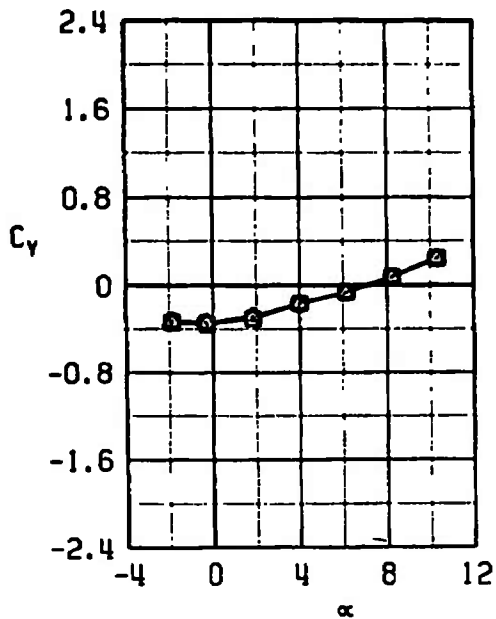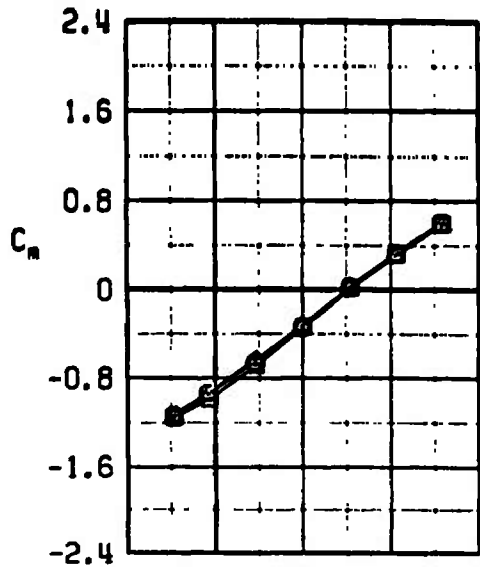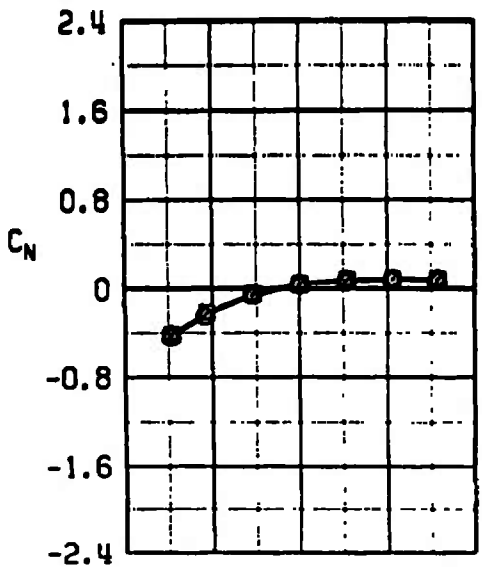
b. $M_\infty = 0.90$
Figure 31. Continued.

SYMBOL
⊙   NO STING
▣   0.4-IN.-DIAM STRAIGHT STING
△   0.4-IN.-DIAM BENT STING
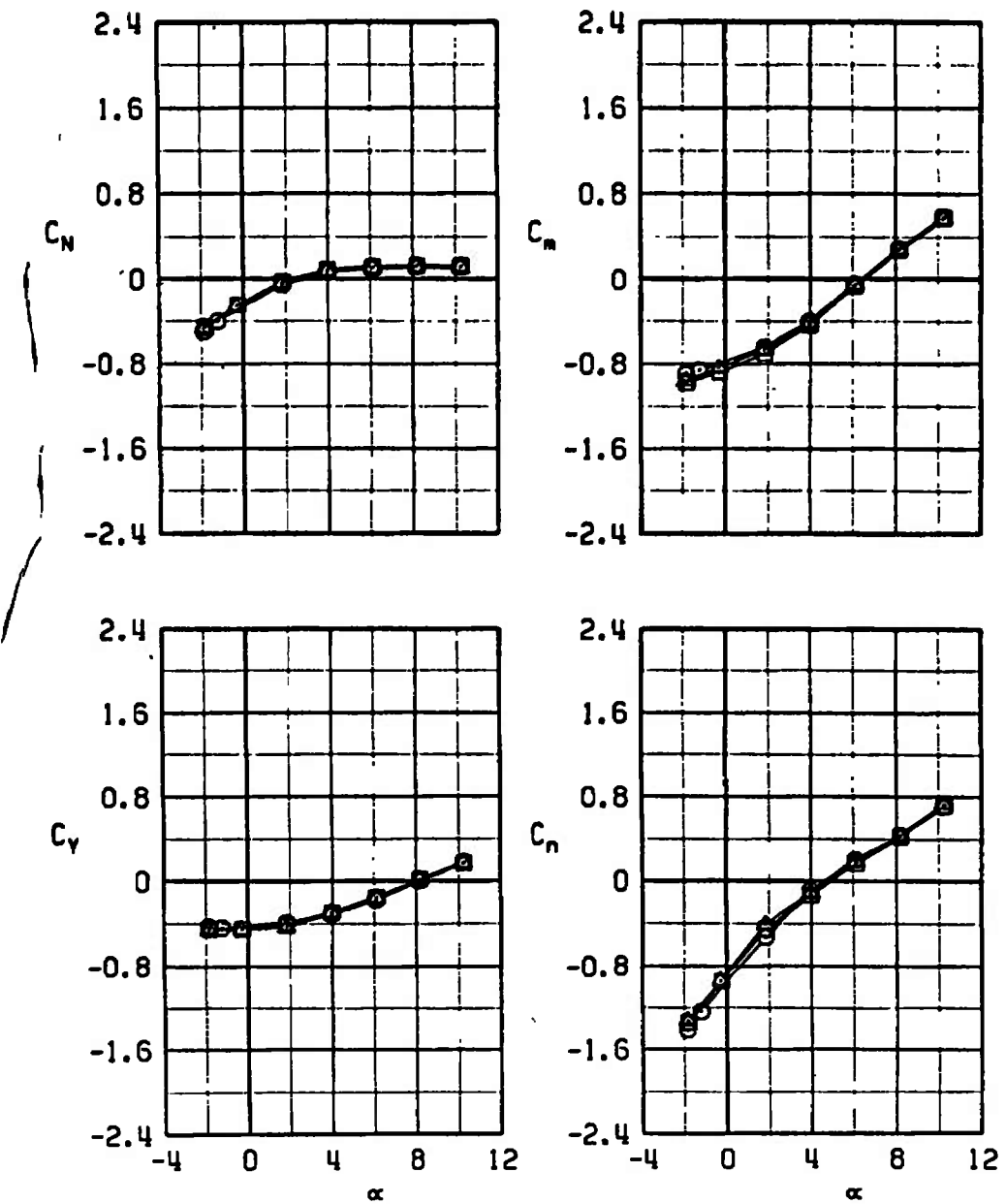
c. M_∞ = 1.05
Figure 31. Concluded.

SYMBOL
⊙ NO STING
⊡ 0.4-IN.-DIAM STRAIGHT STING
△ 0.4-IN.-DIAM BENT STING
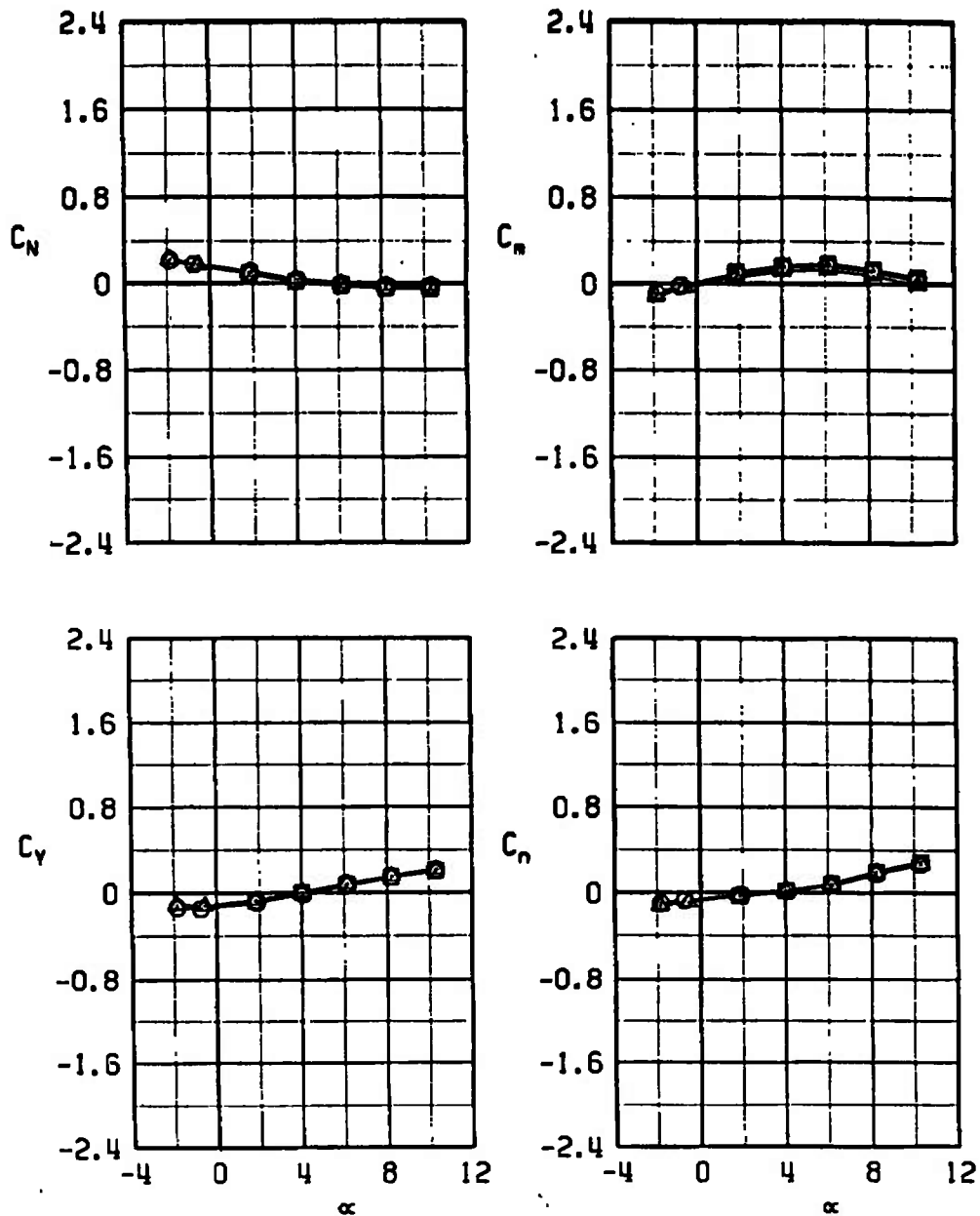
a. $M_\infty = 0.70$
Figure 32. Comparison of modified finned BLU-1C/B carriage-position
aerodynamic coefficients with and without the presence of
the 0.4-in.-diam dummy sting, configuration 3R.

78

SYMBOL

⊙ NO STING
⬚ 0.4-IN.-DIAM STRAIGHT STING
△ 0.4-IN.-DIAM BENT STING
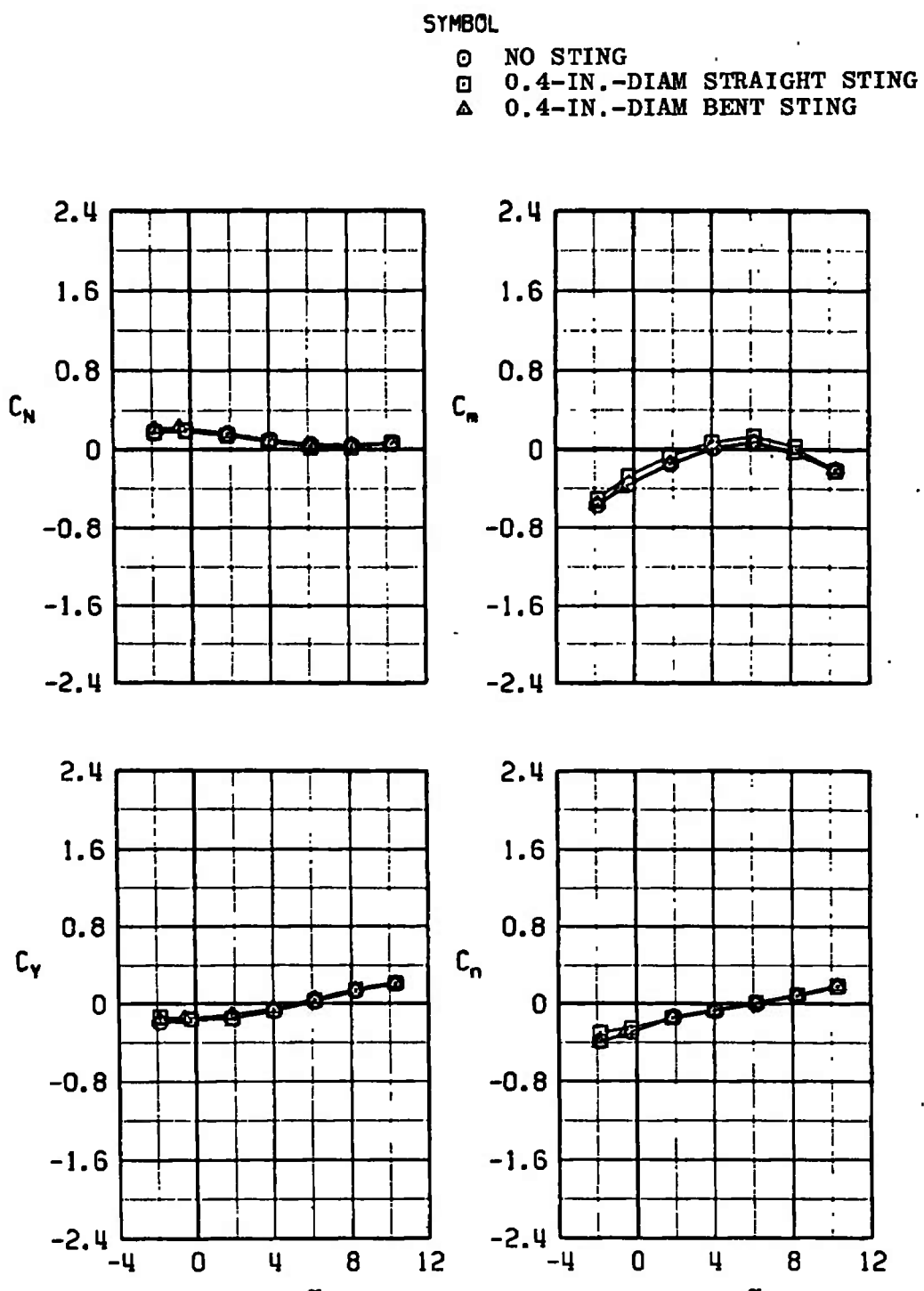
b. $M_\infty = 0.90$
Figure 32. Continued.

79

SYMBOL

⊙   NO STING
⊡   0.4-IN.-DIAM STRAIGHT STING
△   0.4-IN.-DIAM BENT STING
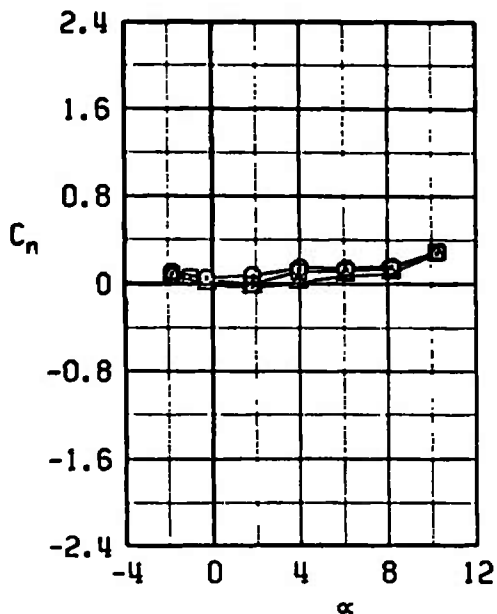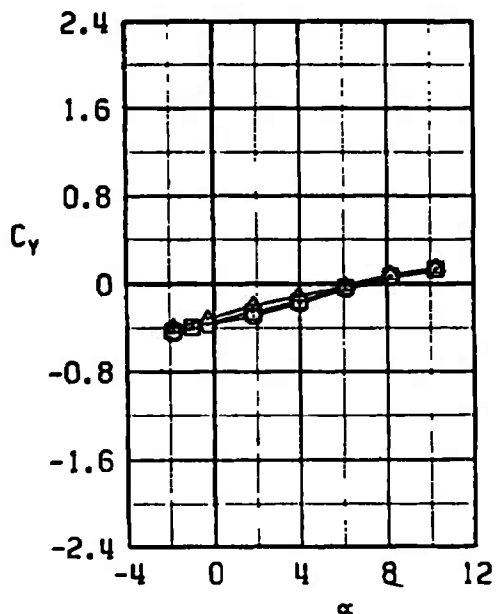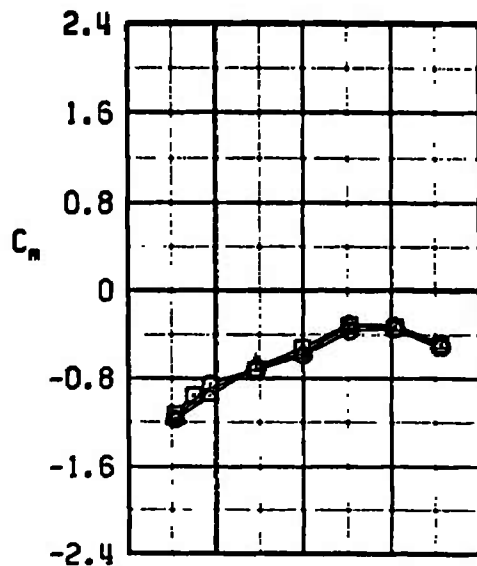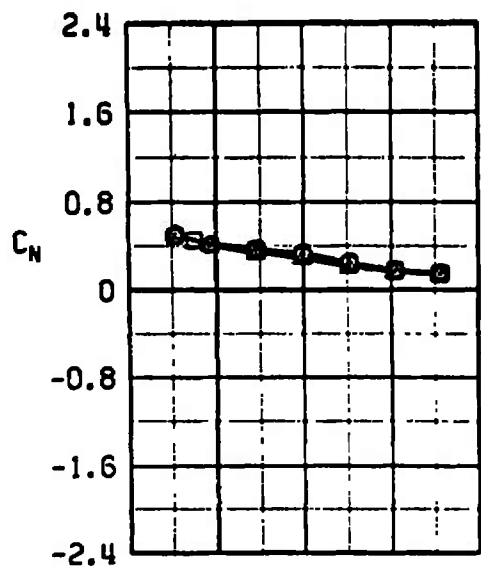
c. M_∞ = 1.05

Figure 32. Concluded.

SYMBOL

⊙   NO STING
⊡   0.4-IN.-DIAM STRAIGHT STING
△   0.4-IN.-DIAM BENT STING
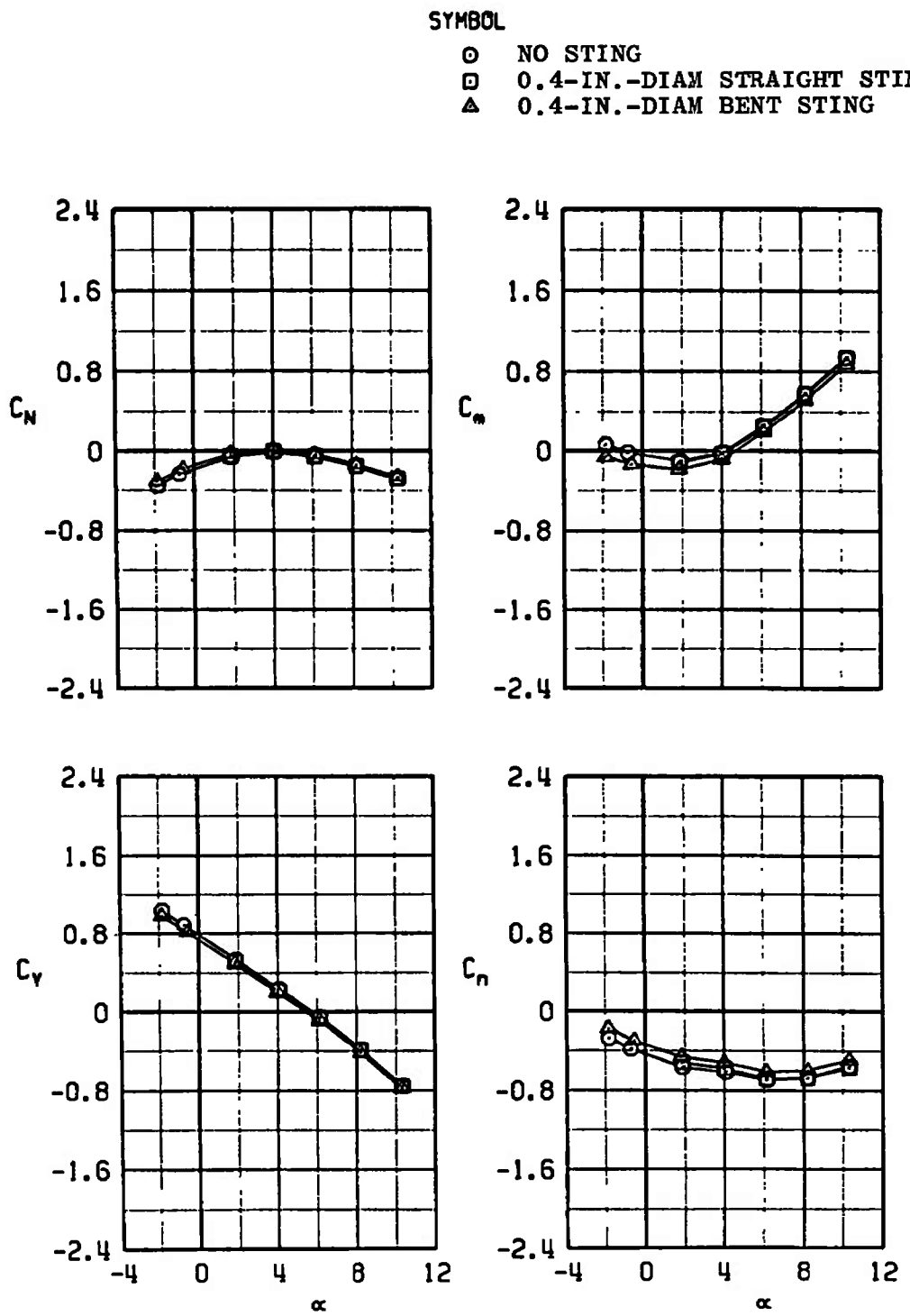
a. M_∞ = 0.70

Figure 33. Comparison of modified finned BLU-1C/B carriage-position
aerodynamic coefficients with and without the presence of
the 0.4-in.-diam dummy sting, configuration 3L.

SYMBOL

⊙   NO STING
⊡   0.4-IN.-DIAM STRAIGHT STING
△   0.4-IN.-DIAM BENT STING
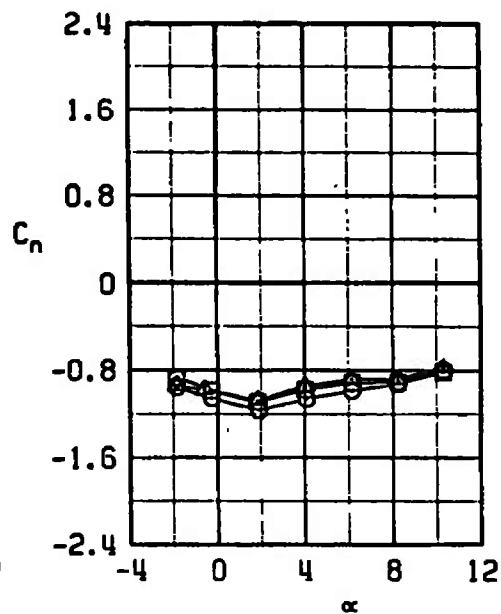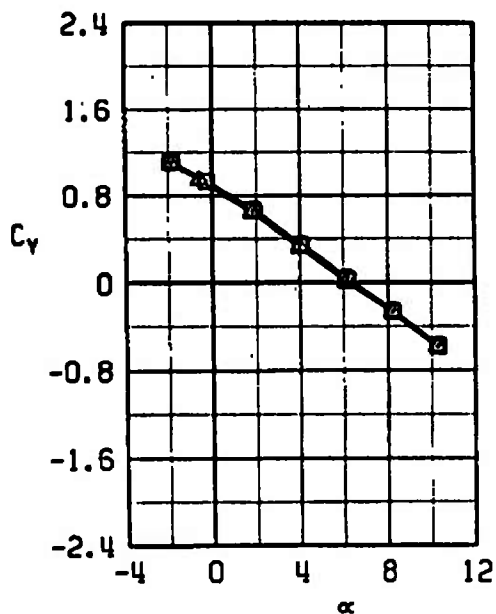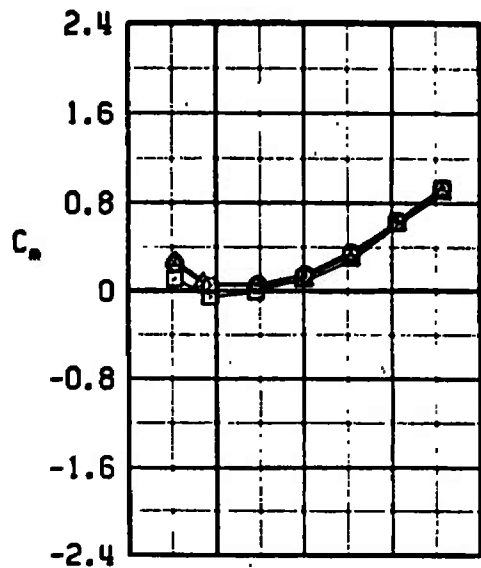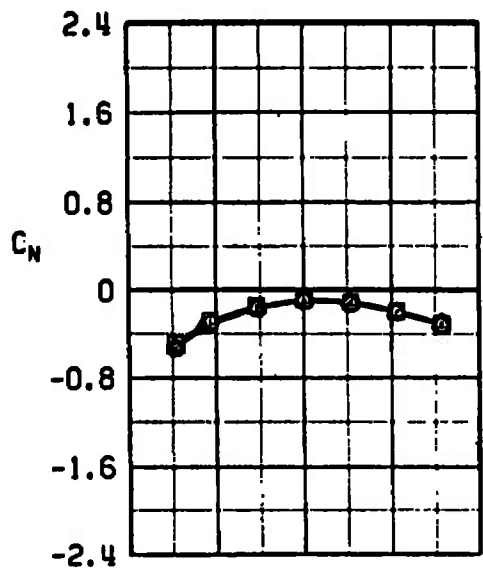
b. $M_\infty = 0.90$
Figure 33. Continued.

SYMBOL
⊙   NO STING
▣   0.4-IN.-DIAM STRAIGHT STING
△   0.4-IN.-DIAM BENT STING
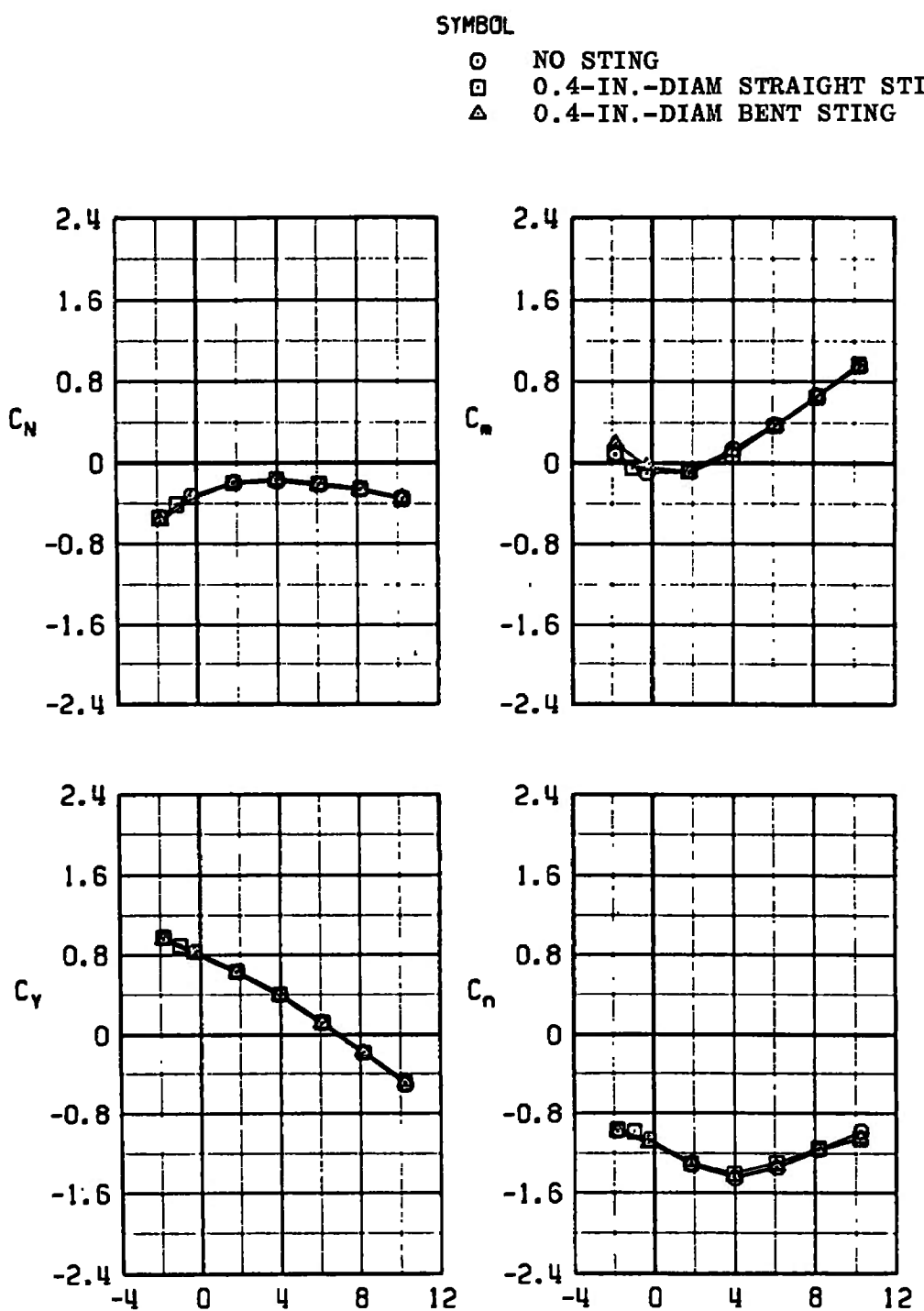
c. $M_\infty = 1.05$
Figure 33. Concluded.
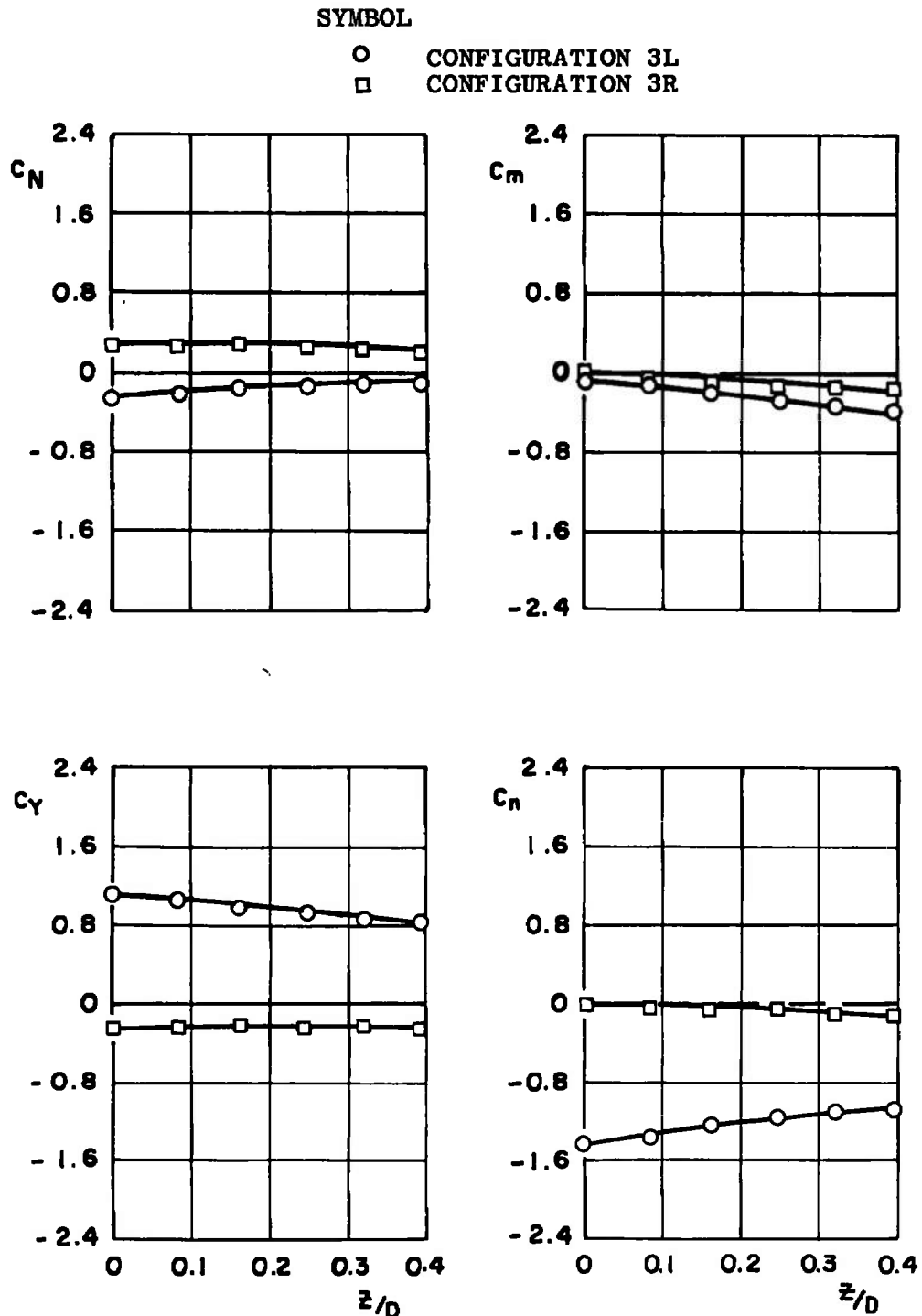
Figure 34. Variation of the finned BLU-1C/B aerodynamic coefficients with distance from the carriage position, $M_\infty = 0.9$, $a = 0$.

SYMBOL

O   CONFIGURATION 2L
△   CONFIGURATION 2R
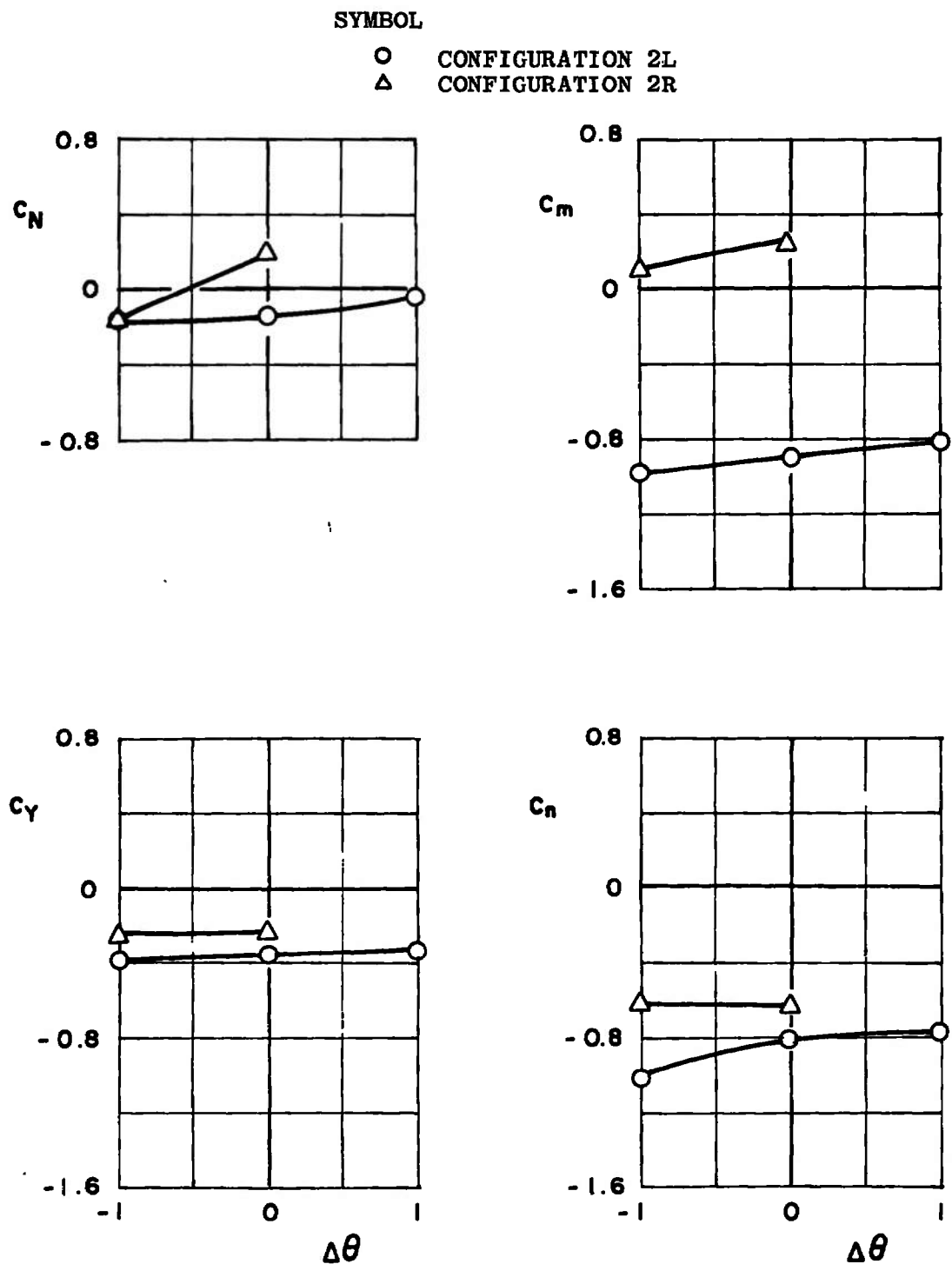
Figure 35. Variation in carriage-position aerodynamic coefficients on the
unfinned BLU-1C/B with pitch attitude, $M_\infty = 0.9$, $a = 0$.

SYMBOL
O   CONFIGURATION 2L
△   CONFIGURATION 2R
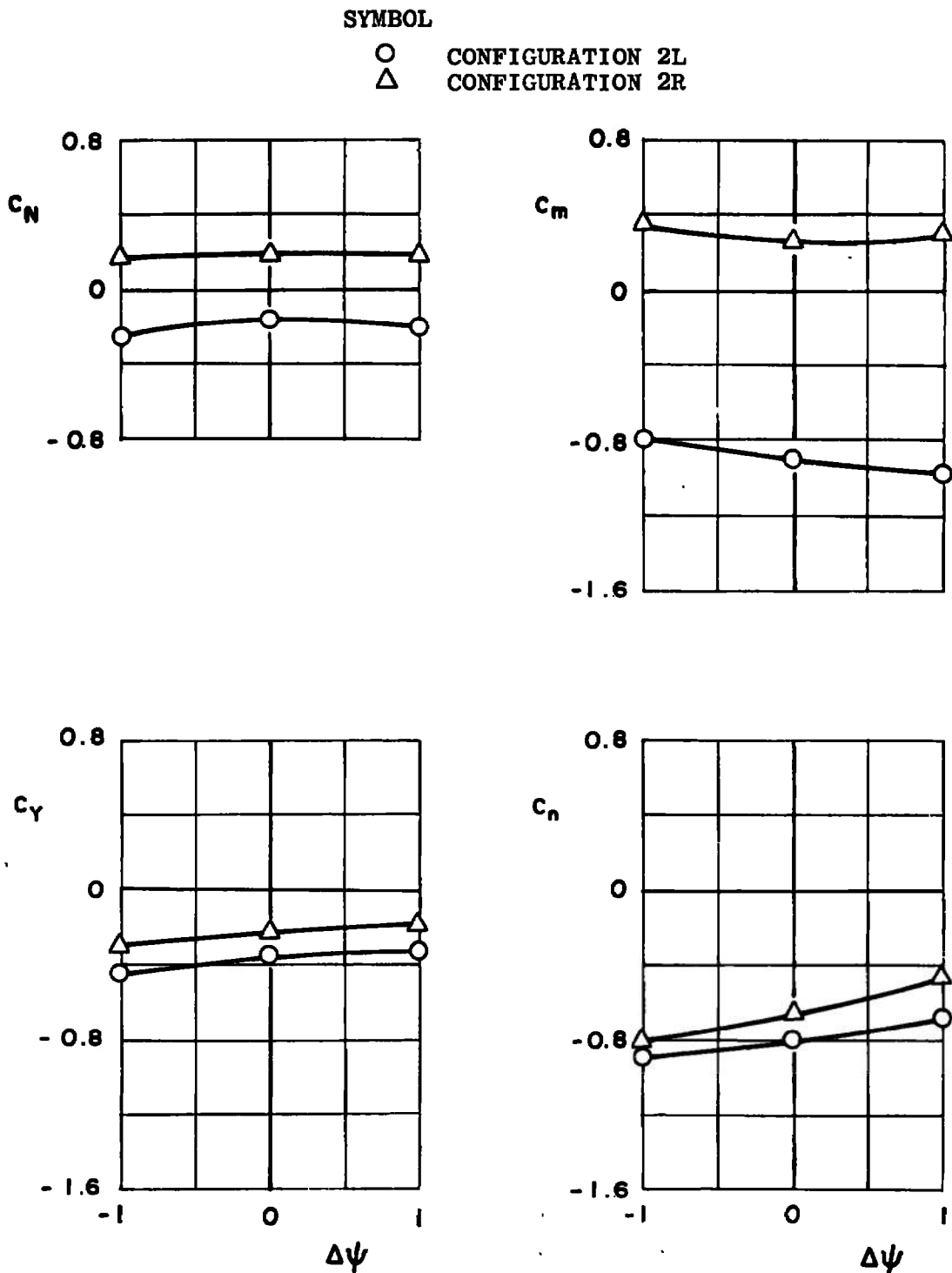
Figure 36. Variation in carriage-position aerodynamic coefficients of the
unfinned BLU-1C/B with store yaw attitude, $M_\infty = 0.9$, $a = 0$.
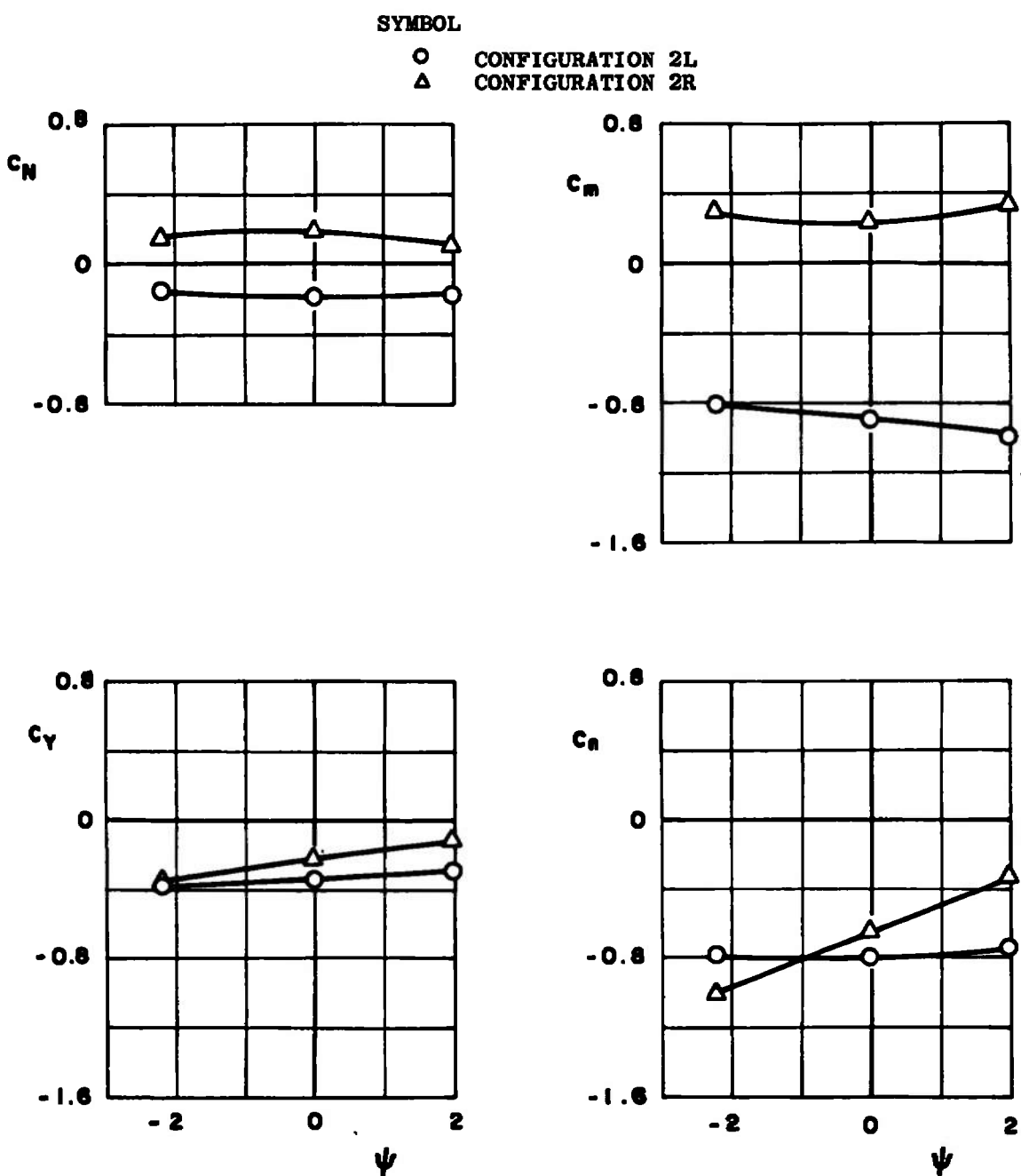
Figure 37. Variation in carriage-position aerodynamic coefficients of the unfinned BLU-1C/B, with aircraft yaw attitude, $M_\infty = 0.9$, $a = 0$.
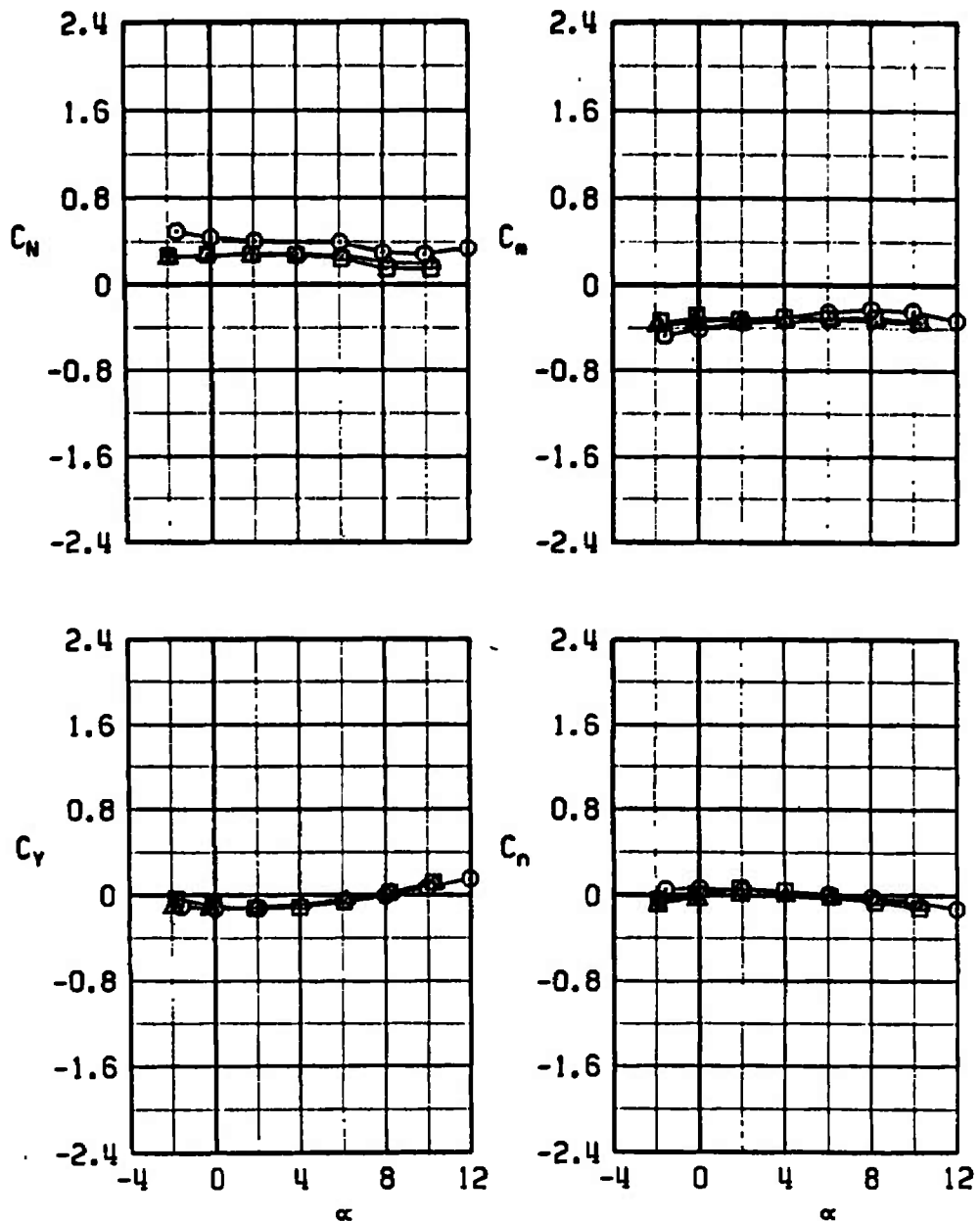
a. $M_\infty = 0.70$

Figure 38. Comparison of M-117 carriage-position aerodynamic coefficients with CTS and rigid loads techniques, configuration 1R.

SYMBOL
- ⊙ MODIFIED – CTS SUPPORTED
- ⊡ MODIFIED – RIGIDLY SUPPORTED
- △ MODIFIED – RIGIDLY SUPPORTED
      0.4–IN.–DIAM STING
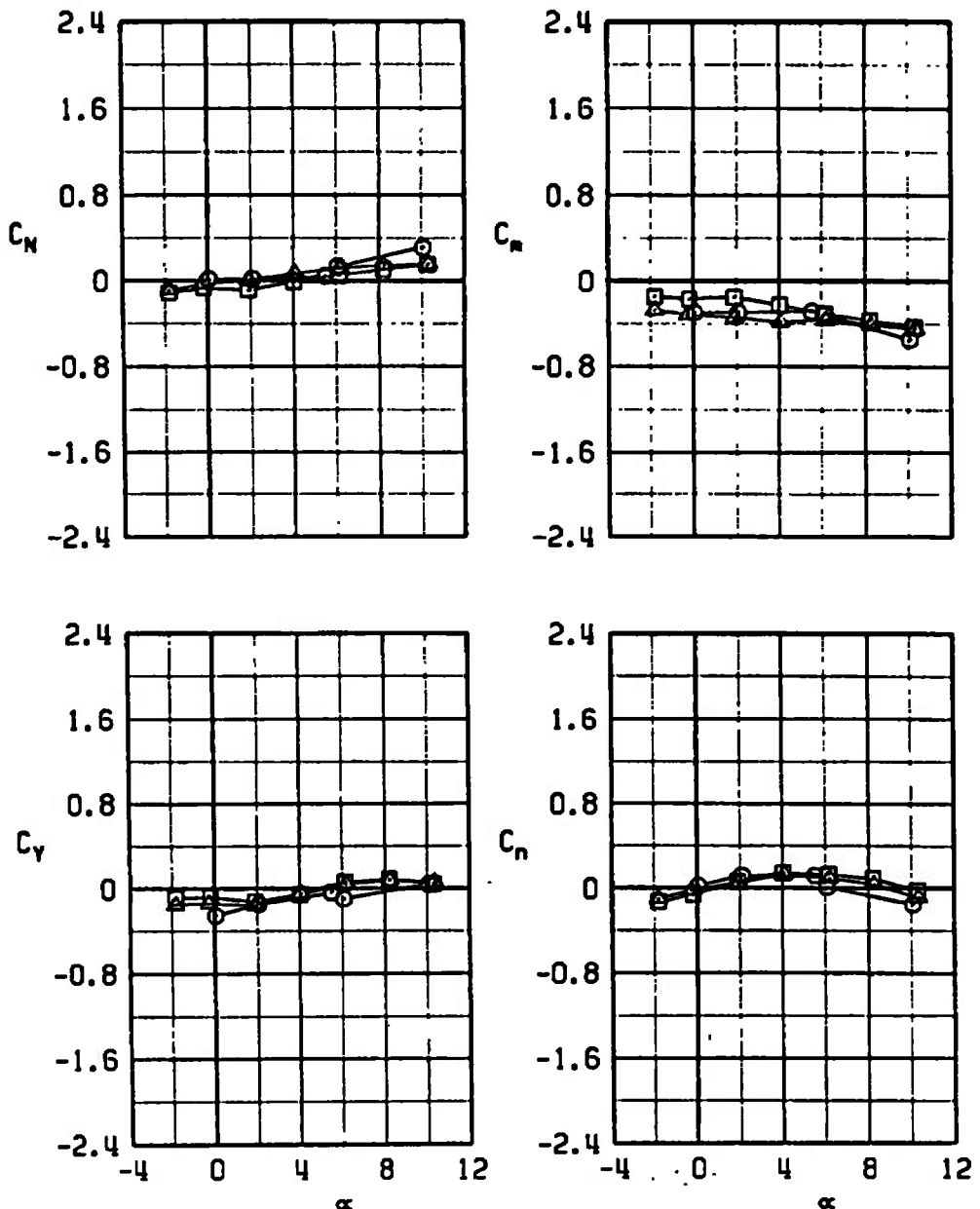
b. $M_\infty = 0.90$
Figure 38. Continued.

SYMBOL

⊙   MODIFIED – CTS SUPPORTED
⊡   MODIFIED – RIGIDLY SUPPORTED
△   MODIFIED – RIGIDLY SUPPORTED
        0.4-IN.-DIAM STING
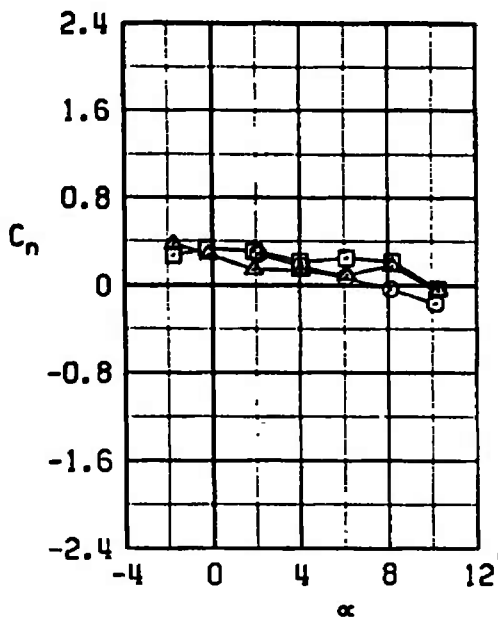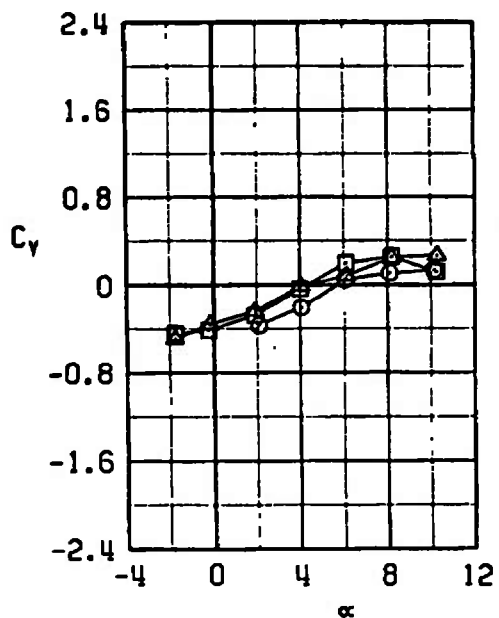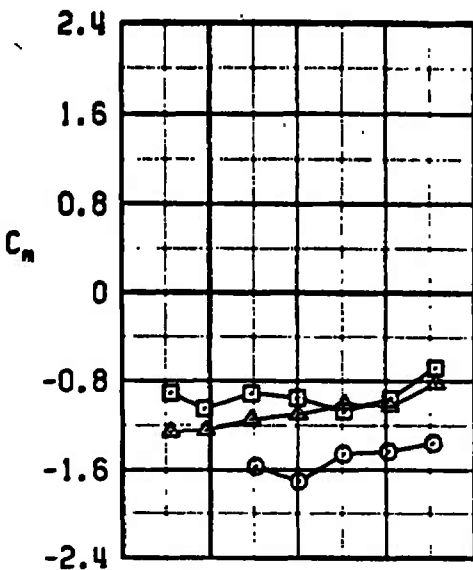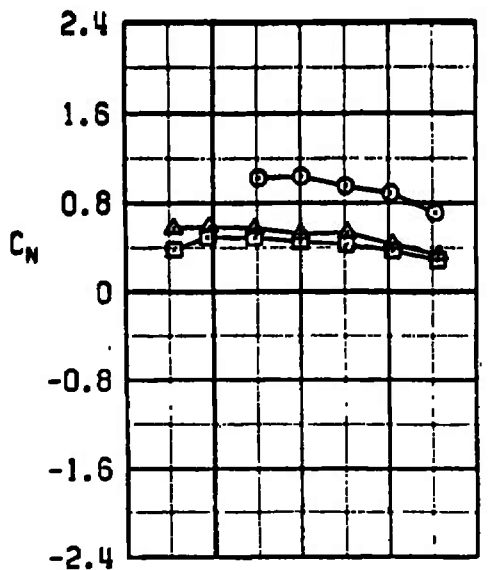
c. $M_\infty = 1.05$
Figure 38. Concluded.

90

SYMBOL
- ⊙ MODIFIED – CTS SUPPORTED
- ⊡ MODIFIED – RIGIDLY SUPPORTED
- △ MODIFIED – RIGIDLY SUPPORTED
  0.4-IN.-DIAM STING
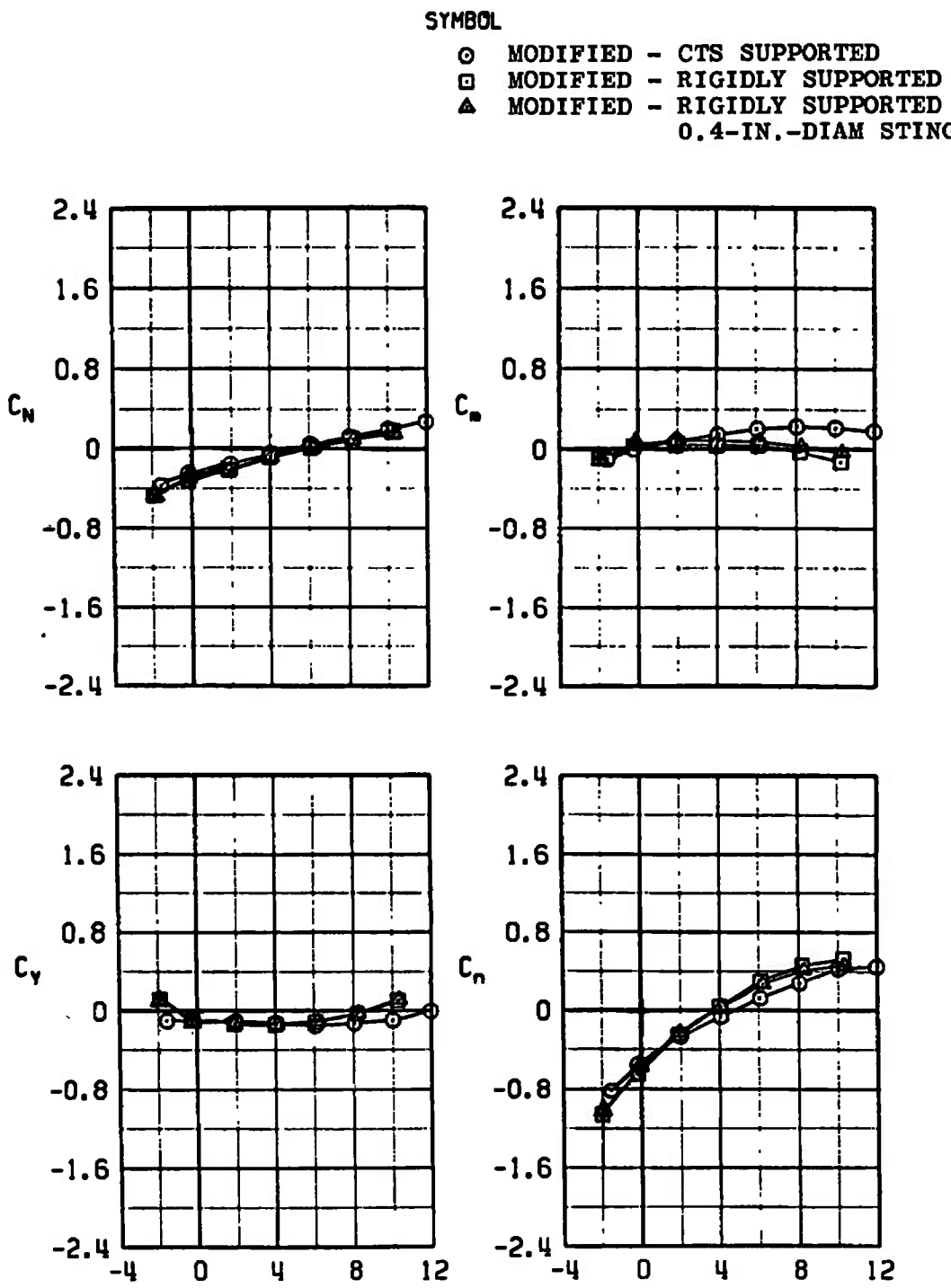
a. $M_\infty = 0.70$

Figure 39. Comparison of M-117 carriage-position aerodynamic coefficients with CTS and rigid loads techniques, configuration 1L.

SYMBOL

⊙   MODIFIED – CTS SUPPORTED
⊡   MODIFIED – RIGIDLY SUPPORTED
△   MODIFIED – RIGIDLY SUPPORTED
        0.4–IN.–DIAM STING
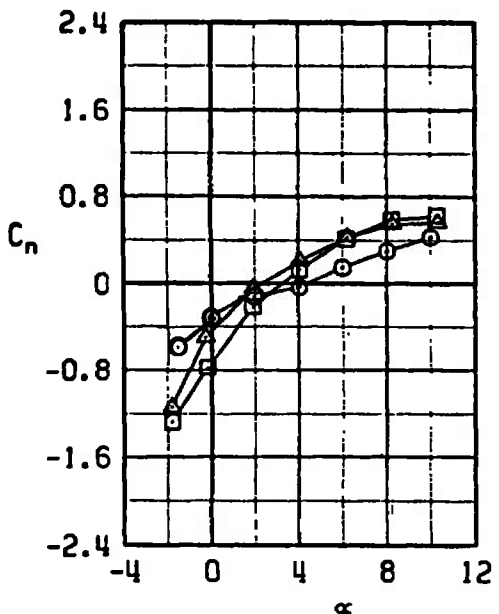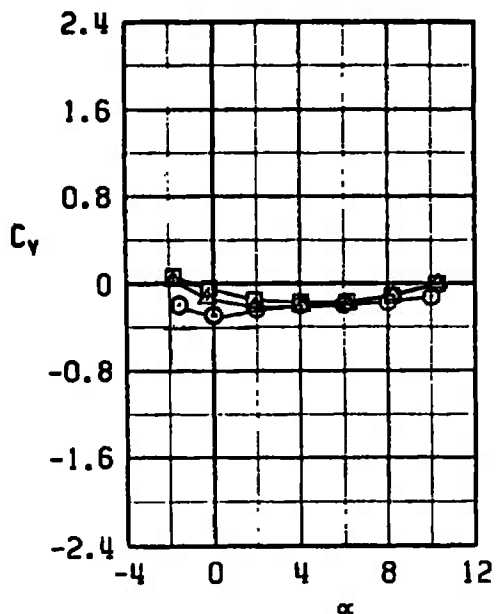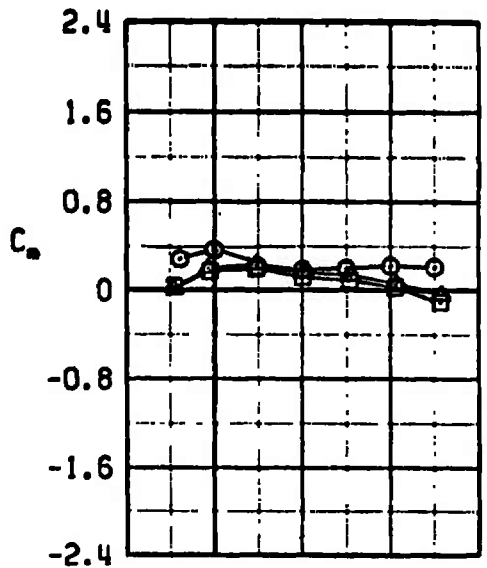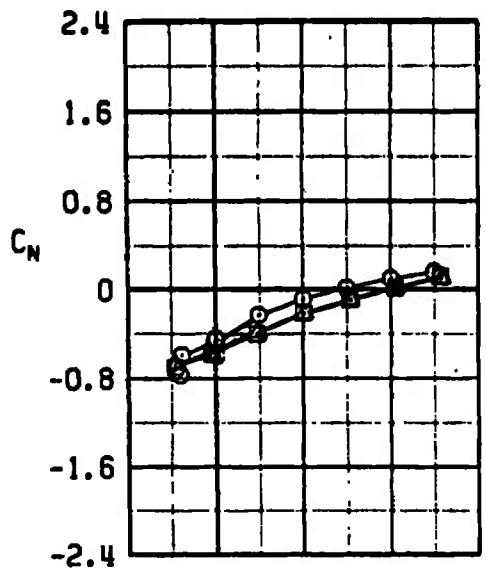
b. $M_\infty = 0.90$
Figure 39. Continued.

SYMBOL

⊙   MODIFIED – CTS SUPPORTED
⊡   MODIFIED – RIGIDLY SUPPORTED
△   MODIFIED – RIGIDLY SUPPORTED
         0.4–IN.–DIAM STING
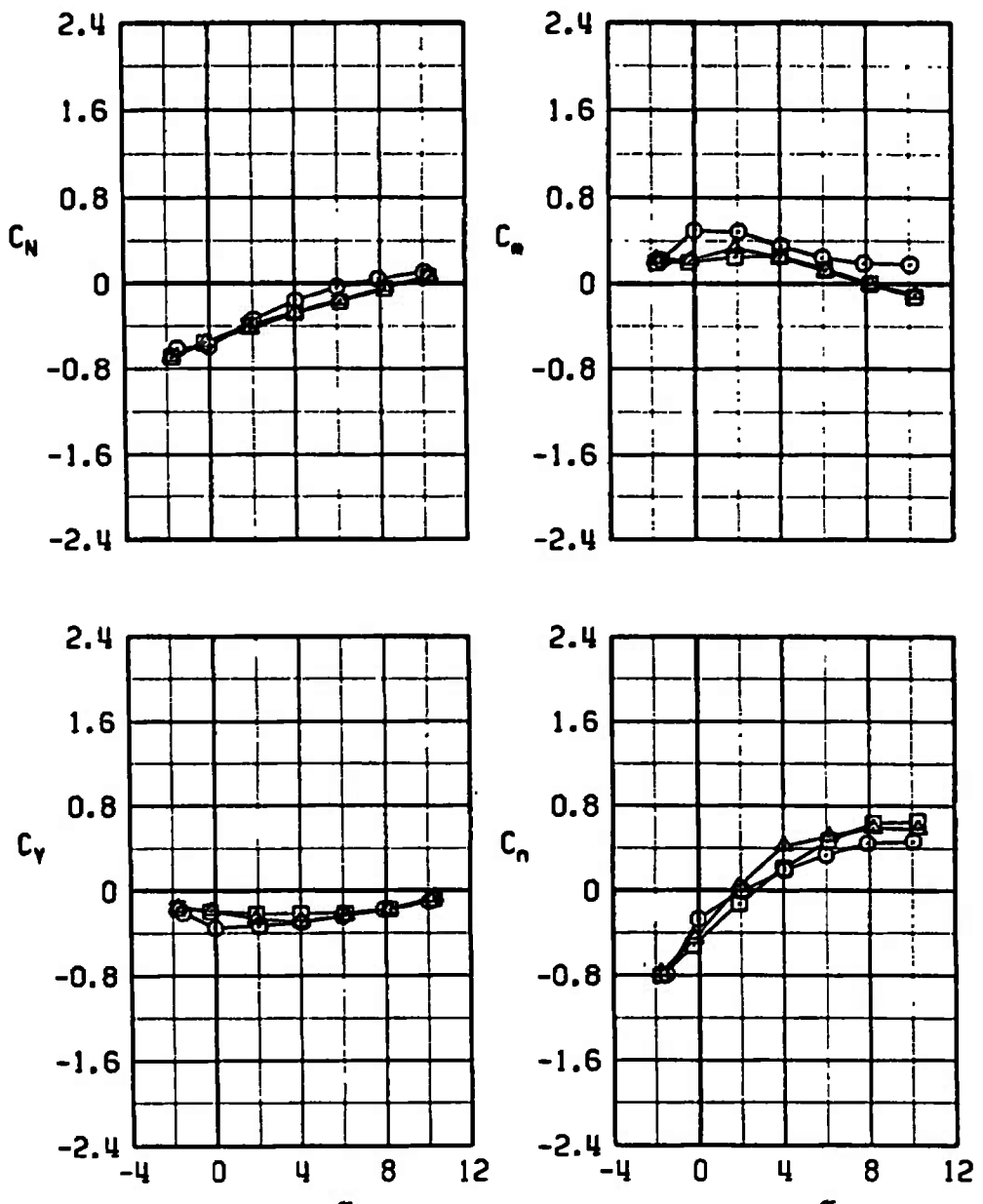
c. $M_\infty = 1.05$
Figure 39. Concluded.

SYMBOL

⊙ MODIFIED – CTS SUPPORTED
▣ MODIFIED – RIGIDLY SUPPORTED
△ MODIFIED – RIGIDLY SUPPORTED
　　0.4–IN.–DIAM
　　STRAIGHT STING
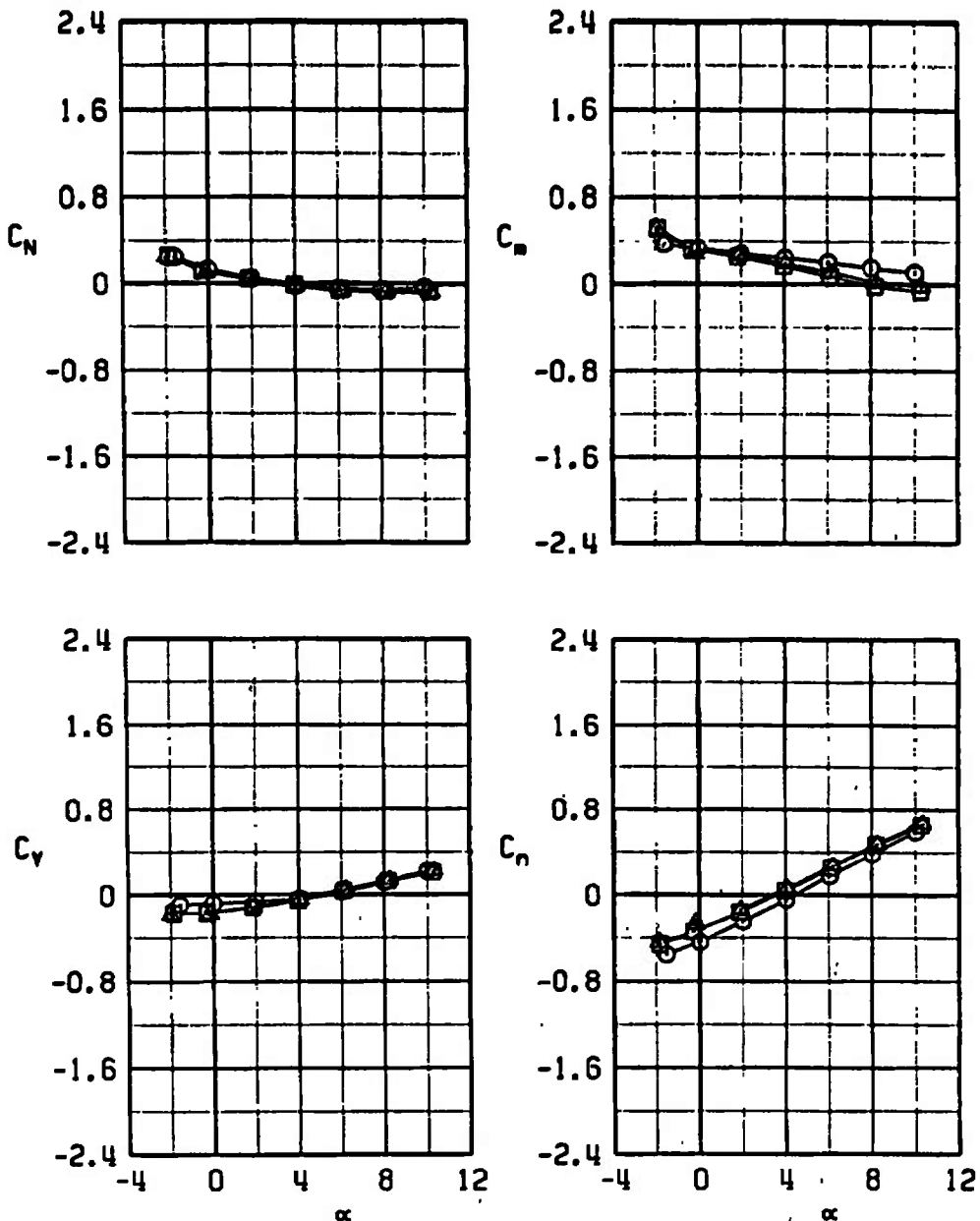
a. $M_\infty = 0.70$

Figure 40. Comparison of unfinned BLU-1C/B carriage-position aerodynamic coefficients with CTS and rigid loads techniques, configuration 2R.

94

SYMBOL

⊙   MODIFIED - CTS SUPPORTED
▣   MODIFIED - RIGIDLY SUPPORTED
△   MODIFIED - RIGIDLY SUPPORTED
      0.4-IN.-DIAM
      STRAIGHT STING
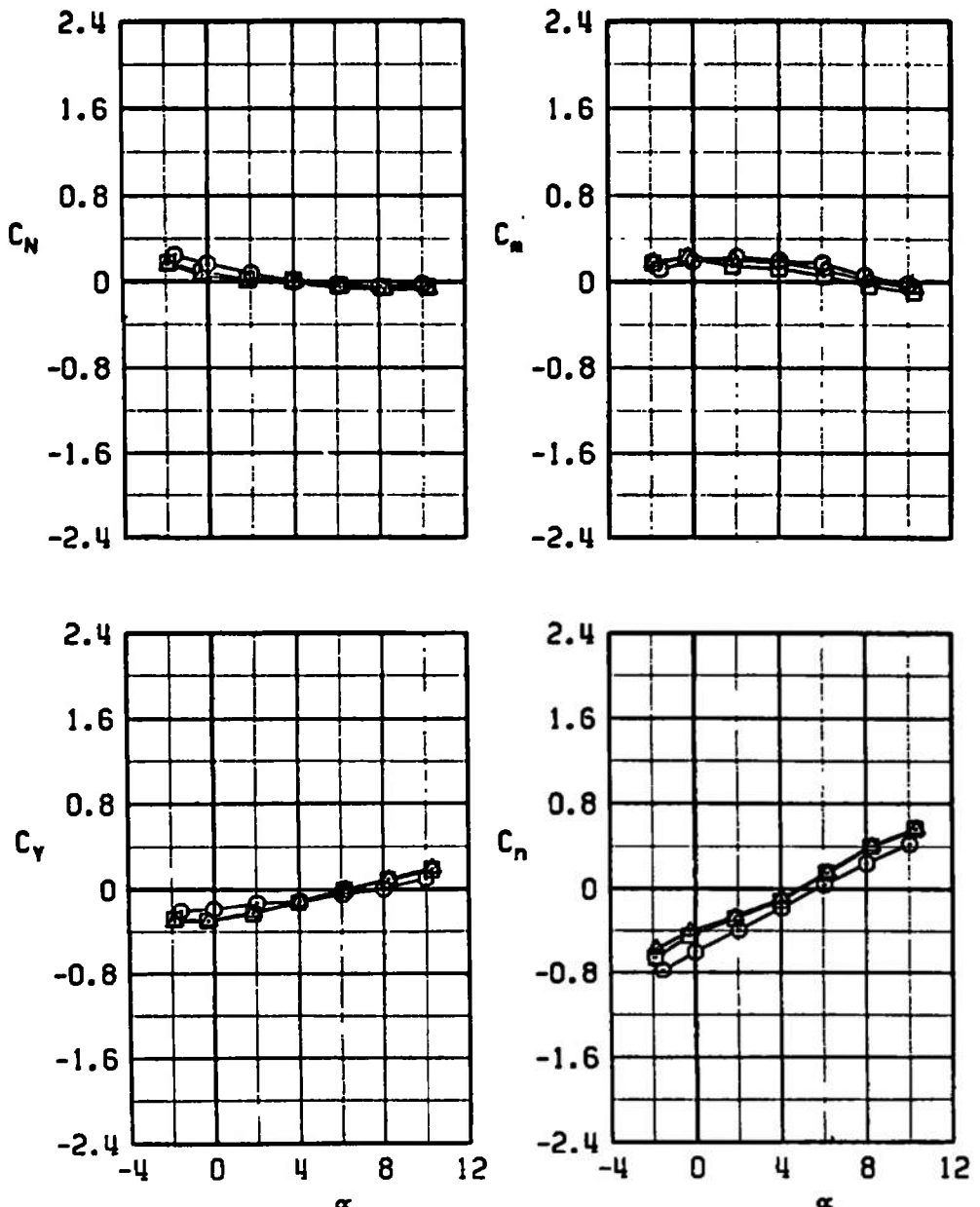
b. M_∞ = 0.90
Figure 40. Continued.

95

SYMBOL
⊙ MODIFIED — CTS SUPPORTED
▣ MODIFIED — RIGIDLY SUPPORTED
△ MODIFIED — RIGIDLY SUPPORTED
0.4-IN.-DIAM
STRAIGHT STING
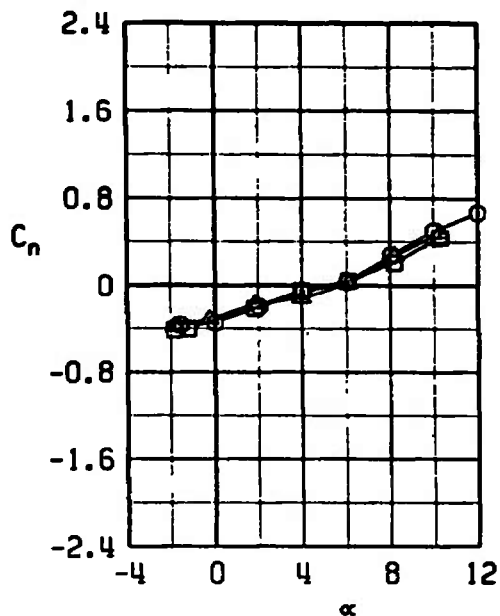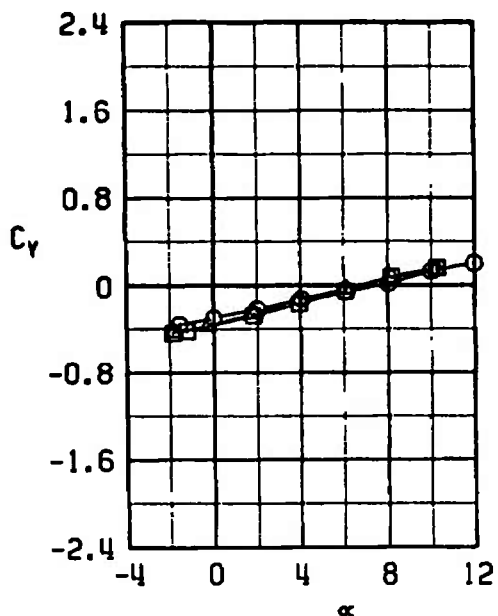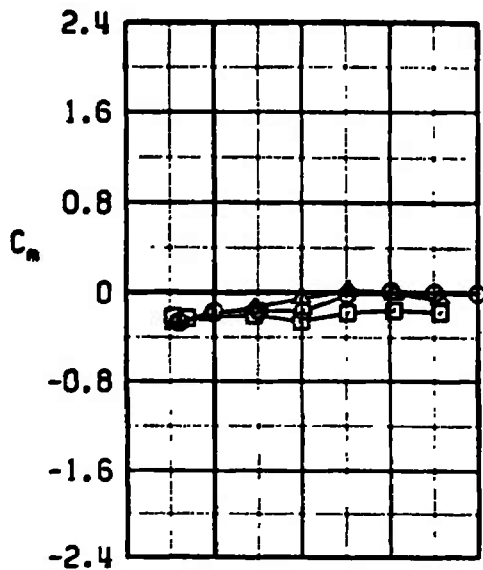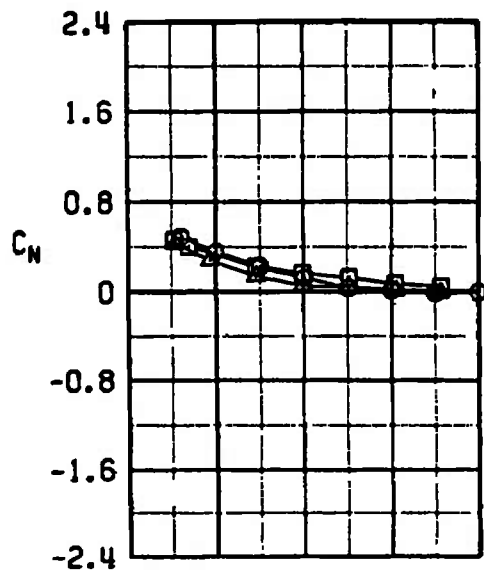
c. $M_\infty = 1.05$
Figure 40. Concluded.

SYMBOL
- ⊙ MODIFIED – CTS SUPPORTED
- ⊡ MODIFIED – RIGIDLY SUPPORTED
- △ MODIFIED – RIGIDLY SUPPORTED
  0.4–IN.–DIAM
  STRAIGHT STING
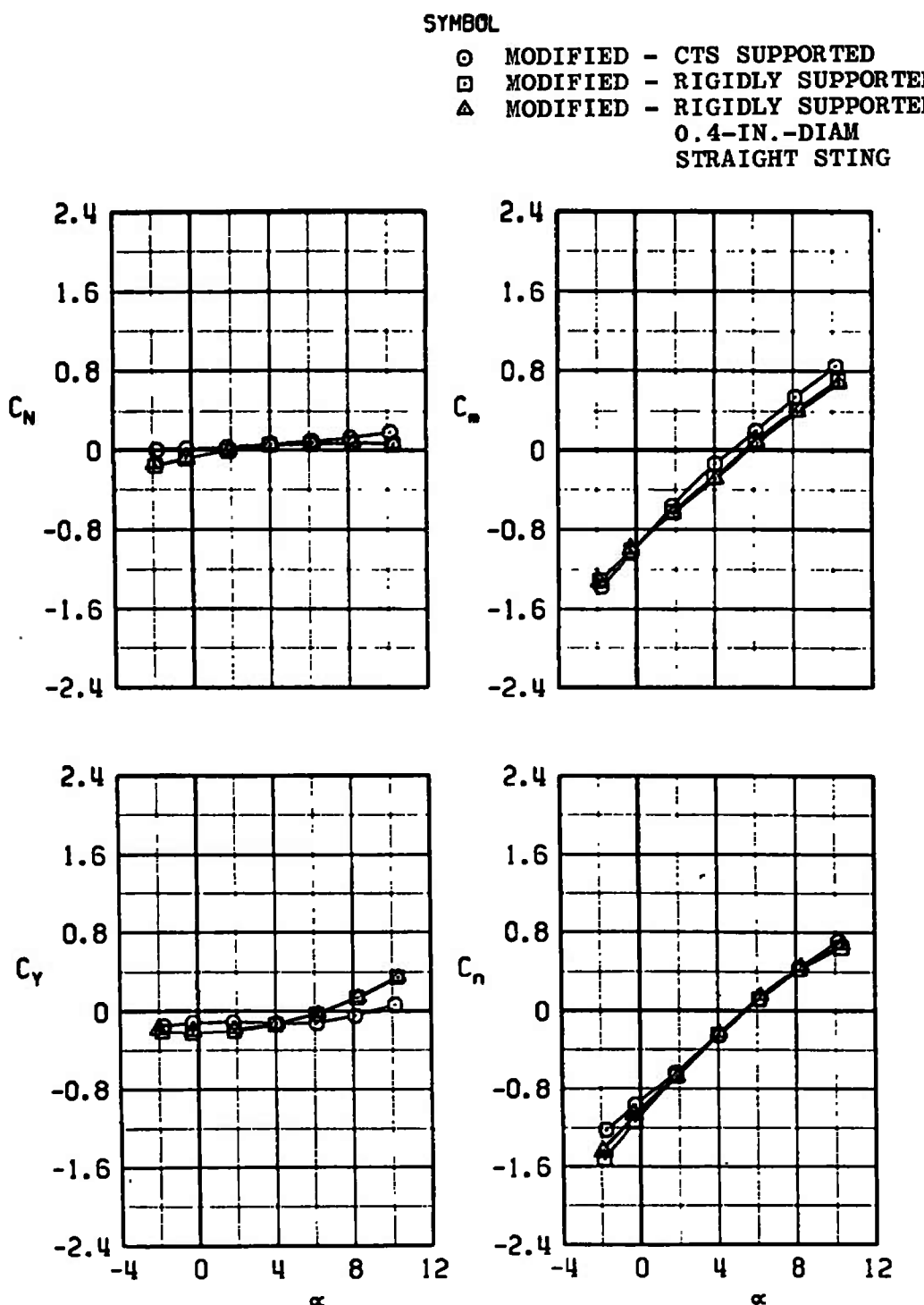
a. $M_\infty = 0.70$

Figure 41. Comparison of unfinned BLU-1C/B carriage-position aerodynamic coefficients with CTS and rigid loads techniques, configuration 2L.

SYMBOL
⊙ MODIFIED – CTS SUPPORTED
⊡ MODIFIED – RIGIDLY SUPPORTED
△ MODIFIED – RIGIDLY SUPPORTED
0.4-IN.-DIAM
STRAIGHT STING
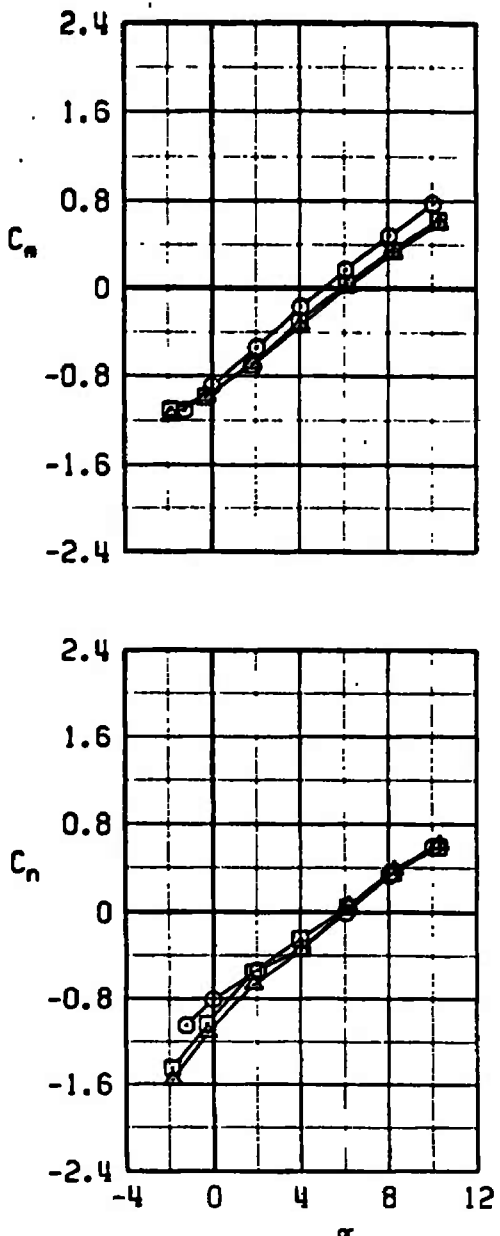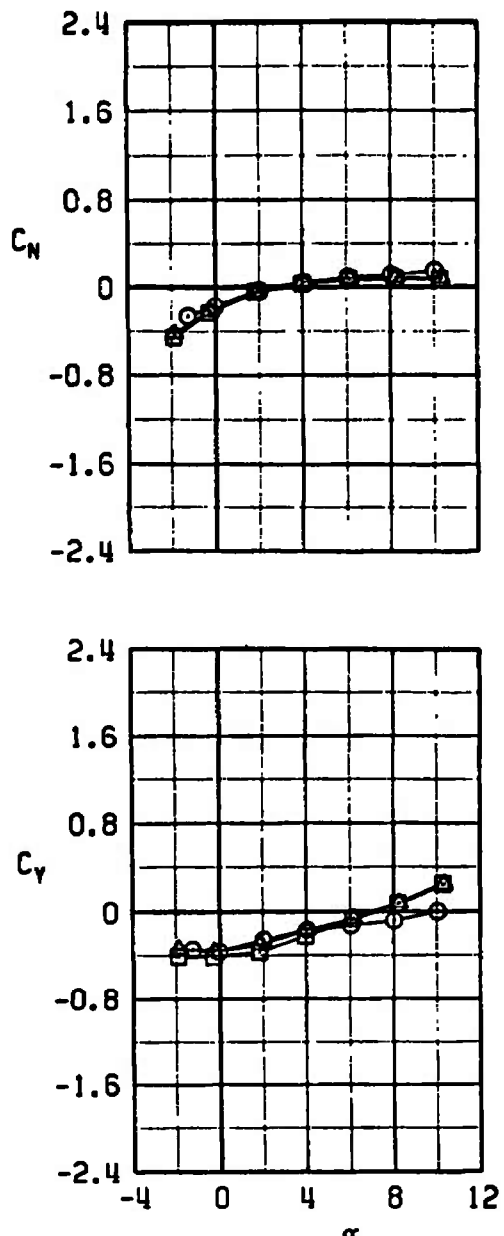
b. $M_\infty = 0.90$
Figure 41. Continued.

SYMBOL

⊙ MODIFIED – CTS SUPPORTED
⊡ MODIFIED – RIGIDLY SUPPORTED
△ MODIFIED – RIGIDLY SUPPORTED
 0.4–IN.–DIAM
 STRAIGHT STING
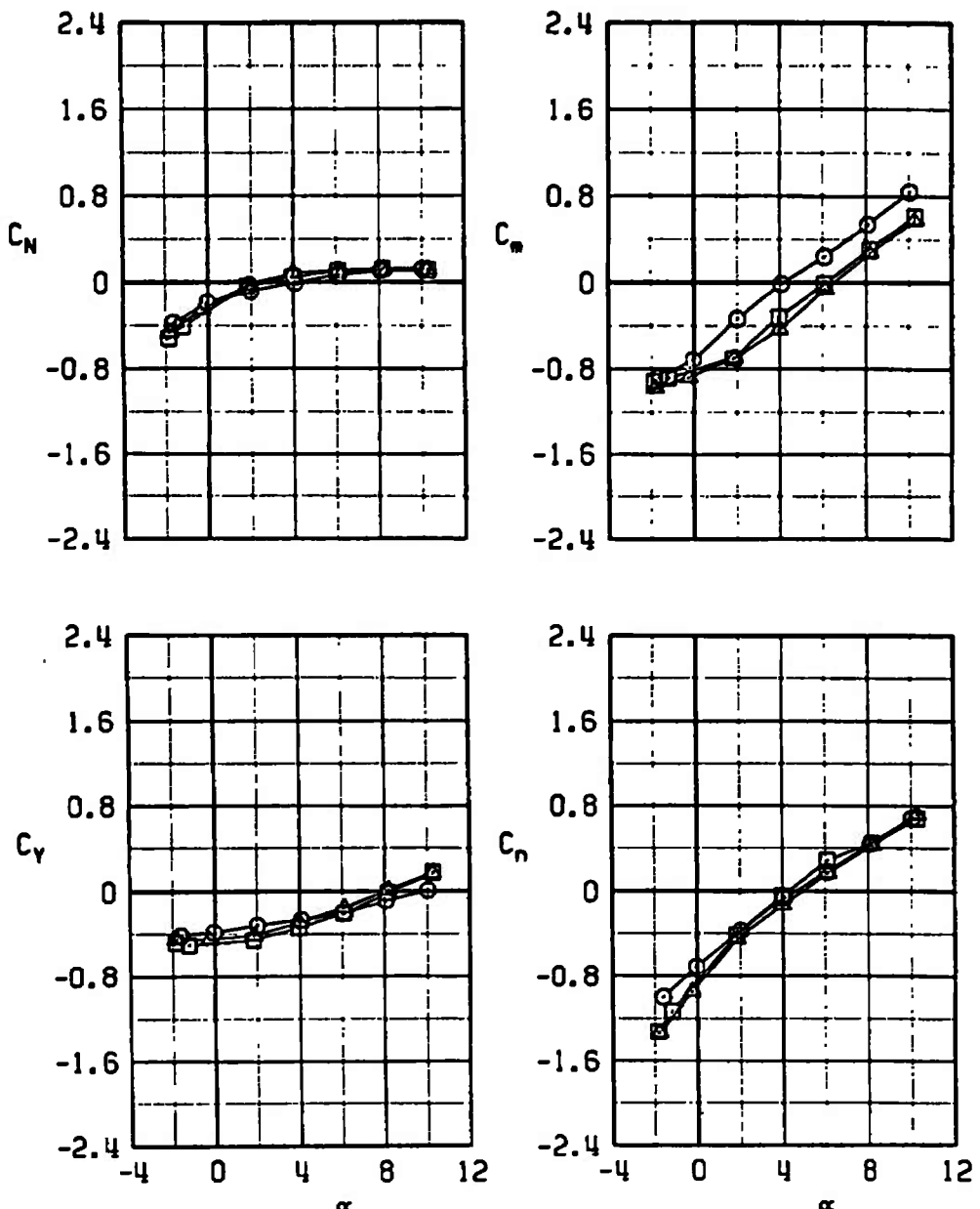
c. $M_\infty = 1.05$
Figure 41. Concluded.

99

SYMBOL

⊙ MODIFIED – CTS SUPPORTED
▣ MODIFIED – RIGIDLY SUPPORTED
▲ MODIFIED – RIGIDLY SUPPORTED
0.4-IN.-DIAM STING
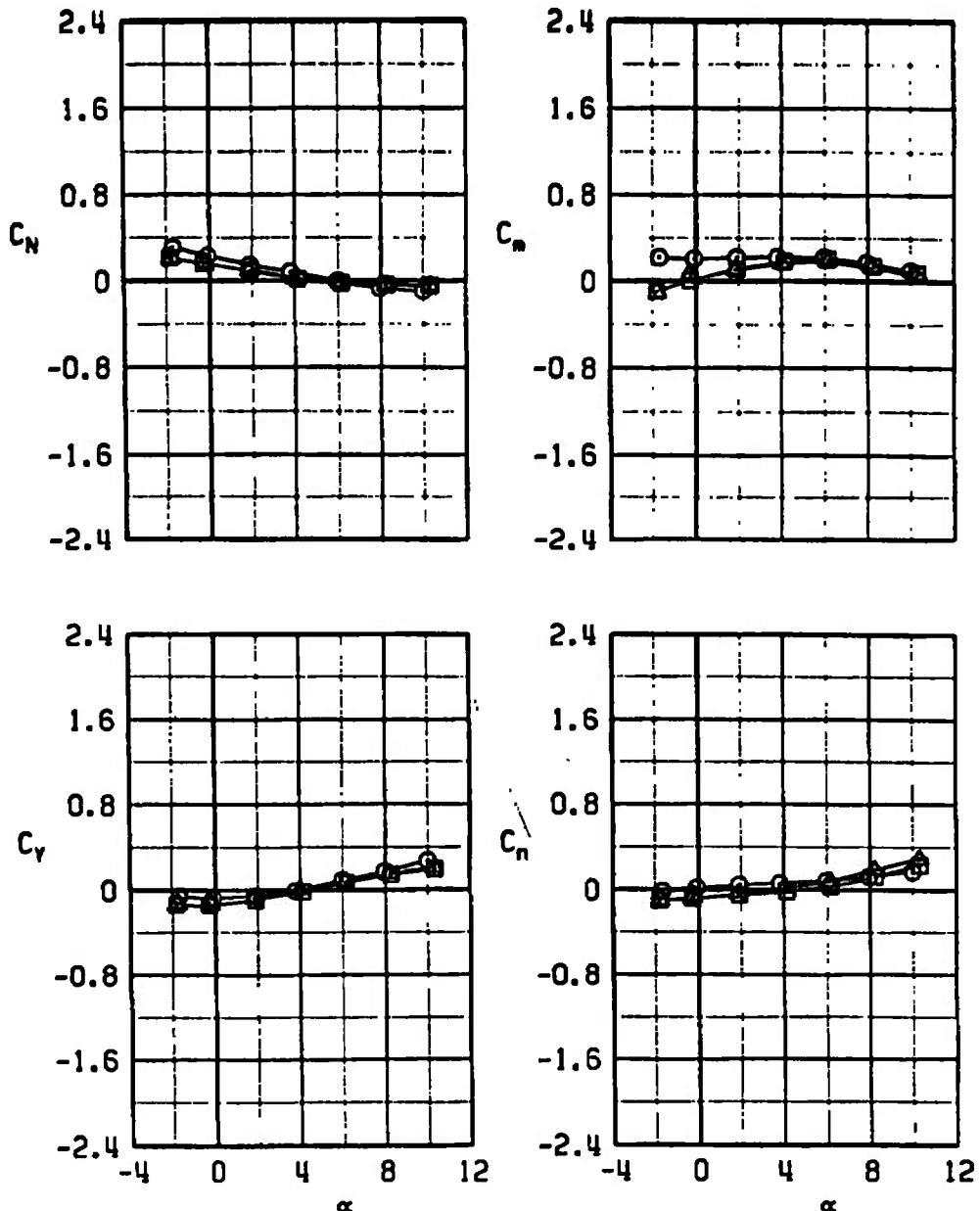
a. $M_\infty = 0.70$

Figure 42. Comparison of finned BLU-1C/B carriage-position aerodynamic coefficients with CTS and rigid loads techniques, configuration 3R.

SYMBOL
- ⊙ MODIFIED – CTS SUPPORTED
- ⊡ MODIFIED – RIGIDLY SUPPORTED
- △ MODIFIED – RIGIDLY SUPPORTED
  0.4-IN.-DIAM STING
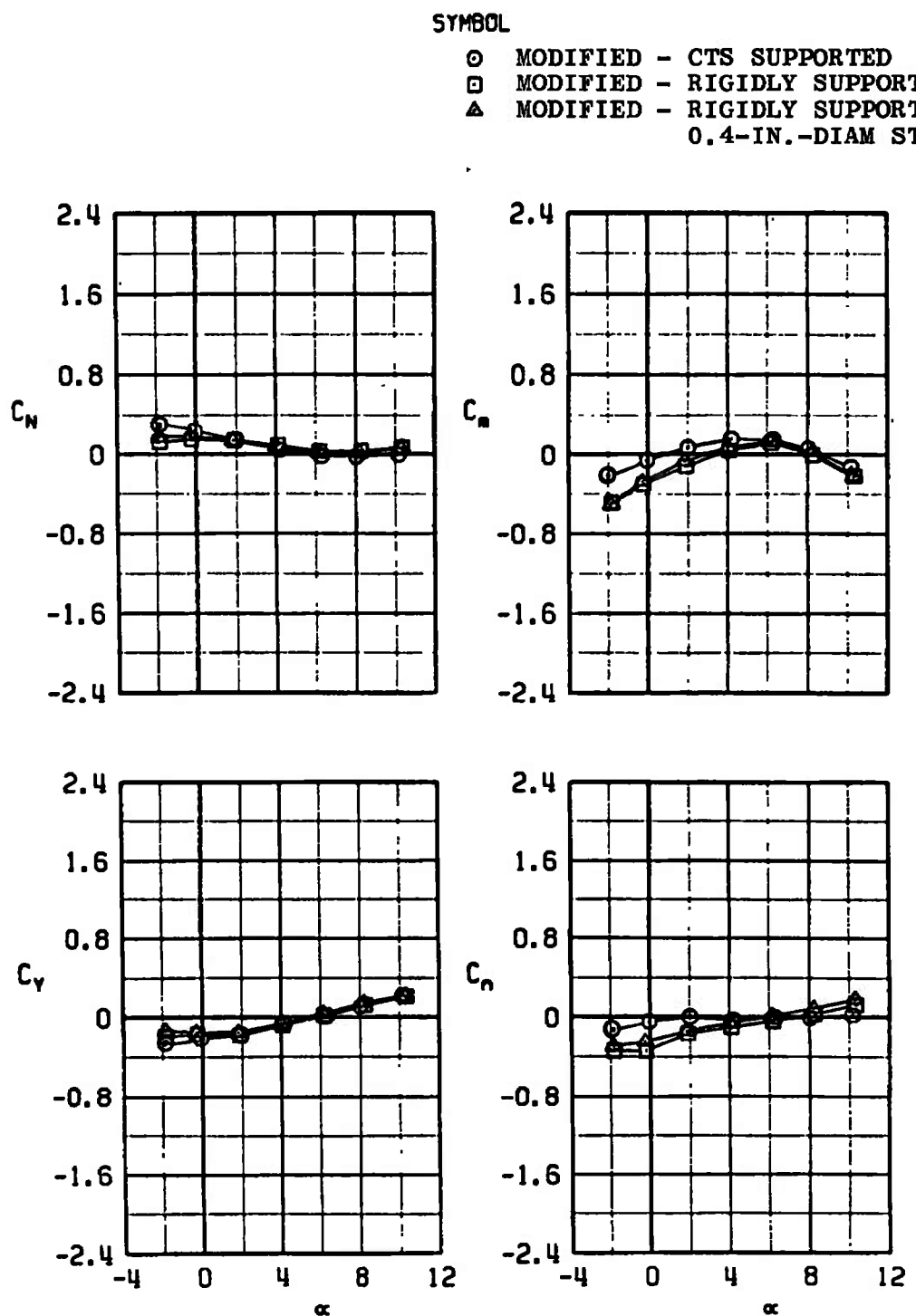
b. $M_\infty = 0.90$
Figure 42. Continued.

101

SYMBOL

⊙ MODIFIED – CTS SUPPORTED
▣ MODIFIED – RIGIDLY SUPPORTED
△ MODIFIED – RIGIDLY SUPPORTED
        0.4-IN.–DIAM STING
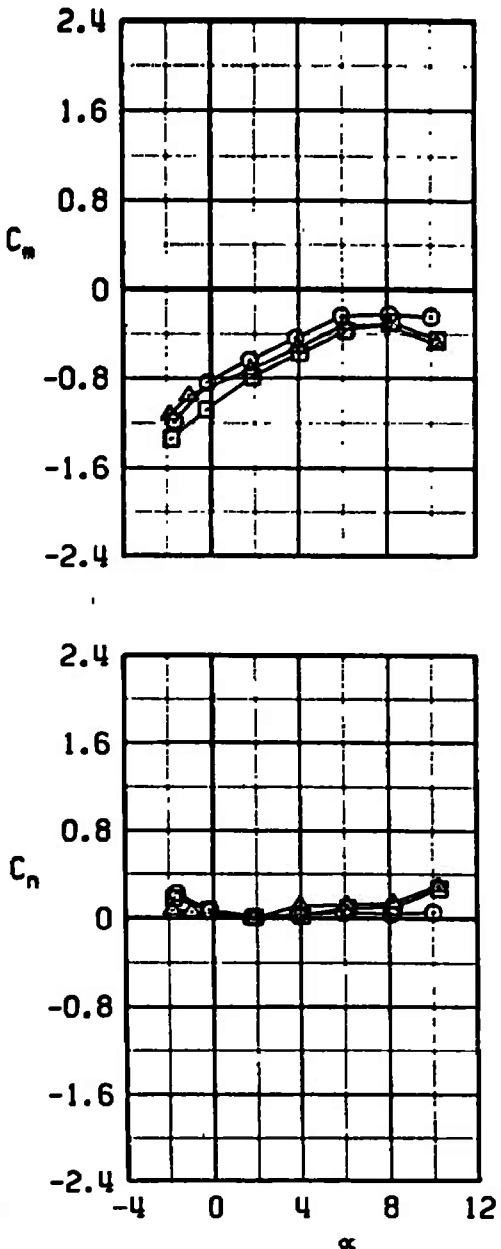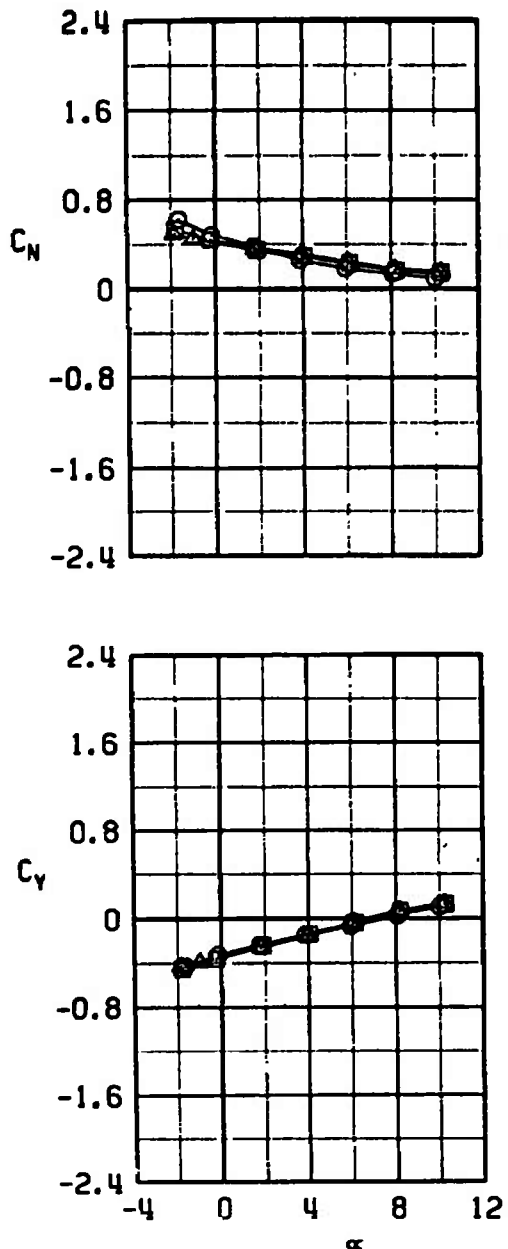
c. $M_\infty = 1.05$
Figure 42. Concluded.

SYMBOL

⊙ MODIFIED – CTS SUPPORTED
⊡ MODIFIED – RIGIDLY SUPPORTED
△ MODIFIED – RIGIDLY SUPPORTED
0.4-IN.-DIAM
STRAIGHT STING
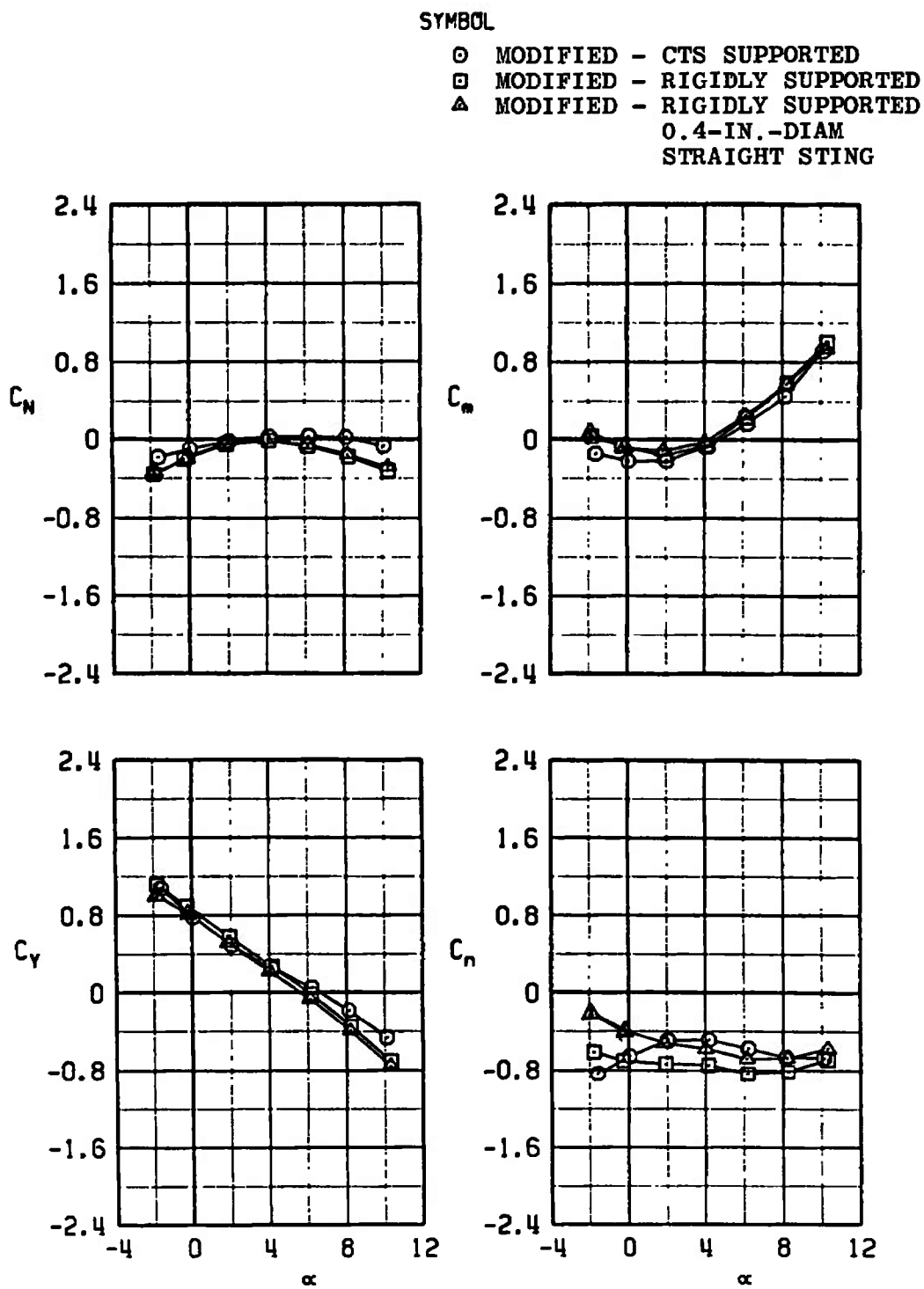
a. $M_\infty = 0.70$

Figure 43. Comparison of finned BLU-1C/B carriage-position aerodynamic coefficients with CTS and rigid loads techniques, configuration 3L.

SYMBOL

⊙ MODIFIED – CTS SUPPORTED
⊡ MODIFIED – RIGIDLY SUPPORTED
△ MODIFIED – RIGIDLY SUPPORTED
0.4–IN.–DIAM
STRAIGHT STING
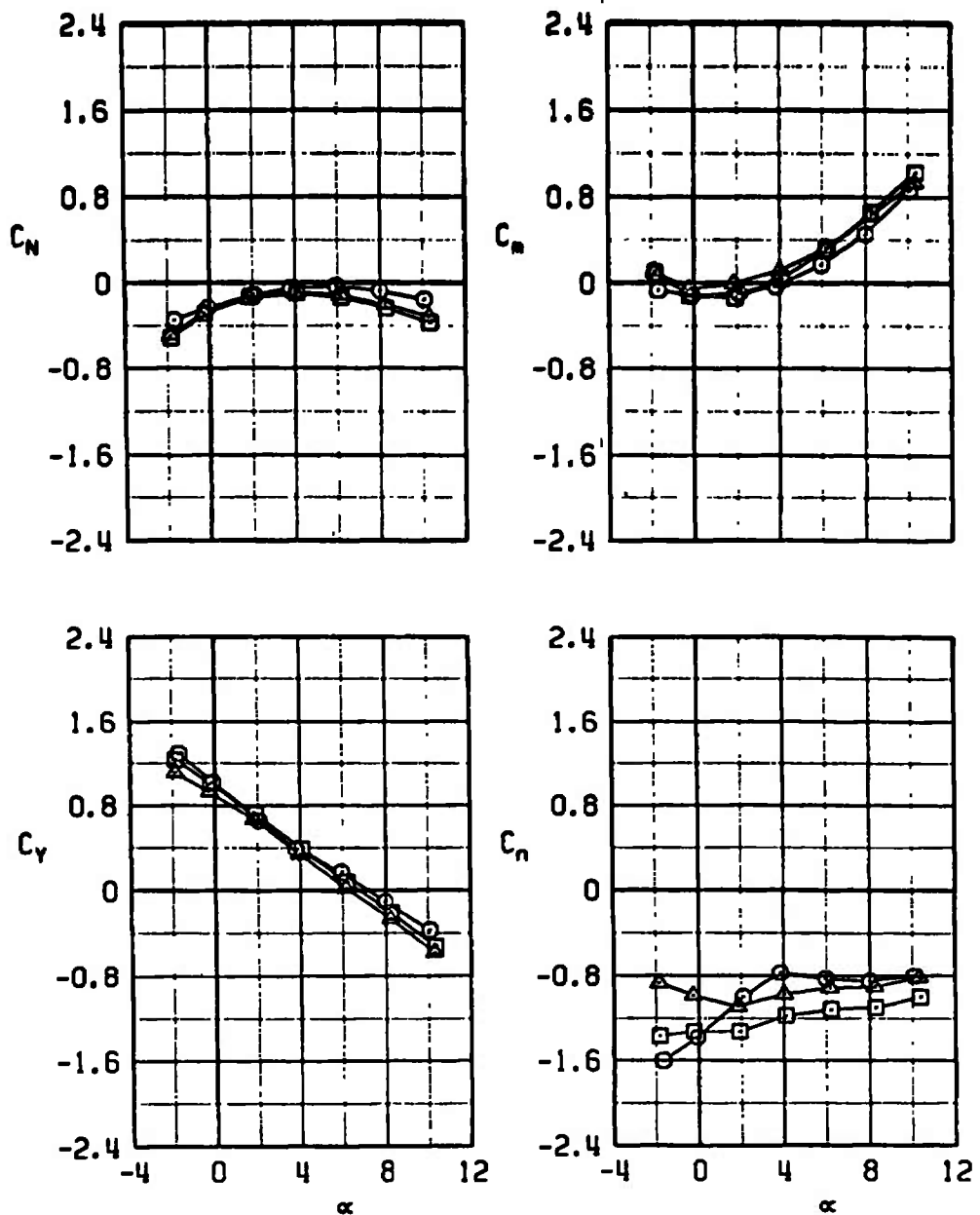
b. $M_\infty = 0.90$
Figure 43. Continued.

SYMBOL
⊙ MODIFIED — CTS SUPPORTED
⊡ MODIFIED — RIGIDLY SUPPORTED
△ MODIFIED — RIGIDLY SUPPORTED
0.4-IN.-DIAM
STRAIGHT STING
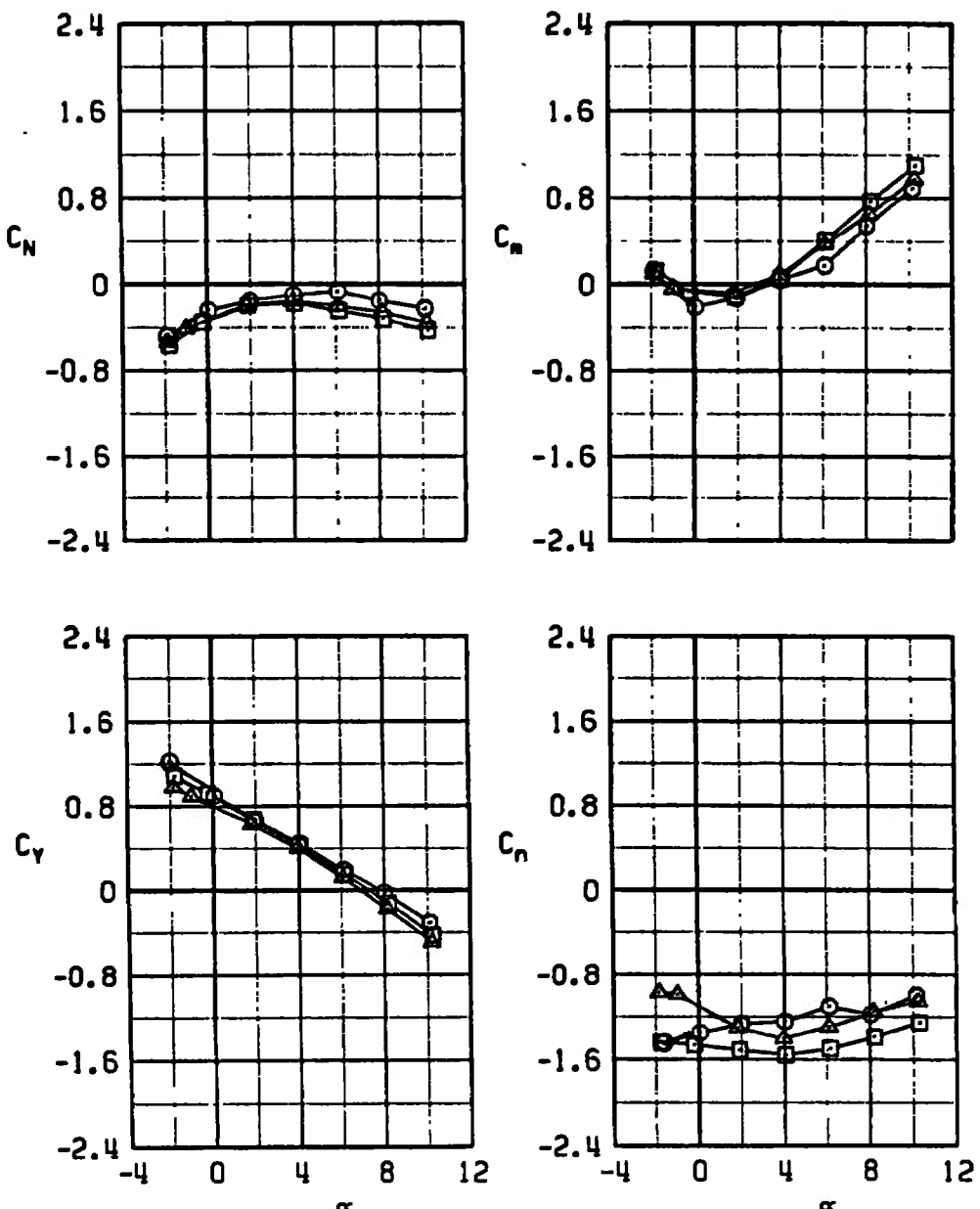
c. M_∞ = 1.05
Figure 43. Concluded.

☑ CTS TECHNIQUE – REPEATABILITY

☒ RIGID LOADS TECHNIQUE – BASIC AND MODIFIED
     – 0.2– AND 0.4–IN.–
     DIAM STING
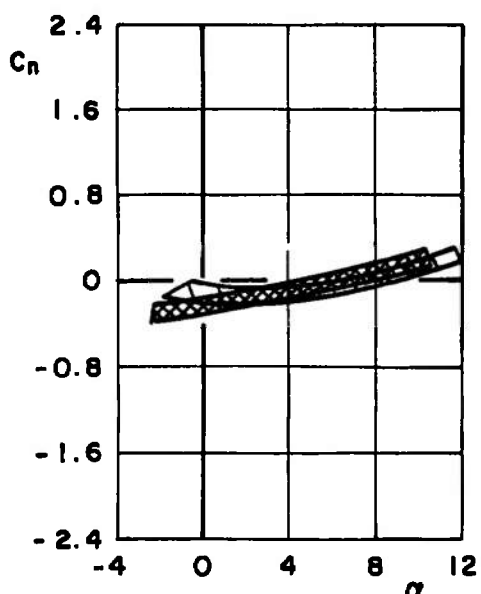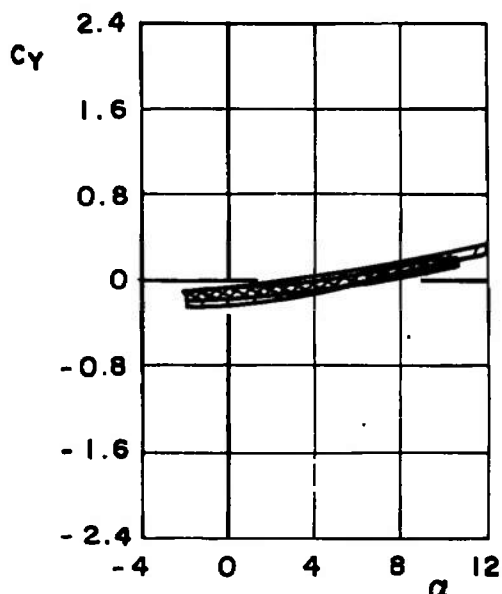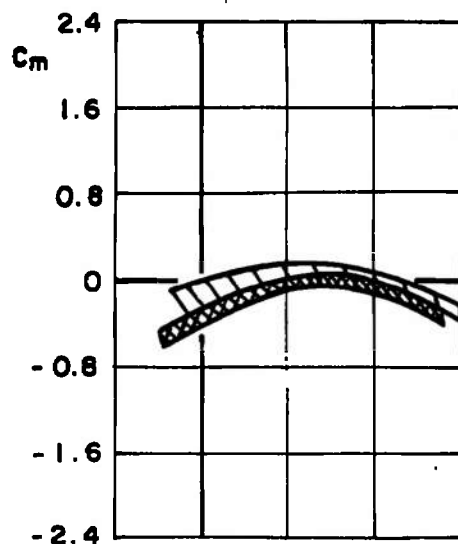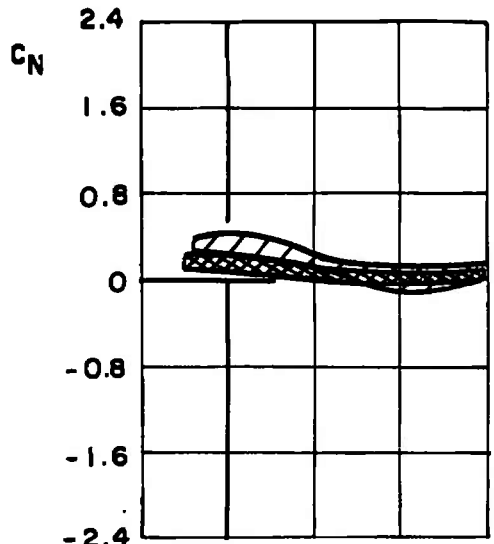
a. Configuration 3R

Figure 44. Summary comparison of finned BLU-1C/B carriage position aerodynamic coefficients between rigid loads and CTS techniques, $M_\infty = 0.9$.

106

⊘ CTS TECHNIQUE – REPEATABILITY
⊗ RIGID LOADS TECHNIQUE – BASIC AND MODIFIED
— 0.2– AND 0.4–IN.
DIAM STING
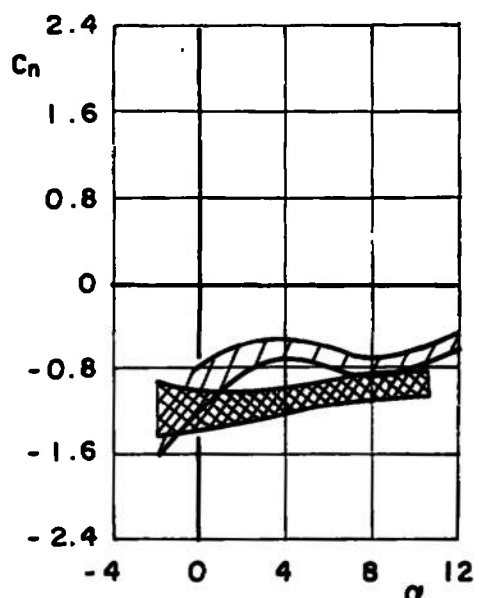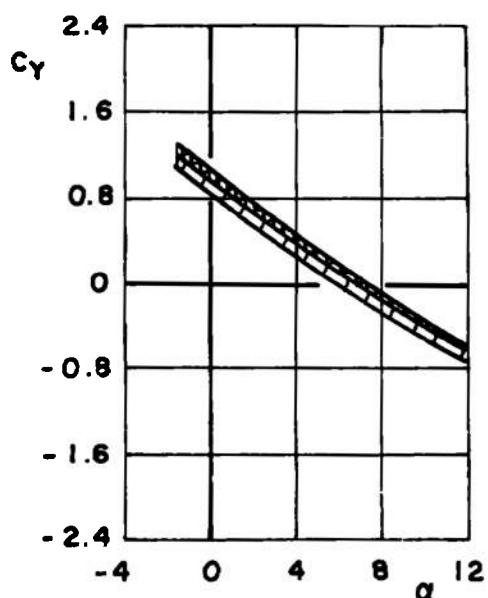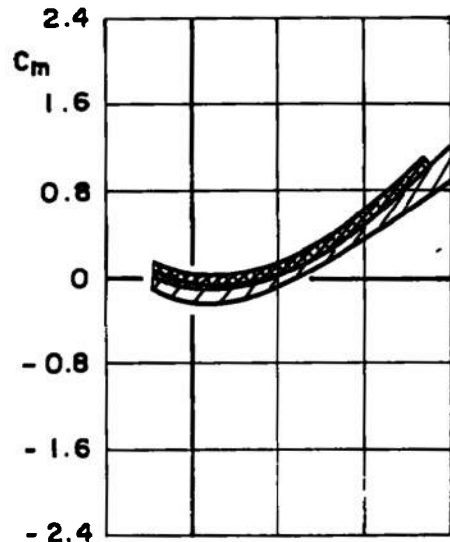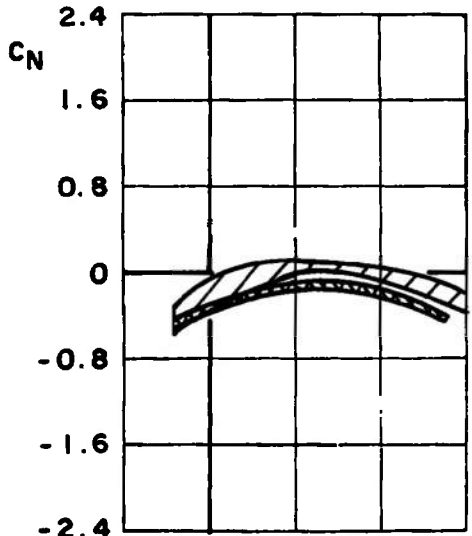
b. Configuration 3L
Figure 44. Concluded.

Table 1. Store Dimensions Used in Data Reduction

Store Actual/Modified	D	S	X_{cg}
M-117	16.0	1.396	2.573
BLU-1C/B (unfinned and finned)	18.6	1.887	5.375

Table 2. Aircraft Wing-Loading Configuration Identification
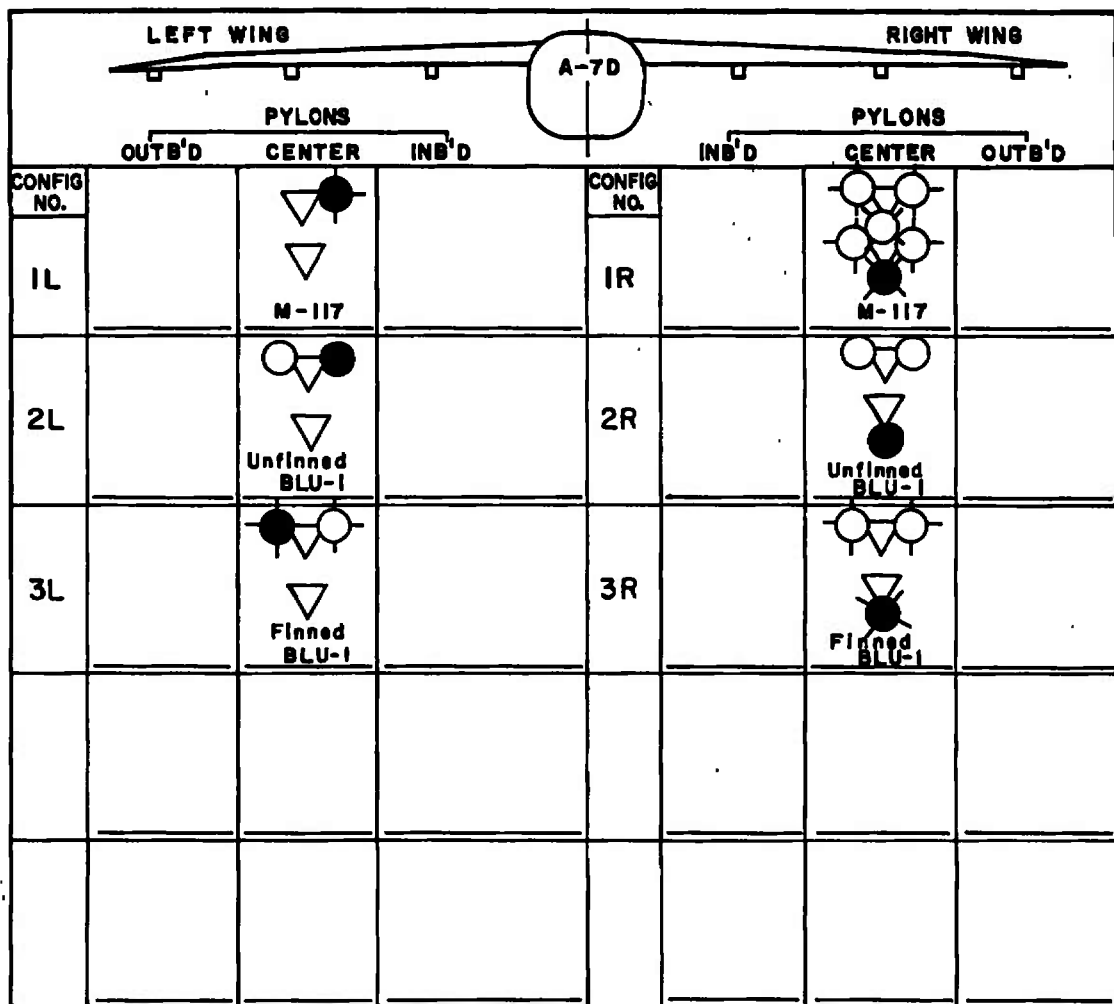
○ DENOTES DUMMY STORE
● DENOTES STING-MOUNTED STORE

▽▽} DENOTES MER

Table 3. Identification of Test Configurations with Test Conditions for CTS Testing

Store/Tail	Parent Yaw	Store Orientation			Wing-Loading Configuration	Mach Number		
		$\Delta\theta$	$\Delta\psi$	ΔZ		0 70	0 90	1.05
BLU-1/Finned	0	0	0	0 to 0 4 in	3L	91	95	96
	0			0 to 0 4 in.	3R	92	94	97
	2.04			0	3L	140	141	144
	2 04				3R	139	142	143
	-2 24				3L	148	149	252
	-2 24				3R	147	250	251
BLU-1/Unfinned	0	0	0	0 to 0 4 in.	2L	42	58	71
		-1	0	0		43	59	72
		1	0			44	66	73
		0	-1			51	70	75
			1			45	67	74
	2 04		0			127	128	131
	-2 24					156	157	160
	0			0 to 0 4 in.	2R	46	55	76
		-1		0		47	56	77
		1				48	57	78
		0	-1			50	65	83
			1			49	65	79
	2 04		0			123/126	129	130
	-2 24					155	158	159
M-117	0			0 to 0.4 in.	1L	18/20	29	34
		-1		0		---	29	35
		1				22	30	36
		0	-1			24	32	38
			1			23	31	37
	2 04		0			134	135	136
	-2 24		0			164	165	166
M-117	0	0	0	0 to 0.4 in.	1R	19/21	33/118	39/119
		-1	0	0		27	29	35
		1	0			29	30	36
		0	-1			24	32	---
		0	1			23	31	---

Note: Above indentification number indicates test part number for test TC-284

Table 4. Identification of Test Configurations with Test Conditions for Rigid Loads Testing

Store/Tail	Parent Yaw	Dummy Sting	Aircraft Horizontal Tail	CTS Rig	Wing-Loading Configuration	Mach Number 0.70	0.90	1.05
M-117/True	0	None	None	None	1L-1R	2, 8	3, 9	10
	0	0.2-in.-diam, Straight				18	17	18
	2.04	None				168	169	170
	-2.24	None				173	174	175
M-117/CTS	0	None				20	21	22
		0.4-in.-diam, Straight				26	27	26
		0.4-in.-diam, Bent				31	34	35
		None		yes	1R	39	42	43
		None		yes	1L	40	41	44
Unfinned BLU/True	0	None		None	2L-2R	48	49	50
	0	0.2-in.-diam, Straight		None		54	55	56
	2.04	None				163	164	165
	-2.24	None				178	179	180
Unfinned BLU/CTS	0	None				59	60	61
Unfinned BLU/CTS		0.4-in.-diam, Straight				64	85	66, 67
Unfinned BLU/CTS		0.4-in.-diam, Bent				71	72	73
Finned BLU/True		None			3L-3R	76, 77	78	79
		None	yes			138	139	140
		0.2-in.-diam,Str.	None			82	83	84
	2.04	None				158	159	160
	-2.24	None				183	184	185
Finned BLU/CTS	0	None				110, 125	111, 126	112, 127
		0.4-in.-diam, Straight				115	116	117
		0.4-in.-diam, Bent				120	121	122
		None		yes	3R	131	134	128
					3L	132	133	135
		None	yes	None	3L-3R	148	149	150
		0.4-in.-diam,Str.	None	None	3L-3R	143	144	145
	2.04	None	None	None	3L-3R	153	154	155

Note: Above identification number indicates test part number for test, TC-296

NOMENCLATURE

BL	Aircraft buttock line from plane of symmetry, in., model scale
C_m	Store pitching-moment coefficient, referenced to the store cg, pitching moment/$q_\infty SD$
C_N	Store normal-force coefficient, normal force/$q_\infty S$
C_n	Store yawing-moment coefficient, referenced to the store cg, yawing moment/$q_\infty SD$
C_Y	Store side-force coefficient, side force/$q_\infty S$
D	Store model reference diameter, full scale, in.
FS	Aircraft fuselage station, in., model scale
M_∞	Free-stream Mach number
p_∞	Free-stream static pressure, psfa
q_∞	Free-stream dynamic pressure, 0.7 $p_\infty M_\infty^2$, psf
S	Store model reference, $\pi/4\ D^2$, ft^2
WL	Aircraft waterline from reference horizontal plane, in., model scale
X_{cg}	Full-scale cg location, ft, from nose of store
Z	Travel of the store cg in the pylon-axis system Z_P direction, measured from the carriage position
α	Parent-aircraft model angle of attack relative to the free-stream velocity vector, deg
$\Delta\theta$	Angle between the store longitudinal axis and its projection in the X_P-Y_P plane, positive when the store nose is raised toward the negative Z_P axis, deg
$\Delta\psi$	Angle between the projection of store longitudinal axis in the X_P-Y_P plane and X_P axis, positive when the store is to the right when looking along the positive X_P axis, deg

ψ Angle between the aircraft model plane of symmetry and the free-stream wind vector, deg, positive when the aircraft nose is to the right looking upstream

PYLON-AXIS SYSTEM COORDINATES

Directions

X_P Parallel to the store longitudinal axis in the carriage position, positive direction is forward as seen by the pilot

Y_P Perpendicular to the X_P axis and parallel to the flight-axis system X_F-Y_F plane, positive direction is to the right as seen by the pilot

Z_P Perpendicular to both the X_P and Y_P axes, positive direction is downward as seen by the pilot

The pylon-axis is coincident with the store cg in the carriage position.

FLIGHT-AXIS SYSTEM COORDINATES

Directions

X_F Parallel to the free-stream vector, positive direction is forward as seen by the pilot

Y_F Perpendicular to the X_F and Z_F directions, positive direction is to the right as seen by the pilot

Z_F In the aircraft plane of symmetry, perpendicular to the free-stream wind vector

The flight-axis origin is coincident with the aircraft cg.